FEATURES OF THE (p, α) REACTION

By

Paul Alexander Smith

A DISSERTATION

Submitted to
Michigan State University
in partial fulfillment of the requirements
for the degree of

DOCTOR OF PHILOSOPHY

Department of Physics

1976

ABSTRACT

FEATURES OF THE (p,α) REACTION

By

Paul Alexander Smith

Theoretical and experimental features of the (p,α) reaction are presented.

A microscopic reaction theory of the 3-nucleon direct pick-up reaction using shell model wavefunctions is developed. This theory involves the calculation of microscopic form factors and spectroscopic amplitudes. Two form factor models are given—the first using harmonic oscillator single-particle wavefunctions, and the second using single-particle wavefunctions of a Woods-Saxon potential. The motion of the nuclear center of mass in a fixed center potential is considered and the microscopic form factors are corrected for this motion. Three nucleon spectroscopic amplitudes are related to two nucleon reduced matrix elements and single nucleon reduced matrix elements which can be calculated using existing shell model codes. Calculations for pure configurations are presented and the features of these calculations are discussed.

Paul Alexander Smit

The Distorted Wave Born Approximation for the (p,α) reaction is investigated. Angular momentum mismatch, finite range effects, and j-dependence are discussed.

The $^{52}Cr(p,\alpha)^{49}V$ and the $^{44}Ca(p,\alpha)^{41}K$ areactions are presented as the experimental side. These reactions have been studied with a beam energy of 35 MeV.

The $^{52}Cr(p,\alpha)^{49}V$ spectra show that the $7/2^-$ ground state, the $3/2^+$, 0.748 MeV proton hole state, and the 1.646 MeV $1/2^+$ proton hole state are strongly excited. Many seniority three transfers are also observed. A comparison of the (p,α) results to (p,t) and (t,α) work is presented. This comparison shows that coherence in the (p,α) reaction is important, since some states found in the (p,t) or (t,α) results are not observed in the (p,α) spectra. Candidates for high spin states are found at 3.612 MeV, 3.745 MeV, and 4.797 MeV. $T = 5/2$ proton hole states (analog states) are observed in the region from 6 to 9.5 MeV. Cluster model DWBA calculations are shown to fit the data successfully. The normalization of the cluster model calculation to the $T = 5/2$, $7/2^-$ angular distribution relative to the corresponding $T = 3/2$ state is about ten times larger than is expected from simple isospin considerations. Microscopic model DWBA calculations are also given. The microscopic calculations are shown to fit the angular distributions reasonably well. The relative normalizations of the DWBA curves to the proton hole state angular distributions are seen to be in good agreement with simple shell model predictions. The general trend of

Paul Alexander Smith

experimental cross sections for the negative parity states is shown to

follow the features of the microscopic model calculations assuming

pure $(0f7/2)^3$ transfer.

The $^{44}Ca(p,\alpha)^{41}K$ spectra show that those states which contain

portions of the sd-shell proton holes are strongly populated. The 0d5/

proton hole is mostly concentrated in a new level at 3.520 MeV. The

$7/2^-$ state at 1.294 MeV is also excited. $T = 5/2$ proton hole states

(analog states) are observed in the excitation region from 8 to 10 MeV.

These states have j^π values of $7/2^-$, $3/2^+$, and $1/2^+$. Clear $\ell = 2$ j-

dependence is observed for this target. Cluster model DWBA calcula-

tions are shown to fit the data well. The normalization of the cluster

model curve to the $7/2^-$, $T = 5/2$ angular distribution is ten times larg

than would be expected from isospin arguments. Microscopic model

DWBA calculations are shown. These do not fit the angular distribu-

tions nearly as well as the cluster model calculations. The relative

normalizations of the sd-shell hole fragments is seen to disagree with

$(d, ^3He)$ results. However, the sums of the fragments are in good

agreement with simple shell model considerations. Microscopic cal-

culations for the $7/2^-$, 1.294 MeV state are found to be in good agree-

ment with the $(d, ^3He)$ result. The possibility of $(0f7/2\ 0d3/2)0d3/2$

pick-up is considered and found to be unnecessary for this transition.

ACKNOWLEDGMENTS

Writing a dissertation is a special occasion for a graduate student. It represents the culmination of many years of hard work, sleepless nights at the cyclotron console, and self-imposed slavery to the project. The dissertation is the end and the beginning.

This is my chance to explain what I have learned to the public. It is my chance to teach you and to thank you. Unfortunately, the language of nuclear physics is a difficult one, which is unfamiliar to the general public and many of my friends. I have, therefore, included an appendix where I hope that some basic nuclear physics is described in more common English. This is my way of saying thanks to my parents and the taxpayers of America and Michigan who have provided enormous resources for my education.

This is also the time when I can say thanks to everyone who has helped me. Everyone means everyone—you have all helped. My teachers, from my parents to my advisor, have provided the information and stimulation necessary for me to learn what little I have. My friends, though many of them know little physics, have managed to delay this moment with good times that have preserved my insanity and made my graduate career a lot of fun. This thesis is for my friends

whose love I have often been unable to share fully because of my commitment to this project. I am especially grateful to the Nuclear Beer Group, which I trust will continue to grow and prosper in the future.

I would like to thank Gary Crawley for suggesting this project.

I am especially thankful for the supervision of my advisor Jerry Nolen. Without his expertise and dedication, this project would never have become a reality.

Roger Markham, Ranjan Bhowmik, Din Shahabuddin, and Joe Finck deserve a great deal of credit for helping in many aspects of this work and plugging away at what has proven to be an immense project.

Finally, no words can describe how the wisdom of the grand old man has influenced me. Few students will ever have the chance to know the golden age of physics the way I have. This thesis is dedicated to an oldtimer—my grandfather, Professor R. A. Wolfe—and his wife.

TABLE OF CONTENTS

LIST OF TABLES

LIST OF FIGURES

viii

CHAPTER I

INTRODUCTION

The field of physics may be divided into the study of bound state problems, such as the solar system, crystals, or atomic structure, and unbound problems, such as the scattering of light or neutron diffraction. The same division applies to nuclear studies. The bound state problem is the study of nuclear structure. The problem to be solved in this instance is the prediction of the energies of the nuclear states and their properties, such as angular momentum and electromagnetic decay rates. The scattering problem is the study of elastic scattering, inelastic scattering, or transfer reactions. Here the problem is to predict the angular distributions and the strengths of the transitions.

The division of the field to which I have alluded is easily made for macroscopic systems, such as the solar system, where the individual components of the system can be examined. The division of nuclear physics in this way cannot be total since we cannot observe the bound system microscopically. Nearly all the information about the details of nuclear structure must come from the observation of free radiation resulting from radioactive decay or artificially induced reactions. Thus bound state models and scattering models must be

1

connected in a way that allows the deduction of nuclear structure information from the results of scattering experiments.

The shell model is commonly used for nuclear structure calculations. This model is based on the idea that a nucleon orbit may be described as that of a particle moving in a central potential created by the average interactions with the other nucleons in the nucleus. In addition, the residual interactions between pairs of nucleons are included in the Hamiltonian. This has the effect of removing degeneracies in the original orbits of the central potential. Nuclear states can be described as distributions of the nucleons in these perturbed orbits.

During the last twenty years many direct reaction studies have concentrated on the deduction of nuclear structure information. As might have been expected, these studies began with the single nucleon transfer reactions and progressed sequentially to more complex reactions. The purpose of this dissertation is to present work aimed toward testing shell model wavefunctions with the direct transfer of three nucleons. Prerequisite goals are to develop a microscopic model for calculations of three nucleon transfer reactions, and to detail the qualitative features of the (p, α) reaction which is the specific three nucleon transfer reaction to be considered in this work.

The simplest nuclear states are those which are described by a single particle or hole outside a closed shell. Such states give the

energies of the single particle orbits in the shell model central potential. Consider ^{41}Ca as an example. A "zero order" shell model would describe ^{41}Ca as a ^{40}Ca inert core plus a neutron in the 0f7/2, 1p3/2, 0f5/2, or 1p1/2 orbit. Given this simple model, ^{41}Ca should have a 7/2$^-$ ground state and 3/2$^-$, 5/2$^-$, and 1/2$^-$ excited states, all of which look like a neutron bound to a ^{40}Ca core. Therefore, if a neutron is added to ^{40}Ca in a nuclear reaction such as ^{40}Ca(d,p)^{41}Ca, the spectrum is expected to contain strong transitions to the 7/2$^-$, 3/2$^-$, 5/2$^-$, and 1/2$^-$ states of ^{41}Ca on the basis of the zero order shell model assumption.

In general, the zero order shell model is not sufficient to explain all the transitions observed experimentally. For the ^{40}Ca(d,p)^{41}Ca example, the zero order shell model not only predicts that 7/2$^-$, 5/2$^-$, 3/2$^-$, and 1/2$^-$ transitions will be observed, but also that they will be the only transitions. The zero order shell model may be improved if the ^{40}Ca core is allowed to contain components with two neutrons in the 0f7/2 shell. In other words, some of the time ^{40}Ca may have vacancies in the 0d3/2 shell. Observation of 3/2$^+$ states in the ^{40}Ca(d,p)^{41}Ca reaction gives a measure of the amplitude of this component of the ^{40}Ca ground state. A complete description of a final state observed in the (d,p) reaction is

$$\psi_f^{J_f} = \sum_{ij} A_{ij} \psi_T^{J_T} \psi_{n_i}^{j}$$

where $\psi_T^{J_T}$ is the target wavefunction, $\psi_{n_i}^{j}$ is the neutron wavefunction

(n$_i$ represents the fact that there is no restriction on the major shell, although contributions from anything other than the lowest shell are usually negligible for low-lying states), and A$_{ij}$ is the amplitude for this component. The A$_{ij}$'s can be deduced from experimental cross sections. In Appendix II and Chapter II the details of the reaction theory called the DWBA (Distorted Wave Born Approximation) are discussed. For the moment, a short summary is all that is necessary to see the role of the A$_{ij}$'s in the cross section prediction. The idea behind the DWBA is that the operator which causes transitions is a small part of the total Hamiltonian that describes the scattering problem. The transition operator is treated as a perturbation causing transitions between elastic scattering states (distorted waves) which are the eigenstates of the rest of the Hamiltonian. The cross section is proportional to the square of the transition matrix element. The transition matrix element can be "factored" (see Chapter II) so that the overlap of the target wavefunction and the final wavefunction is isolated. In other words, the cross section is proportional to $|\langle \psi_p | \psi_r \rangle|^2$ which is proportional to $|A_{ij}|^2$. A nice example of how the values of the A$_{ij}$'s are determined is given by Barry Preedom in his notes on nuclear reactions (I.1, page 72). The simplicity of single nucleon transfer lies in the fact that only one term in the final wavefunction contributes to a given transition if the target wavefunction has $J_T \equiv 0$. In other words, only one of the A$_{ij}$'s is deduced for each transition. However, the signs of the amplitudes are not determined.

Two-nucleon structures are the next in order of complexity.
There are not many simple two-nucleon structures observed experimen-
tally. As an example, let us use ^{40}Ca as a core again and consider
the ^{40}Ca(p,t)^{38}Ca reaction. Final states with $j^{\pi}=0^+$ are relatively
simple because the only way two neutrons can have zero angular
momentum is if they both come from the same orbit. For our example,
the two neutrons picked up can come from the 0f7/2, 0d3/2, 1s1/2, or
0d5/2 orbits. Because of the residual interaction, a given 0^+ final
state will look like ^{40}Ca+A_1(0f7/2)$^{-2}$+A_2(0d3/2)$^{-2}$+A_3(1s1/2)$^{-2}$+
A_4(0d5/2)$^{-2}$. Other transitions may have more components since the
neutrons can come from different orbits for final states that do not have
$j^{\pi}=0^+$. This discussion can be written more precisely as

$$\psi_f^{J_f} = \sum_{jkL} A_{jk}^L \psi_T^{J_T} (\psi_{n_j} \psi_{n_k})^L$$

where the ψ_{n_j} (ψ_{n_k}) indicate that a neutron is removed from the jth (kth)
orbit and $(\ )^L$ indicates vector coupling of the neutron angular momenta
to the value L. If we consider the overlap of the target and the final
state wavefunction as was done before, it is seen that, in general,
many shell model configurations contribute coherently to the cross sec-
tion for a given transition in the (p,t) reaction. Therefore, it is not
possible to extract the values of the A_{jk}'s directly from the data.
Instead, we must work in the other direction by calculating the A_{jk}'s
as overlaps of shell model wavefunctions and using the results in a
reaction model. Because many configurations contribute coherently to

the cross section, the phases of the A_{jk}'s are important. Whereas single nucleon transfer cannot measure these phases, multi-nucleon transfer has the advantage of being sensitive to them. The ability to predict the data tests both the shell model and the reaction model simultaneously.

The progression from single nucleon transfer to two-nucleon transfer results in an enormous increase in complexity, hence one might ask, "Why study three-nucleon transfer?" The answer lies in the hope that there might be simple features of reactions such as (p, α) which are less complex than two-nucleon transfer, as well as other specific reasons discussed below. Because of the problems previously encountered in the analysis of two-nucleon transfer reactions, detailed agreement between a microscopic (p, α) reaction model and the data is not expected. Hence, this thesis is primarily concerned with prediction of the qualitative features of this reaction and their identification in the data.

One of the simple properties of the (p, α) reaction is the population of the same single proton hole states that are seen in single proton pick-up. The target ^{52}Cr can be used as a good example. Much of the time the neutron pairs in the closed shell will have an internal angular momentum of zero. If one of these pairs and a proton are removed, we will see the single proton hole states that would be observed in the $^{50}Cr(d, {}^{3}He)^{49}V$ reaction. This was one of the first observations made by the pioneers in this area (I.2, I.3, I.4, I.5). Sherr (I.2) used the

^{58}Fe$(p, \alpha)^{55}$Mn reaction to demonstrate this feature. The ^{55}Mn ground state has $j^\pi = 5/2^-$. In a zero order shell model the neutrons would be coupled to zero angular momentum since there are an even number of them. Therefore, the ^{55}Mn ground state must be primarily a seniority three-proton state. The term "seniority" means the number of particles that are not part of nucleon pairs that have zero angular momentum. The ^{55}Mn ground state has a pair of protons that have nonzero angular momentum and an odd 0f7/2 proton, making it a seniority three-state. The ^{58}Fe ground state looks like four 1p3/2 neutrons and three pairs of zero coupled protons. Removal of a pair of neutrons and a proton will lead to a $7/2^-$ state which is not the ground state. The data showed that the ground state was weakly excited and that the $7/2^-$ first excited state was very strong. The inverse reaction ^{55}Mn$(\alpha, p)^{58}$Fe, presented at the same conference, showed excellent agreement in that the ground state of ^{58}Fe was not observed (I.6).

Although the strongest states will be those that can be made via seniority one transfers (a seniority zero neutron pair and a seniority one proton), there will be seniority three pick-ups where the pair of neutrons does not have zero angular momentum. Some of the time a neutron from two different pairs will be picked up leading to a transferred pair with nonzero angular momentum. If a pair of neutrons is removed with nonzero angular momentum along with a 0f7/2 proton, final states with spins different from $7/2^-$ can be populated. Since the 0f7/2 neutron pair may have angular momentum as high as six, it is

possible to populate states in ^{49}V with spins up to 19/2. In recent

years high spin states have been studied intensively with $(\alpha, xn\gamma)$ and

$(HI, xn\gamma)$ reactions. The (p, α) reaction and other multi-particle trans-

fer reactions may be useful for differentiating between high spin states

due to simple shell model configurations and those which are collective

rotations of a deformed nucleus. Four recent experiments have

observed $j^{\pi} = 13/2^+$ transfers which is the maximum $(0d5/2)^3$ coupling.

$13/2^+$ levels have been observed in $^{12}C(\alpha, p)^{15}N$, $^{16}O(\alpha, p)^{19}F$, and

$^{24,26}Mg(p, \alpha)^{21,23}Na$, while an 8^+ state was observed in

$^{23}Na(p, \alpha)^{20}Ne$ (I.7, I.8, I.9, I.10).

In principle, the (p, α) reaction may also be used to locate states

with isospin greater than the ground state ($T_>$ states) that are not

allowed in the $(d, ^3He)$ reaction because of isospin selection rules.

Thus single nucleon spectroscopic factors and Coulomb energies can

be deduced for levels that cannot be made by single nucleon pick-up.

This feature of the (p, α) reaction has not been confirmed in previously

published experiments.

The determination of both the total angular momentum and parity

of a nuclear state can be a difficult problem. In many cases more than

one experiment is necessary. Gamma-ray decay studies often deter-

mine the total angular momentum but not the parity. When the state

of interest can be made by single nucleon transfer, the orbital angular

momentum but not the total angular momentum is usually determined.

The parity in this case is given by $(-1)^{\ell}$. One of the observations

made during the first (p,α) reaction studies was the marked dependence
of the angular distributions on the value of j for $\ell = 1$ transitions (I.11,
I.12, I.4, I.5). The angular distribution for the $1/2^-$ transfer is
characterized by deep minima, while the $3/2^-$ distribution is feature-
less. There is promise that the (p,α) reaction may be used to deter-
mine both j and π. Lee et al. (I.13) have shown that this effect is a
consequence of spin orbit coupling in the proton channel. The j-
dependence for $\ell = 2$ and higher is currently not well documented and,
in fact, different experiments have reached different conclusions (I.13,
I.14, I.15, I.16). This point is pursued in Chapters IV and V of this
thesis.

The (p,α) reaction has the potential for reaching states that
cannot be reached by single proton pick-up in nuclei where proton
pick-up can be done. It also can be used to reach single proton hole
states in nuclei that cannot be reached by single proton pick-up
because the targets do not exist or are hard to obtain, thereby per-
mitting the measurement of single nucleon spectroscopic information in
these otherwise inaccessible cases. If simple models explain the
properties of the spectra observed in nuclei that can be studied with
proton pick-up, then these models may be extended to new nuclei to
further study the systematics of hole states, Coulomb energies, high
spin states, etc.

Even though there are simple features that make three-nucleon

transfer attractive for spectroscopic studies, detailed study of the

reaction for all states is even more difficult than for two-nucleon trans-

fer. The additional complication may be illustrated if the final wave-

function for the (p,α) reaction is expanded as before

$$\psi_f^{J_f} = \sum_{\substack{rst \\ \ell_{12}j}} A_{rst}^{j} \psi_T^{J_T} \left[(\psi_{n_r} \psi_{n_s})^{\ell_{12}} \psi_{p_t} \right]^{j}$$

where $\psi_T^{J_T}$ is the target wavefunction, ψ_{n_r} (ψ_{n_s}) is the wavefunction for

a neutron hole in the rth (s^{th}) orbit, ℓ_{12} is the angular momentum cou-

pling of the two neutrons, and ψ_{p_t} is the wavefunction for a proton

hole in the tth orbit. There is a sum over shell model configurations

as in two-nucleon transfer, but in addition there is a sum over all the

allowed values of the neutron pair angular momentum. A discussion of

the internal degrees of freedom associated with the (p,α) reaction and

some of the consequences within the 0f7/2 shell has been given by

Bayman (I. 17).

A microscopic model for the (p,α) and (α,p) reactions is pre-

sented in Chapter II, including the details of the connection between

the shell model and the DWBA. The remaining chapters are devoted to

testing this theory and documenting the qualitative features of the

reaction. The experimental considerations are described in Chapter III,

with the fourth and fifth chapters being devoted to the $^{52}Cr(p,\alpha)^{49}V$

and $^{44}Ca(p,\alpha)^{41}K$ reactions. The general features are discussed and

DWBA calculations using both phenomonological cluster form factors and microscopic form factors based on simple pure configuration wavefunctions are compared to the data. Microscopic calculations using sd-shell wavefunctions are currently in progress and will be presented at a later date. These calculations are being done for the ^{26,24}Mg$(p,\alpha)^{23,21}$Na data (I.9).

Two appendices are included to help less experienced readers to understand the body of the text. The first appendix is for the general public which has supported this project. The second is a discussion of the basic reaction theory for the purpose of helping students who may wish to learn about nuclear reactions.

REFERENCES FOR CHAPTER I

I.1   Barry Preedom, Michigan State University Cyclotron Report, MSUCL-27.

I.2   B. F. Bayman, F. P. Brady, and R. Sherr, Proceedings of the Rutherford Jubilee International Conference, 553 (1962).

I.3   R. Sherr, B. F. Bayman, H. O. Funsten, N. R. Roberson, and E. Rost, Proceedings of the Conference on Direct Reaction Mechanisms, 1025 (1962).

I.4   J. A. Nolen, Jr., Ph.D. thesis, Princeton University (1965), unpublished.

I.5   J. A. Nolen, Jr., C. M. Glashausser, and M. E. Rickey, Phys. Lett. $\underline{21}$ (1966), 705.

I.6   T. Yamazaki, M. Kondo, S. Yamabe, Proceedings of the Conference on Direct Reaction Mechanisms, 1079 (1962).

I.7   W. R. Falk, A. Djaloeis, and D. Ingham, Nucl. Phys. $\underline{A252}$ (1975), 452.

1.8   K. van der Borg, R. J. deMeijer, and A. van der Woude, to be published in Nucl. Phys.

I.9   R. K. Bhomik, R. G. Markham, M. A. M. Shahabuddin, P. A. Smith, and J. A. Nolen, Jr., Bull. Am. Phys. Soc., private communication.

I.10   H. T. Fortune, P. A. Smith, J. A. Nolen, Jr., and R. G. Markham, private communication.

I.11   L. L. Lee, Jr., and J. P. Schiffer, Phys. Rev. Lett. $\underline{12}$ (1964), 108.

I.12   L. L. Lee, Jr., and J. P. Schiffer, Phys. Rev. $\underline{136B}$ (1964), 405.

I.13 L. L. Lee, Jr., A. Marinov, C. Mayer-Boricke, J. P. Schiffer, R. H. Bassel, R. M. Drisko, and G. R. Satchler, Phys. Rev. Lett. $\underline{14}$ (1965), 261.

I.14 L. S. August, P. Shapiro, and L. R. Cooper, Phys. Rev. Lett. $\underline{23}$ (1969), 537.

I.15 L. S. August, P. Shapiro, L. R. Cooper, and C. D. Bond, Phys. Rev. $\underline{C4}$ (1971), 2291.

I.16 J. E. Glenn, C. D. Zafiratos, and C. S. Zaidins, Phys. Rev. Lett. $\underline{26}$ (1971), 328.

I.17 B. F. Bayman, Nuclear Spectroscopy with Direct Reactions II, Argonne National Lab. Report ANL-6878, 335 (1964).

CHAPTER II

THEORETICAL CONSIDERATIONS

A. Introduction

The (p,α) and (α,p) reactions have been shown to proceed primarily by direct three-nucleon transfer for incident energies greater than about 17 MeV (II.1, II.2, II.3, II.4). These reactions have the attractive features of reaching nuclei and nuclear states that cannot be reached by simpler reactions. An important class of states that may be populated via these reactions are high spin states that are described by relatively simple shell model wavefunctions.

Much of the Distorted Wave Born Approximation (DWBA) analysis that has been done in previous work has employed mass three-cluster form factors (II.5, II.6, II.7). Calculations of this type can give good fits to the shapes of many angular distributions. Unfortunately, this simple model cannot produce different shapes for angular distributions for final states which have the same j^{π} value. Differences of this type have been observed in the sd-shell (II.8). Furthermore, the "spectroscopic factors" which are derived from this model are not easily related to nuclear structure models.

The first microscopic form factor model was due to Bayman and

Rost (II.9). Although this model was never published, it may be found

in Nolen's thesis (II.2) and Ginaven's thesis (II.10). This model used

harmonic oscillator single-particle wavefunctions and a technique

developed by Mang (II.11) to project out the "triton" internal and

center of mass coordinates. Nolen (II.2) used this model to study the

(p,α) reaction on Cu and Zn isotopes while Ginaven applied the model

to the (α,p) reaction on the Ca isotopes (II.10, II.12).

Nolen's analysis assumed that the two neutrons were coupled to

zero angular momentum. The j-transfer was then the total angular

momentum of the proton. This simplification was necessary because

complete wavefunctions were not available for these targets. Since

Nolen studied the same states that were strongly populated by the

$(d, {}^{3}He)$ reaction, the assumption of simple seniority wavefunctions

was probably reasonable.

The study of proton hole states by the (p,α) reaction has resulted

in models based on the seniority one assumption (II.13, II.14). It is

assumed that the three nucleon wavefunction is the product of a

di-neutron wavefunction and a proton wavefunction. The models differ

in the way that the di-neutron wavefunction is calculated.

Ginaven's calculations (II.10, II.12) went a step beyond those of

Nolen's to include the coherence in the di-neutron angular momentum

coupling. $(0f7/2)^3$ MBZ (II.15) wavefunctions were used to describe the Sc isotopes with the exception of ^{51}Sc.

A semi-microscopic model which includes coherence over intermediate couplings and configurations has been devised by Smits et al. (II.16, II.17) recently. Their method is a weak coupling model. Good agreement has been obtained with Sn(p,α) data. This model has the drawback of using mass three-cluster form factors. Thus, shape differences in the angular distributions of states with the same j^π value cannot be reproduced. Such effects are apparently weak in heavier nuclei, but may be important in lighter nuclei. In addition, the model is limited to those cases where the weak coupling assumption is appropriate.

Falk et al. (II.18, II.19) have developed a microscopic model which uses the principle of expanding single particle wavefunctions that are generated in a Woods-Saxon potential in terms of harmonic oscillator wavefunctions. The resulting oscillator wavefunctions are coupled together with a generalized Talmi transformation (II.20) to make a "triton" wavefunction. The results for the ^{12}C$(\alpha,p)^{15}$N reaction are quite good when the coherent sums over all allowed couplings are performed.

In this work we present a theory for the (p,α) and (α,p) reactions which is derived from a generalization of the Bayman and Kallio method of calculating two nucleon form factors (II.21). In the first

section the problem is formulated in terms of the single nucleon transfer theory as presented by Tamura (II.22). In the second section the spin part is separated from the spatial part of the wavefunction and the spin coupling factors that enter multi-nucleon transfer calculations are determined. In the third section harmonic oscillator single particle wavefunctions are used to rederive the theory of Bayman and Rost in a slightly different way. The fourth section shows how single particle wavefunctions generated in a Woods-Saxon well may be used. Section five is devoted to correcting for the center of mass motion in a fixed center harmonic oscillator potential. A method of deriving cluster model spectroscopic factors from microscopic considerations is given for the harmonic oscillator model in the sixth section. In section seven we show how to calculate spectroscopic amplitudes as sums of products of two nucleon spectroscopic amplitudes and single particle spectroscopic amplitudes. Sample calculations using form factors calculated with the models presented in sections three, four and five are presented in section eight. The last section is devoted to studying the features of DWBA calculations for the (p,α) reaction. Finite range calculations and zero range calculations are compared, angular momentum matching effects are investigated, and the j-dependence in the DWBA calculations is discussed.

B. Distorted Waves Formalism

Since certain factors appear in the DWBA formalism for all trans-
fer reactions, it will be useful to look at structureless cluster transfer
to display the elements of the analysis that are present for all reac-
tions. Then it will be possible to concentrate on those features which
are unique to three-nucleon transfer. To develop the cluster transfer
formalism, we borrow the elegant treatment of Tamura (II.22).

The transition matrix element from a particular initial state to a
particular final state is

$$T_{M_B m_b M_A m_a} = \oint \sum_{m_b' m_a'} \int dr_a \, dr_b \, \chi^{(-)}_{m_b' m_b} (k_b, r_b)$$

$$\langle I_B M_B s_b m_b' | V | I_A M_A s_a m_a' \rangle \, \chi^{(+)}_{m_a' m_a} (k_a, r_a) \qquad \text{II.1}$$

if spin-orbit coupling is present in both the entrance and exit channels
Table II.1 contains a list of the notation used in this work.

The coordinates for a pick-up reaction are shown in Figure II.1.
The internal matrix in Equation II.1 is an integral over the coordinates
ξ_B, ξ_x, and ξ_a which can be factored if the interaction is assumed to
act between the center of masses of a and x.

$$\langle I_B M_B s_b m_b' | V | I_A M_A s_a m_a' \rangle = \int \langle I_B M_B | I_A M_A \rangle$$

$$\langle s_b m_b' | V(r_2) | s_a m_a' \rangle d\xi_x. \qquad \text{II.2}$$

The first matrix element under the integral in Equation II.2 is an inte-
gral over ξ_B and the second is an integral over ξ_a, so that both are

Figure II. 1

Coordinates for cluster pick-up.
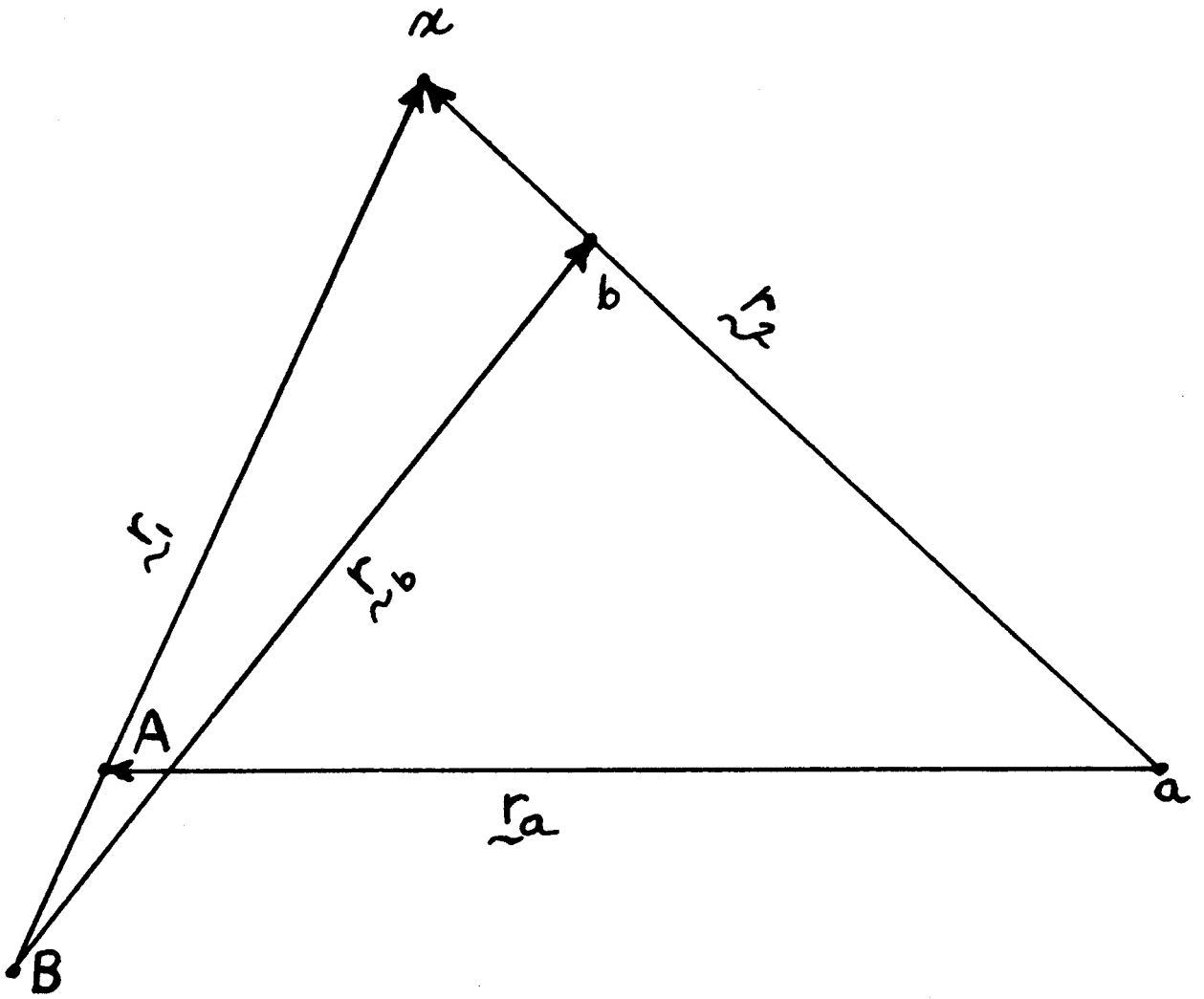
Figure II. 1

TABLE II.1

A LIST OF SYMBOLS

Symbol	Explanation
a, b, x, A, B	Projectile, ejectile, transferred cluster, target, final nucleus
$\mathcal{J}$	Jacobian for transforming to relative coordinates
$\underset{\sim}{r}_a, \underset{\sim}{r}_b$	Relative coordinates for the aA and Bb systems (See Figure II.1)
$\underset{\sim}{k}_a, \underset{\sim}{k}_b$	Incoming and outgoing wave vectors
$\chi_{m'm}^{(\pm)}(\underset{\sim}{k}, r)$	Optical wavefunction including spin-orbit coupling
I_B, I_A	Spins of the residual and target nuclei
M_B, M_A	Magnetic substates for I_B and I_A
s_b, s_a	Spins of the ejectile and projectile
m_b, m_a	Magnetic substates for s_b, s_a
ξ's	Internal coordinates for the target nucleons relative to an origin located at the center of the core (See Figure II.2)
$C_{n_1 \mathcal{L}_1 s_x \alpha_x j}^{(A)}$	Expansion coefficient for the decomposition of the target wavefunction in terms of a core and a cluster with quantum numbers $(n_1, \mathcal{L}_1, s_x, \alpha_x, j)$
φ	Wavefunctions—superscripts denote angular momentum—subscripts are for magnetic substates or principle quantum number

TABLE II.1—Continued

Symbol	Explanation
$\left[\varphi^{\mathcal{L}_1}(\underset{\sim}{r}_1)\varphi^{s_x}(\xi_x)\right]^j_{m_j}$	Angular momentum vector coupling $$\left[\varphi^{\mathcal{L}_1}(\underset{\sim}{r}_1)\varphi^{s_x}(\xi_x)\right]^j_{m_j} =$$ $$= \sum_{m_1 m_x} (\mathcal{L}_1 m_1 s_x \mid j\, m_j)$$ $$\cdot\, \varphi^{\mathcal{L}_1}_{m_1}(\underset{\sim}{r}_1)\varphi^{s_x}_{m_x}(\xi_x)$$
$(j_1 m_1 j_2 m_2 \mid j_3 m_3)$	Vector coupling (Clebsch-Gordon) coefficients
$\underset{\sim}{\ell},\ \underset{\sim}{s},\ \underset{\sim}{j}$	Orbital angular momentum transfer, spin transfer, total angular momentum transfer $\underset{\sim}{j} = \underset{\sim}{\ell} + \underset{\sim}{s}$
n	Principle quantum number (oscillator convention)
$\underset{\sim}{r}_1,\underset{\sim}{r}_2$	Separation of the cluster from the residual nucleus and projectile (See Figure II.1)
α,β	Oscillator size parameters for target and α-particle
$C^{(b)}_{n_2 \mathcal{L}_2 s'_x \alpha'_x s}$	Expansion coefficient for decomposition of the ejectile in terms of the projectile plus cluster
s'_x, α'_x	Spin and other quantum numbers of the cluster when part of the ejectile (not necessarily the same as s_x, α_x)
$\varphi^{\widetilde{\mathcal{L}}_2}_{m_2}$	$\sim$ indicates time reversal conjugation $$\varphi^{\widetilde{\mathcal{L}}_2}_{m_2} = (-1)^{\mathcal{L}_2 - m_2}\varphi^{\mathcal{L}_2}_{-m_2}$$ and $(j_1 m_1 j_2 m_2 \mid j_3 \widetilde{m}_3) = (-1)^{j_3 - m_3}$ $$\cdot (j_1 m_1 j_2 m_2 \mid j_3 -m_3)$$
$d^{j\ell s}$	Spectroscopic amplitude for a $j\ell s$-transfer

TABLE II.1—<u>Continued</u>

Symbol	Explanation
$f^{\mathcal{L}_1 n_1 \, \mathcal{L}_2 n_2}_{\ell m_\ell}(\underline{r}_1, \underline{r}_2)$	Finite range form factor
$W(\mathcal{L}_1 \mathcal{L}_2 js; \ell s_x)$	Racah coefficient related to 6-j symbol by $$(\mathcal{L}_1 \mathcal{L}_2 js; \ell s_x) = (-1)^{\mathcal{L}_1 + \mathcal{L}_2 + j + s}$$ $$\begin{Bmatrix} \mathcal{L}_1 & \mathcal{L}_2 & \ell \\ j & s & s_x \end{Bmatrix}$$
$\{n_i \, \ell_i \, j_i\}$	Set of quantum numbers which describe the single particle orbits
$\ell_{12}, \, s_{12}, \, j_{12}$	Di-neutron angular momentum couplings
$\begin{bmatrix} \ell_1 & \ell_2 & \ell_{12} \\ s_1 & s_2 & s_{12} \\ j_1 & j_2 & j_{12} \end{bmatrix}$	Transformation coefficients for changing j-s to ℓ-s coupling— related to -j symbols by $$\begin{bmatrix} \ell_1 & \ell_2 & \ell_{12} \\ s_1 & s_2 & s_{12} \\ j_1 & j_2 & j_{12} \end{bmatrix} =$$ $$= \sqrt{(2\ell_{12}+1)(2s_{12}+1)(2j_1+1)(2j_2+1)}$$ $$\begin{Bmatrix} \ell_1 & \ell_2 & \ell_{12} \\ s_1 & s_2 & s_{12} \\ j_1 & j_2 & j_{12} \end{Bmatrix}$$
$C^{(A)}_{\{n_i \ell_i j_i\}\ell_{12} \alpha_x j}$	Expansion coefficient for decomposing the target wavefunction into a core and three nucleons with quantum numbers $\{n_i \ell_i j_i\}\ell_{12}\alpha_x j$
χ^s	Spin functions

TABLE II.1—Continued

Symbol	Explanation
$\left\langle \begin{array}{cc\|cc} n_1 & \ell_1 & \nu_1 & \lambda_1 \\ n_2 & \ell_2 & \nu_2 & \lambda_2 \\ & \ell_{12} & & \lambda_{12} \\ n_3 & \ell_3 & \nu_3 & \lambda_3 \end{array} \right\rangle$	Transformation coefficient for changing from nuclear coordinates to internal and center of mass coordinates (See Figure II.2) ν's and λ's are the principle quantum numbers and angular momenta in the transformed coordinates
$\langle n_1\ell_1 n_2\ell_2 : \ell_{12} \mid (n'-\nu_2)\ell_{12}\nu_2 0 : \ell_{12} \rangle_{11}$	Transformation coefficient to relative and center of mass coordinates for the di-neutron
$\langle (n'-\nu_2)\ell_{12} n_3\ell_3 : \ell \mid \nu_1\ell_1\nu_3 0 : \ell \rangle_{21}$	Transformation coefficient from the di-neutron C.M. and proton to triton C.M. and internal coordinates.
$f^{\ell_{12}}_{\lambda_{12},\Lambda}$	Transformation coefficient for transforming two nucleon coordinates to relative and C.M. coordinates in a Woods-Saxon well
$\zeta, \underline{r}_t$	Internal coordinates in a fixed center potential
T's	Isospin quantum numbers
N's	z projection of T's ($N=+\frac{1}{2}$ for a proton)
$\mathcal{A}$	Antisymmeterizer
(‖ ‖)	Reduced matrix element—reduced in spin only
(Ⅱ Ⅱ)	Reduced matrix element—reduced in spin and isospin

functions of ξ_x. The core may be integrated away if the target is expanded in terms of a core plus the transferred nucleon cluster. Thi[s] procedure yields:

$$\langle I_B M_B | I_A M_A \rangle = \sum_{\substack{n_1 \mathcal{L}_1 j \\ s_x \alpha_x}} C^{(A)}_{n_1 \mathcal{L}_1 s_x \alpha_x j} \left(I_B M_B j m_j | I_A M_A \right) \left[\varphi^{\mathcal{L}_1}_{n_1}(r_1) \varphi^{s_x}_{\alpha_x}(\xi_x) \right]^j \qquad \text{II}[.3]$$

where α_x represents other quantum numbers that may be used to describe the cluster. It is in Equation II.3 that the structureless clus[ter] ter assumption has been realized by separating the center of mass coordinate from the internal "triton" coordinates. We will return to this point later.

The ejectile can also be expanded as a projectile core plus the transferred group.

$$\langle s_b m_b' | V(r_2) | s_a m_a' \rangle = \sum_{\substack{n_2 \mathcal{L}_2 s \\ s_x \alpha_x}} C^{(b)}_{n_2 \mathcal{L}_2 s_x \alpha_x s} \left(s_b m_b' s m_s | s_a m_a' \right) \left[\tilde{\Phi}^{\tilde{\mathcal{L}}_2}_{n_2}(r_2) \varphi^{s_x}_{\alpha_x}(\xi_x) \right]$$

$$\text{II}[.4]$$

where

$$\Phi^{\tilde{\mathcal{L}}_2}_{n_2}(r_2) = V(r_2) \varphi^{\tilde{\mathcal{L}}_2}_{n_2}(r_2) \qquad \text{II}[.5]$$

and $\sim$ denotes time reversal conjugation (see Table II.1). $\Phi^{\tilde{\mathcal{L}}_2}_{n_2}(r_2)$ contains the separation of the projectile from the cluster center of mas[s]. If this function is not taken to be a delta function (zero range approxi-mation), then the six-dimensional finite range integral must be per-formed (Equation II.1).

If the results of Equations II.3 and II.4 are used in Equation II.2 and, at the same time, we change to l-s coupling, the transition matrix element for pick-up is seen to be

$$\langle I_B M_B s_b m'_b | V(\underset{\sim}{r}_2) | I_A M_A s_a m'_a \rangle = \sum_{j\ell s} \left\{ \sum_{\mathcal{L}_1 n_1 \mathcal{L}_2 n_2} d^{j\ell s}_{\mathcal{L}_1 n_1 \mathcal{L}_2 n_2} f^{\mathcal{L}_1 n_1 \mathcal{L}_2 n_2}_{\ell m_\ell}(\underset{\sim}{r}_1, \underset{\sim}{r}_2) \right\}$$

$$\cdot (-1)^{I_B + s_a + j + 2s + m_s - m'_b - M_A}(2s+1)(2I_B+1)(I_A M_A I_B - M_B | jm_j)$$

$$\cdot (s_a m'_a s_b - m'_b | sm_s)(jm_j sm_s | \ell - m_\ell). \qquad \text{II.6}$$

The quantities $d^{j\ell s}_{\mathcal{L}_1 n_1 \mathcal{L}_2 n_2}$ and $f^{\mathcal{L}_1 n_1 \mathcal{L}_2 n_2}_{\ell m_\ell}(\underset{\sim}{r}_1, \underset{\sim}{r}_2)$ are defined to be

$$d^{j\ell s}_{\mathcal{L}_1 n_1 \mathcal{L}_2 n_2} = \sum_{s_x \alpha_x} C^{(A)}_{n_1 \mathcal{L}_1 s_x \alpha_x j} C^{(b)}_{n_2 \mathcal{L}_2 s_x \alpha_x s}(-1)^{s + \mathcal{L}_2 - s_x} W(\mathcal{L}_1 \mathcal{L}_2 js; \ell s_x) \qquad \text{II.7}$$

and

$$f^{\mathcal{L}_1 n_1 \mathcal{L}_2 n_2}_{\ell m_\ell}(\underset{\sim}{r}_1, \underset{\sim}{r}_2) = \left[\varphi^{\mathcal{L}_1}_{n_1}(\underset{\sim}{r}_1) \Phi^{\mathcal{L}_2}_{n_2}(\underset{\sim}{r}_2) \right]^{\tilde{\ell}}. \qquad \text{II.8}$$

Because expression II.6 is exact, these are complicated looking equations. The meaning of $d^{j\ell s}_{\mathcal{L}_1 n_1 \mathcal{L}_2 n_2}$ and $f^{\mathcal{L}_1 n_1 \mathcal{L}_2 n_2}_{\ell m_\ell}(\underset{\sim}{r}_1, \underset{\sim}{r}_2)$ becomes clearer if we look briefly at their zero range cousins for, say, the (p,d) reaction. Under these conditions

$$n_2 = 0; \quad \mathcal{L}_2 = 0; \quad \mathcal{L}_1 = \ell; \quad C^{(b)}_{n_2 \mathcal{L}_2 s_x \alpha_x s} = 1;$$

$$W(\mathcal{L}_1 \mathcal{L}_2 js; \ell s_x) = 1$$

and $d^{j\ell s}_{\mathcal{L}_1 n_1 \mathcal{L}_2 n_2}$ is seen to reduce to a single spectroscopic amplitude. $f^{\mathcal{L}_1 n_1 \mathcal{L}_2 n_2}_{\ell m_\ell}(\underset{\sim}{r}_1, \underset{\sim}{r}_2)$ reduces to the usual form factor

$$f^{\ell m_1}_{\ell m_\ell}(\underset{\sim}{r}_1, \underset{\sim}{r}_2) = \varphi^{\ell}_{n_1}(\underset{\sim}{r}_1) V(r_2) \varphi_\alpha(\underset{\sim}{r}_2) \cong D_o \delta(\underset{\sim}{r}_2) \varphi^{\ell}_{n_1}(\underset{\sim}{r}_1).$$

Since our particular interest is the (p,α) reaction, we will now write Equations II.6, II.7, and II.8 again in the specific form that applies to "triton" transfer.

For (p,α) we must have

$$\mathcal{L}_2 = 0; \quad \mathcal{L}_1 = \ell; \quad s = \tfrac{1}{2}; \quad C^{(b)}_{n_2 \mathcal{L}_2 s_x \alpha_x s} =$$

$$W(\mathcal{L}_1 \mathcal{L}_2 js; \ell s_x) = 1.$$

These conditions imply

$$\langle I_B M_B s_b m'_b | V | I_A M_A s_a m'_a \rangle = \sum_{j\ell} \left\{ \sum_{n_1} d^{j\ell\frac{1}{2}}_{n_1} f^{\ell n_1}_{\ell m_\ell} (\underset{\sim}{r}_1, \underset{\sim}{r}_2) \right\}$$

$$\cdot (-1)^{I_B + (3/2) + j + m_s - M_A} 2(2I_B + 1)(I_A M_A I_B - M_B | jm_j)(jm_j \tfrac{1}{2} m_a | \ell - m_\ell) \qquad \text{II.6a}$$

$$d^{j\ell s}_{n_1} = 2 \sum_{\alpha_x} C^{(A)}_{n_1 \ell \frac{1}{2} \alpha_x j} \qquad \text{II.7a}$$

$$f^{\ell n_1}_{\ell m_\ell} (\underset{\sim}{r}_1, \underset{\sim}{r}_2) = \varphi^{\tilde{\ell}}_{n_1} (\underset{\sim}{r}_1) \Phi^o_o (\underset{\sim}{r}_2) . \qquad \text{II.8a}$$

The quantity on which we need to concentrate in the future is the quantity in brackets { } in Equation II.6. We will not specify whether the zero range approximation is being made or not. Instead, the function $\Phi^o_o (\underset{\sim}{r}_2)$ will be carried along through all steps.

C. Decomposition of the Orbital and Spin Parts

In the last section we saw that all the reaction information is contained in the quantities $d^{j\ell s}$ and $f_{\ell m_\ell} (\underset{\sim}{r}_1, \underset{\sim}{r}_2)$. The function $f_{\ell m_\ell} (\underset{\sim}{r}_1, \underset{\sim}{r}_2)$ contains only the spatial parts of the wavefunctions. In order to isolate $f_{\ell m_\ell} (\underset{\sim}{r}_1, \underset{\sim}{r}_2)$ for the (p,α) reaction we must, therefore, separate the spin and orbital angular momenta of the wavefunctions that are involved. If k nucleons are involved, there will be (k-1) 9-j

symbols which come from the transformation from j-j coupling to l-s coupling.

We show this for the (p,α) reaction by making the expansion of the target wavefunction (Equation II.3) again

$$\langle I_B M_B | I_A M_A \rangle = \sum_{\substack{\{n_i \ell_i j_i\} \\ j_{12}\alpha_x j}} C^{(A)}_{\substack{\{n_i \ell_i j_i\} \\ j_{12}\alpha_x j}} \varphi^{\{(j_1 j_2)^{j_{12}} j_3\}^j}_{\substack{(\xi_1 \xi_2 \xi_3) \\ \{n_i \ell_i j_i\}}} (I_B M_B jm_j | I_A M_A). \qquad \text{II.3a}$$

The difference between Equations II.3 and II.3a is that some of the quantum numbers that were previously part of α_x have been written explicitly and (ξ_x, r_1) have been replaced by (ξ_1, ξ_2, ξ_3).

The change to l-s coupling is accomplished by

$$\varphi^{\{(j_1 j_2)^{j_{12}} j_3\}^j}_{\substack{(\xi_1 \xi_2 \xi_3) \\ \{n_i \ell_i j_i\}\alpha_x}} = \sum_{\substack{\ell_{12} s_{12} \\ \ell}} \begin{bmatrix} \ell_{12} & \ell_3 & \ell \\ s_{12} & \frac{1}{2} & \frac{1}{2} \\ j_{12} & j_3 & j \end{bmatrix} \begin{bmatrix} \ell_1 & \ell_2 & \ell_{12} \\ \frac{1}{2} & \frac{1}{2} & s_{12} \\ j_1 & j_2 & j_{12} \end{bmatrix}$$

$$\begin{bmatrix} \varphi^{\{(\ell_1 \ell_2)^{\ell_{12}} \ell_3\}^{\ell}}_{\substack{(\xi_1 \xi_2 \xi_3) \\ \{n_i \ell_i j_i\}}} & X & \{(\tfrac{1}{2} \tfrac{1}{2})^{s_{12}} \tfrac{1}{2}\}^s \end{bmatrix}^j \qquad \text{II.9}$$

Choose particles 1 and 2 to be the two neutrons. Since they must go into the 0s orbit in the α-particle, the Pauli principle requires $s_{12}=0$ and $j_{12}=\ell_{12}$. Using these conditions and Equation II.9 in the expression for $\langle I_B M_B | I_A M_A \rangle$ gives

$$\langle I_B M_B | I_A M_A \rangle = \sum_{\substack{\{n_i \ell_i j_i\} \\ \ell_{12}\alpha_x j\ell}} C^{(A)}_{\substack{\{n_i \ell_i j_i\} \\ \ell_{12}\alpha_x j}} \begin{bmatrix} \ell_{12} & \ell_3 & \ell \\ 0 & \frac{1}{2} & \frac{1}{2} \\ \ell_{12} & j_3 & j \end{bmatrix} \begin{bmatrix} \ell_1 & \ell_2 & \ell_{12} \\ \frac{1}{2} & \frac{1}{2} & 0 \\ j_1 & j_2 & \ell_{12} \end{bmatrix}$$

$$\cdot (I_B M_B j m_j | I_A M_A) \begin{bmatrix} \{(\ell_1 \ell_2)^{\ell_{12}} \ell_3\}^{\ell} & \{(\tfrac{1}{2}\tfrac{1}{2})^0 \tfrac{1}{2}\} \\ \varphi_{(\xi_1 \xi_2 \xi_3)} & X \\ \{n_i \ell_i j_i\} & \end{bmatrix}^j . \quad \text{II.10}$$

Comparing Equations II.10 and II.3, we see that they have the same form except for the recoupling terms. Therefore, the term in brackets in Equation II.6a can be written as

$$\sum_{\substack{\{n_i \ell_i j_i\} \\ \ell_{12}}} d^{j\ell\frac{1}{2}}_{\substack{\{n_i \ell_i j_i\} \\ \ell_{12}}} f^{\{n_i \ell_i j_i\}}_{\ell m_\ell} (\underset{\sim}{r}_1, \underset{\sim}{r}_2) . \quad \text{II.11}$$

The spectroscopic amplitude is given by

$$d^{j\ell\frac{1}{2}}_{\substack{\{n_i \ell_i j_i\} \\ \ell_{12}}} = \sum_{\alpha_x} C^{(A)}_{\substack{\{n_i \ell_i j_i\} \\ \ell_{12}\alpha \, j}} \begin{bmatrix} \ell_{12} & \ell_3 & \ell \\ 0 & \frac{1}{2} & \frac{1}{2} \\ \ell_{12} & j_3 & j \end{bmatrix} \begin{bmatrix} \ell_1 & \ell_2 & \ell_{12} \\ \frac{1}{2} & \frac{1}{2} & 0 \\ j_1 & j_2 & \ell_{12} \end{bmatrix} . \quad \text{II.12}$$

In order to write an expression for $f^{\{n_i \ell_i j_i\}}_{\ell m_\ell} (\underset{\sim}{r}_1, \underset{\sim}{r}_2)$, it is necessary to choose a wavefunction for the α-particle. We make the following Gaussian choice

$$\varphi = \eta e^{-\beta/2 (\rho_{12}^2 + \rho_{123}^2 + a r_z^2)}$$

where ρ_{12} and ρ_{123} are related to $\underset{\sim}{r}_{12}$ and $\underset{\sim}{r}_{123}$, which are the "triton" internal coordinates that are shown in Figure II.2. This choice allows some of the overlap integrals to be done analytically in the oscillator model.

Figure II. 2

Nucleon coordinates in the target nucleus.
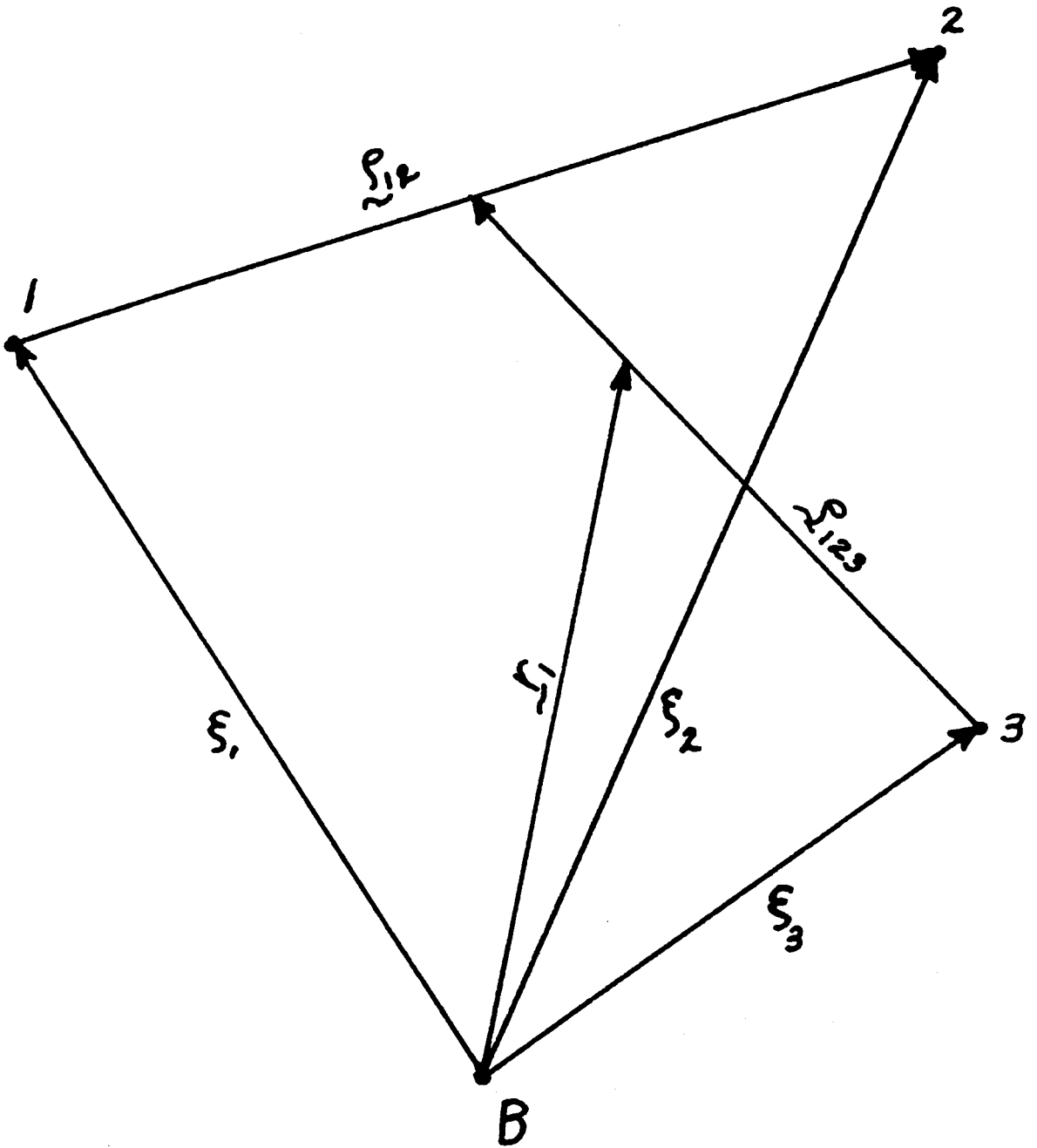
Figure II.2

Using this choice gives

$$f_{\ell m_\ell}^{\{n_i \ell_i j_i\}\ell_{12}}(\underset{\sim}{r}_1, \underset{\sim}{r}_2) = \eta \Phi_o^o(\underset{\sim}{r}_2) \int \varphi_{(\xi_1\xi_2\xi_3)}^{\{(\ell_1\ell_2)^{\ell_{12}}\ell_3\}^\ell} e^{-\beta/2(\rho_{12}^2 + \rho_{123}^2)} d\underset{\sim}{\rho}_{12} d\underset{\sim}{\rho}_{123}.$$

$$\{n_i \ell_i j_i\}$$

II.13

$\underset{\sim}{r}_1$ is not explicitly shown on the right hand side of Equation II.13 because (ξ_1, ξ_2, ξ_3) must still be transformed to $(\underset{\sim}{\rho}_{12}, \underset{\sim}{\rho}_{123}, \underset{\sim}{r}_1)$. This is the subject of the next three sections.

D. The (p, α) Form Factor: Harmonic Oscillator Model

In order to reduce the right hand side of Equation II.13 to a function of $(\underset{\sim}{r}_1, \underset{\sim}{r}_2)$, the nuclear coordinates (ξ_1, ξ_2, ξ_3) must be transformed to center of mass and internal coordinates $(\underset{\sim}{\rho}_{12}, \underset{\sim}{\rho}_{123}, \underset{\sim}{r}_1)$ (see Figure II.2).

The function $\varphi_{(\xi_1, \xi_2, \xi_3)\alpha_x}^{\{(\ell_1\ell_2)^{\ell_{12}}\ell_3\}^\ell}$ may be written in the anti-symmetric form

$$\varphi_{(\xi_1\xi_2\xi_3)\{n_i\ell_ij_i\}\alpha_x}^{\{(\ell_1\ell_2)^{\ell_{12}}\ell_3\}^\ell} = \frac{\left\{\left[\varphi_{n_1}^{\ell_1 j_1}(\xi_1)\varphi_{n_2}^{\ell_2 j_2}(\xi_2) - \varphi_{n_1}^{\ell_1 j_1}(\xi_2)\varphi_{n_2}^{\ell_2 j_2}(\xi_1)\right]^{\ell_{12}}\varphi_{n_3}^{\ell_3 j_3}(\xi_3)\right\}^\ell}{\sqrt{2(1 + \delta_{n_1 n_2}\delta_{\ell_1 \ell_2}\delta_{j_1 j_2})}}$$

II.14

where the convention that particles 1 and 2 are the neutrons is used.

In this section the single particle wavefunctions are taken to be harmonic oscillator wavefunctions.

We need to determine the expansion coefficients defined by Equation II.15

$$\frac{\left\{\left[\varphi_{n_1}^{\ell_1 j_1}(\xi_1)\varphi_{n_2}^{\ell_2 j_2}(\xi_2) - \varphi_{n_1}^{\ell_1 j_1}(\xi_2)\varphi_{n_2}^{\ell_2 j_2}(\xi_1)\right]^{\ell_{12}}\varphi_{n_3}^{\ell_3 j_3}(\xi_3)\right\}^{\ell}}{\sqrt{2(1+\delta_{n_1 n_2}\delta_{\ell_1 \ell_2}\delta_{j_1 j_2})}}$$

$$= \sum_{\substack{\lambda_1 \nu_1 \lambda_2 \nu_2 \\ \lambda_3 \nu_3 \Lambda}} \left\langle \begin{array}{cc|cc} \nu_1 & \lambda_1 & n_1 & \ell_1 \\ \nu_2 & \lambda_2 & n_2 & \ell_2 \\ & \Lambda & & \ell_{12} \\ \nu_3 & \lambda_3 & n_3 & \ell_3 \end{array} \right\rangle \frac{\left[\varphi_{\nu_1}^{\lambda_1}(\underset{\sim}{r}_1)\varphi_{\nu_2 \nu_3}^{(\lambda_2 \lambda_3)\Lambda}(\underset{\sim}{\rho}_{12},\underset{\sim}{\rho}_{123})\right]^{\ell}}{\sqrt{2(1+\delta_{n_1 n_2}\delta_{\ell_1 \ell_2}\delta_{j_1 j_2})}} \qquad \text{II.1}$$

where

$$\sum_{i=1}^{3}(2n_i + \ell_i) = \sum_{i=1}^{3}(2\nu_i + \lambda_i) = N \qquad \text{II.1}$$

is required to conserve oscillator quanta.

The transferred "triton" should have zero internal angular momen-
tum if it is to fit into the α-particle. This condition implies that only
the terms with $\lambda_1 = 0$, $\lambda_2 = 0$, and $\Lambda = 0$ should be saved. Terms with
nonzero ν_2 and ν_3 need not be zero, however. If the size parameter
of the α-particle (β) is different from the size parameter of the target
wavefunctions (α), there will be nonzero overlaps for the $\nu_2, \nu_3 \neq 0$
terms. Equation II.15 may be written again including these conditions.

$$\mathbb{P}\left\{\left[\varphi_{n_1}^{\ell_1 j_1}(\xi_1)\varphi_{n_2}^{\ell_2 j_2}(\xi_2) - \varphi_{n_1}^{\ell_1 k_1}(\xi_2)\varphi_{n_2}^{\ell_2 j_2}(\xi_1)\right]^{\ell_{12}}\varphi_{n_3}^{\ell_3 j_3}(\xi_3)\right\}^{\ell}$$

$$= \sum_{\nu_1 \nu_2 \nu_3} \left\langle \begin{array}{cc|cc} \nu_1 & \ell & n_1 & \ell_1 \\ \nu_2 & 0 & n_2 & \ell_2 \\ & 0 & & \ell_{12} \\ \nu_3 & 0 & n_3 & \ell_3 \end{array} \right\rangle \varphi_{\nu_1}^{\ell}(\underset{\sim}{r}_1)\varphi_{\nu_2 \nu_3}^{(00)0}(\underset{\sim}{\rho}_{12},\underset{\sim}{\rho}_{123})$$

$$\text{II.15a}$$

where $\mathbb{P}$ is a projection operator that picks out the portion of the wave-
function that has nonzero overlap with $e^{-\beta/2(\rho_{12}^2+\rho_{123}^2)}$.

It is our goal to relate these expansion coefficients to Talmi-Moshinsky coefficients. Proceed by examining the two-nucleon part of the wavefunction

$$\left[\varphi^{\ell_1 j_1}_{n_1}(\xi_1)\varphi^{\ell_2 j_2}_{n_2}(\xi_2) - \varphi^{\ell_1 j_1}_{n_1}(\xi_2)\varphi^{\ell_2 j_2}_{n_2}(\xi_1)\right]^{\ell_{12}} = 2\sum_{\substack{\lambda_R \nu_R \\ \lambda_{12}\nu_2}}$$

$$\cdot \langle \nu_R \lambda_R \nu_{12}\lambda_{12}:\ell_{12} | n_1\ell_1 n_2\ell_2:\ell_{12}\rangle_{11} \left[\varphi^{\lambda_R}_{\nu_R}(\underset{\sim}{R})\varphi^{\lambda_{12}}_{\nu_2}(\underset{\sim}{\rho}_{12})\right]^{\ell_{12}}_{N'} \quad \text{II.17}$$

where

$$N' = (N - n) + \frac{(\ell-\ell_3-\ell_{12})}{2}$$

$$\nu_R = N' - \nu_2 . \qquad \text{II.18}$$

The $\langle n_1\ell_1 n_2\ell_2:\ell_{12} | \nu_R \lambda_R \nu_{12}\lambda_{12}:\ell_{12}\rangle_{11}$ are the normal Talmi-Moshinsky transformation coefficients for equal mass particles. The subscripts 11 denote that the masses involved are both single nucleon masses.

The vector $\underset{\sim}{R}$ runs from the center of the core (B) to the center of mass of the di-neutron. The condition that there be no internal angular momentum implies that $\lambda_{12}=0$ and $\lambda_R=\ell_{12}$.

This result may be inserted into the left hand side of Equation II.15a to get

$$2 \sum_{\nu_2} \langle (N'-\nu_2)\ell_{12}\nu_2 0:\ell_{12} | n_1\ell_1 n_2\ell_2:\ell_{12} \rangle_{11} \left[\varphi^{\ell_{12}}_{(N'-\nu_2)}(\underset{\sim}{R})\varphi^{\circ}_{\nu_2}(\underset{\sim}{\rho}_{12})\varphi^{\ell_3 j_3}_{n_3}(\xi_3) \right]^\ell$$

$$= \sum_{\nu_1\nu_2\nu_3} \left\langle \begin{matrix} \nu_1 & \ell & \vline & n_1 & \ell_1 \\ \nu_2 & 0 & \vline & n_2 & \ell_2 \\ & 0 & \vline & & \ell_{12} \\ \nu_3 & 0 & \vline & n_3 & \ell_3 \end{matrix} \right\rangle \varphi^\ell_{\nu_1}(r_1)\varphi^{(00)\circ}_{\nu_2\nu_3}(\underset{\sim}{\rho}_{12},\underset{\sim}{\rho}_{123}). \quad \text{II.19}$$

The function in brackets on the left hand side of Equation II.19 can be expanded in a similar way

$$\varphi^{\circ}_{\nu_2}(\rho_{12})\left[\varphi^{\ell_{12}}_{(N'-\nu_2)}(\underset{\sim}{R})\varphi^{\ell_3 j_3}_{n_3}(\xi_3) \right]^\ell = \sum_{\substack{\lambda_1\nu_1 \\ \lambda_3\nu_3}}$$

$$\cdot \langle \nu_1\lambda_1\nu_3\lambda_3:\ell | (N'-\nu_2)\ell_{12}n_3\ell_3:\ell \rangle_{21} \varphi^{\circ}_{\nu_2}(\underset{\sim}{\rho}_{12})\left[\varphi^{\lambda_1}_{\nu_1}(\underset{\sim}{r}_1)\varphi^{\lambda_3}_{\nu_3}(\underset{\sim}{\rho}_{123}) \right]^\ell.$$

$$\text{II.20}$$

The subscripts 21 denote that the mass on the left hand side of the bracket is two nucleon masses while the right hand side is for a single nucleon. Again the requirement of zero internal angular momentum can be applied so that $\lambda_3 = 0$ and $\lambda_1 = \ell$.

Using Equation II.20 in Equation II.19 yields the relation

$$\left\langle \begin{matrix} \nu_1 & \ell & \vline & n_1 & \ell_1 \\ \nu_2 & 0 & \vline & n_2 & \ell_2 \\ & 0 & \vline & & \ell_{12} \\ \nu_3 & 0 & \vline & n_3 & \ell_3 \end{matrix} \right\rangle = 2 \langle (N'-\nu_2)\ell_{12}\nu_2 0:\ell_{12} | n_1\ell_1 n_2\ell_2:\ell_{12} \rangle_{11}$$

$$\cdot \langle \nu_1\ell\nu_3 0:\ell | (N'-\nu_2)\ell_{12}n_3\ell_3:\ell \rangle_{21}. \quad \text{II.21}$$

The $\langle | \rangle_{21}$ coefficient is the Talmi-Moshinsky transformation for a mass two particle and a mass one particle (II.20).

We may use Equation II.21 in Equation II.15a and then insert the result in Equation II.13 to yield

$$f_{\ell m_\ell}^{\{n_i \ell_i j_i\}}(\underset{\sim}{r}_1, \underset{\sim}{r}_2) = \frac{2\eta}{\sqrt{2(1+\delta_{n_1 n_2}\delta_{\ell_1 \ell_2}\delta_{j_1 j_2})}} \sum_{\nu_1 \nu_2 \nu_3}$$

$$\cdot \langle (N'-\nu_2)\ell_{12}\nu_2 0 : \ell_{12} | n_1 \ell_1 n_2 \ell_2 : \ell_{12} \rangle_{11}$$

$$\cdot \langle \nu_1 \ell \nu_3 0 : \ell | (N'-\nu_2)\ell_{12} n_3 \ell_3 : \ell \rangle_{21} \; \varphi_{\nu_1}^{\ell}(\underset{\sim}{r}_1) \Phi_0^0(\underset{\sim}{r}_2)$$

$$\left(\int \varphi_{\nu_2}^0(\underset{\sim}{\rho}_{12}) \varphi_{\nu_3}^0(\underset{\sim}{\rho}_{123}) e^{-\beta/2(\rho_{12}^2 + \rho_{123}^2)} d\underset{\sim}{\rho}_{12} \, d\underset{\sim}{\rho}_{123} \right). \quad \text{II.22}$$

The integral in parentheses in Equation II.22 can be factored into two integrals of the form

$$I = \int \varphi_\nu^0(\rho) e^{-\beta/2 \, \rho^2} \rho^2 d\rho . \quad \text{II.23}$$

This integral can be done analytically if we use the oscillator function

$$\varphi_\nu^0(\rho) = \sqrt{\frac{2^{2-\nu}(2\nu+1)!!\,\alpha^{3/2}}{\sqrt{\pi}\;\nu!}} \sum_{\kappa=0}^{\nu} \left\{ \frac{(-2\alpha)^\kappa}{(2\kappa+1)!!} \binom{\nu}{\kappa} \rho^{2\kappa} \right\} e^{-\alpha/2 \, \rho^2} . \quad \text{II.24}$$

The result is

$$I = \pi^{\frac{1}{4}} \sqrt{\frac{(2\nu+1)!!}{\nu!\;2^\nu}} \; \frac{\alpha^{3/4}}{(\beta+\alpha)^{3/2}} \left(\frac{\beta-\alpha}{\beta+\alpha} \right)^\nu . \quad \text{II.25}$$

Equation II.22 may now be written

$$f_{\ell m_\ell}^{\{n_i \ell_i j_i\}}(\underset{\sim}{r}_1, \underset{\sim}{r}_2) = \frac{2\eta}{\sqrt{2(1+\delta_{n_1 n_2}\delta_{\ell_1 \ell_2}\delta_{j_1 j_2})}} \sum_{\nu_1 \nu_2 \nu_3}$$

$$\cdot \langle (N'-\nu_2)\ell_{12}\nu_2 0 : \ell_{12} | n_1 \ell_1 n_2 \ell_2 : \ell_{12} \rangle_{11}$$

$$\cdot \langle \nu_1 \ell \nu_3 0 : \ell | (N'-\nu_2)\ell_{12} n_3 \ell_3 : \ell \rangle_{21} \; A_{\nu_2 \nu_3} \; \varphi_{\nu_1}^\ell(\underset{\sim}{r}_1) \Phi_0^0(\underset{\sim}{r}_2)$$

$$\text{II.22a}$$

where

$$A_{\nu_2\nu_3} = \pi^{\frac{1}{2}} \sqrt{\frac{(2\nu_2+1)!!\,(2\nu_3+1)!!}{\nu_2!\,\nu_3!\quad 2^{\nu_2+\nu_3}}}\;\; \frac{\alpha^{3/2}}{(\beta+\alpha)^3}\left(\frac{\beta-\alpha}{\beta+\alpha}\right)^{\nu_2+\nu_3}. \qquad \text{II.26}$$

The last result is very similar to one obtained by Bayman and Rost (II.9). It is purely a result of allowing the oscillator size parameters for the α-particle and the target to be different. If $\alpha = \beta$, ν_2 and ν_3 must be zero and the problem is easily simplified.

A recipe for the harmonic oscillator model calculation is as follows. For allowed combinations of (ν_1,ν_2,ν_3), calculate the $A_{\nu_2\nu_3}$ and the two Talmi-Moshinsky coefficients. The form factor can be calculated via equation II.22a. The spectroscopic amplitudes are given by Equation II.12. The transition matrix element is then found by substituting these values into expression II.11.

E. The (p,α) Form Factor:
Woods-Saxon Model

Once again we wish to reduce the right hand side of Equation II.13 so that it is explicitly a function of r_1 and r_2 only. Again, the triton wavefunction is taken to be as given in Equation II.14. We will work in the same general pattern as the last section.

As before, begin by expanding the two-nucleon part of Equation II.14, but this time follow the Bayman and Kallio (II.21) two-nucleon expansion

$$\frac{\left[\varphi_{n_1}^{\ell_1 j_1}(\xi_1)\varphi_{n_2}^{\ell_2 j_2}(\xi_2) - \varphi_{n_1}^{\ell_1 j_1}(\xi_2)\varphi_{n_2}^{\ell_2 j_2}(\xi_1)\right]^{\ell_{12}}}{\sqrt{2(1+\delta_{n_1 n_2}\delta_{\ell_1\ell_2}\delta_{j_1 j_2})}} = \sum_{\lambda_{12}\Lambda}\frac{f_{\lambda_{12}\Lambda}^{\ell_{12}}(\rho_{12},R)}{\rho_{12}R}$$

$$\cdot\left[Y^{\lambda_{12}}(\hat{\rho}_{12})Y^{\Lambda}(\hat{R})\right]^{\ell_{12}}. \qquad \text{II.27}$$

Since the internal angular momentum is required to be zero, only terms

with $\lambda_{12}=0$ and $\Lambda=\ell$ need to be saved.

This result may be used in Equation II.13 to yield

$$f_{\ell m_\ell}^{\{n_i\ell_i j_i\}}(\mathfrak{r}_1,\mathfrak{r}_2) = \eta\Phi_0^0(\mathfrak{r}_2)\sum_{m_{12}m_3}(\ell_{12}m_{12}\ell_3 m_3|\ell m_\ell)\int d\rho_{123}e^{-\beta/2\,\rho_{123}^2}$$

$$\cdot\varphi_{n_3}^{\ell_3 j_3}(\xi_3)\left(\int d\rho_{12}e^{-\beta/2\,\rho_{12}^2}\frac{f_{0\ell_{12}}^{\ell_{12}}(\rho_{12},R)}{\rho_{12}R}Y_0^0(\hat{\rho}_{12})Y_{m_{12}}^{\ell_{12}}(\hat{R})\right).$$

$$\text{II.28}$$

The inner integral in Equation II.28 is the normal two-nucleon

form factor that Bayman and Kallio calculate. Call this integral

$F^{(2)}(R)Y_{m_{12}}^{\ell_{12}}(\hat{R})$ where $\underset{\sim}{R}$ is the coordinate of the center of mass of the

di-neutron as defined in the last section. Using this notation in Equa-

tion II.28 and recoupling the angular momenta yields

$$f_{\ell m_\ell}^{\{n_i\ell_i j_i\}}(\mathfrak{r}_1,\mathfrak{r}_2) = \eta\Phi_0^0(\mathfrak{r}_2)\int d\rho_{123}e^{-\beta/2\,\rho_{123}^2}\left[F^{(2)}(R)Y^{\ell_{12}}(\hat{R})\varphi^{\ell_3}(\xi_3)\right]^\ell. \qquad \text{II.29}$$

The quantity in brackets can be expanded as

$$\left[F^{(2)}(R)Y^{\ell_{12}}(\hat{R})\varphi^{\ell_3}(\xi_3)\right]^\ell = \sum_{\lambda_{123}}\frac{f_{\lambda_{123}\tau}^\ell(r_1,\rho_{123})}{r_1\rho_{123}}\left[Y^{\lambda_{123}}(\hat{\rho}_{12})Y^\tau(\hat{r}_1)\right]^\ell. \qquad \text{II.30}$$

As before, take only terms with $\lambda_{123} = 0$, and hence $\tau = \ell$, so that

$$f_{\ell m_\ell}^{\{n_i \ell_i j_i\}} (\underline{r}_1, \underline{r}_2) = \eta \, \Phi_0^0(\underline{r}_2) \int d\rho_{123} e^{-\beta/2 \, \rho_{123}^2} \frac{f_{0\ell}^\ell (r_1, \rho_{123})}{r_1 \rho_{123}} \left[Y_0^0(\hat{\rho}_{123}) Y^\ell(\hat{r}_1) \right]^\ell .$$

<div align="right">II.31</div>

The integral in Equation II.31 has the same form as the two-nucleon form factor. However, one of the particles is a di-neutron. It is possible to redefine the coordinates in the Bayman and Kallio paper to handle the unequal mass problem. Roger Markham has written a code to perform this calculation for three-nucleon or four-nucleon transfer (II.23).

If single particle wavefunctions generated in a Woods-Saxon potential are used, the prescription is to first calculate the two-nucleon wavefunction $F^{(2)}(R) Y^{\ell_{12}}(R)$ then use this to calculate the three-nucleon form factor, which is given by Equation II.31. The transition matrix element can then be found by using the spectroscopic amplitudes given by Equation II.12.

F. Correction for the Center of Mass Motion

The steps leading to Equation II.22a involved integrating over the coordinates of $\langle I_B M_B |$ in Equation II.3a. We implicitly assumed that all the coordinates were internal, which they are in the coordinate system whose origin is the center of the core (see Figure II.2). However, this is really incorrect since the core (B) is moving about the center of mass of nucleus (A) which is fixed in our reference frame.

Hence the coordinate system shown in Figure II.3 is the correct one. In this system the appropriate coordinates for $\langle I_B M_B |$ are ξ_B and $\underset{\sim}{R}_B$ and we are interested in determining the effect of motion about $\underset{\sim}{R}_B$ on the form factor. We begin by expanding $|I_A M_A\rangle$ again

$$|I_A M_A\rangle = \sum_{\substack{\{n_i \ell_i j_i\} \\ j_{12}\alpha_x j}} C^{(A)}_{\substack{\{n_i \ell_i j_i\} \\ j_{12}\alpha_x j}} \frac{\left\{ \psi^{J_B}(\xi_B, \underset{\sim}{R}_B) \left(\left[\varphi^{j_1}(\underset{\sim}{\zeta}_1) \varphi^{j_2}(\zeta_2) - \varphi^{j_1}(\zeta_2)\varphi^{j_2}(\zeta_2) \right]^{j_{12}} \varphi^{j_3}(\zeta_3) \right)^j \right\}^{I_A}}{\sqrt{2(1+\delta_{n_1 n_2}\delta_{\ell_1 \ell_2}\delta_{j_1 j_2})}} .$$

II.32

At this point we can change to LS coupling and apply the two Moshinsky transformations outlined in Equations II.15 through II.21 to get

$$|I_A M_A\rangle = \sum_{\substack{\{n_i \ell_i j_i\} \\ \ell_{12}\alpha_x j}} \sum_{\nu_1 \nu_2 \nu_3} C^{(A)}_{\substack{\{n_i \ell_i j_i\} \\ j_{12}\alpha_x j}} \frac{2}{\sqrt{2(1+\delta_{n_1 n_2}\delta_{\ell_1 \ell_2}\delta_{j_1 j_2})}}$$

$$\begin{bmatrix} \ell_1 & \ell_2 & \ell_{12} \\ \frac{1}{2} & \frac{1}{2} & 0 \\ j_1 & j_2 & \ell_{12} \end{bmatrix} \begin{bmatrix} \ell_{12} & \ell_3 & \ell \\ 0 & \frac{1}{2} & \frac{1}{2} \\ \ell_{12} & j_3 & j \end{bmatrix} \langle (N'-\nu_2)\ell_{12}\nu_2 0:\ell_{12}|n_1\ell_1 n_2\ell_2:\ell_{12}\rangle_{11}$$

$$\langle \nu_1 \ell \nu_3 0:\ell | (N'-\nu_2)\ell_{12}n_3\ell_3:\ell\rangle_{21} \; \varphi^O_{\nu_2}(\rho_{12})\varphi^O_{\nu_3}(\rho_{123})$$

$$\left\{ \left(\varphi^\ell_\nu(\underset{\sim}{r}) \times^{((\frac{1}{2}\frac{1}{2})O\frac{1}{2})^{\frac{1}{2}}} \right)^j \psi^{J_B}(\xi_B, R_B) \right\} .$$

II.33

We assume that there is no spurious center of mass motion which means that the center of mass motion does not have any oscillator quanta associated with it. In other words,

Figure II. 3

Nucleon coordinates in a fixed potential.
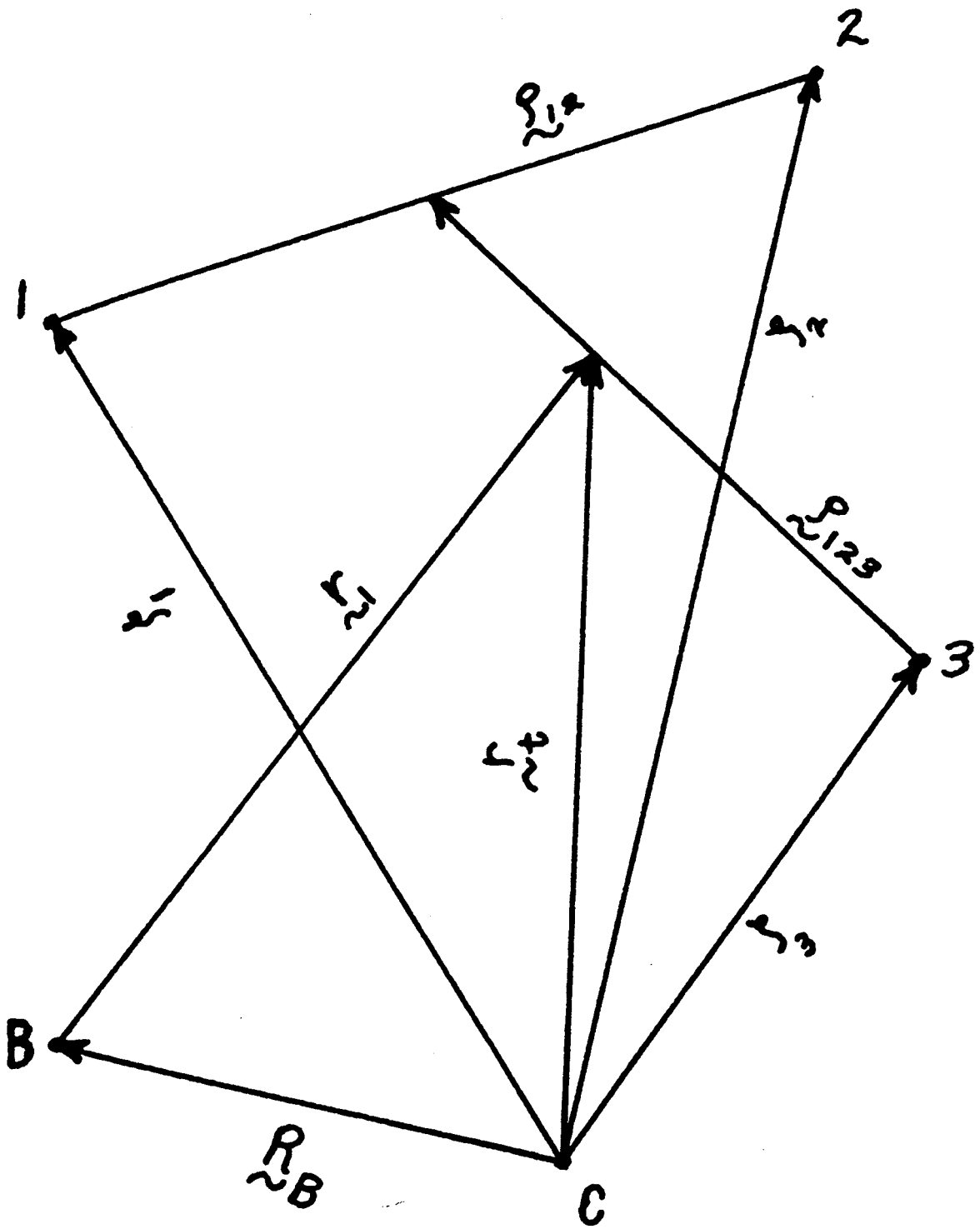
Figure II. 3

$$\psi^{J_B}(\xi_B, \underset{\sim}{R}_B) = \psi^{J_B}(\xi_B)\varphi_o^o(\underset{\sim}{R}_B). \qquad \text{II.34}$$

We may now perform another generalized Moshinsky transformation on the term in brackets in Equation II.33, where the masses involved are B and 3.

$$\varphi_{\nu_1}^{\ell}(\underset{\sim}{r}_t)\varphi_o^o(\underset{\sim}{R}_B) = \langle 00\nu_1\ell:\ell \mid 00\nu_1\ell:\ell\rangle_{B3} \; \varphi_o^o(R_A)\varphi_{\nu_1}^{\ell}(\underset{\sim}{R})$$

$$= \left(\frac{A}{A-3}\right)^{\nu_1+\ell/2} \varphi_o^o(R_A)\varphi_{\nu_1}^{\ell}(\underset{\sim}{R}). \qquad \text{II.35}$$

If Equation II.35 is used to replace the term in { } in Equation II.33 and the result is compared with II.22a, it is evident that the effect of the center of mass motion is to make the replacement

$$\varphi_{\nu_1}^{\ell}(\underset{\sim}{r}_1) \longrightarrow \left(\frac{A}{A-3}\right)^{\nu_1+\ell/2} \varphi_{\nu_1}^{\ell}(\underset{\sim}{r}_1).$$

Similar analysis for cluster transfer has been presented by Ichimura et al. (II.24). Our result reduces to the cluster result if we require equal size parameters, which is the equivalent of the cluster transfer form factor. It is intriguing to note that the correction is different for 0s, 1s, 2s, . . . internal motions for realistic size parameters, thereby changing the shape as well as the magnitude of the form factor.

G. The Microscopic Basis for Cluster Model Spectroscopic Factors

In the harmonic oscillator model the importance of 1s, 2s, 3s, . . . terms in the "triton" wavefunction is a function of the difference of oscillator parameters $(\alpha-\beta)$. In principle, this difference is fixed by

the α-particle radius and the nuclear radius. However, it is instruc-

tive to consider the case where $\alpha = \beta$.

If $(\alpha-\beta)$ is zero, there is no contribution from the 1s, 2s, 3s . . .

terms. In this instance, $\nu_2 = \nu_3 = 0$ and the triton is structureless.

Therefore, $(\alpha-\beta) = 0$ implies mass three cluster transfer. Furthermore,

the center of mass correction reduces to the cluster center of mass cor-

rection given in Reference II.24.

It was pointed out in the introduction that "spectroscopic fac-

tors" deduced from a cluster model calculation are not easily related to

nuclear shell structure. In the sense that a harmonic oscillator cluster

model is given by $(\alpha-\beta) = 0$, we can derive a spectroscopic amplitude by

investigating the expression II.11 and Equation II.22a.

For single nucleon transfer, or cluster transfer, II.11 becomes

$$d^{j\ell\frac{1}{2}}f_{\ell m_\ell}(\underset{\sim}{r}_1,\underset{\sim}{r}_2) = d^{j\ell\frac{1}{2}}\Phi_{o}^{o}(\underset{\sim}{r}_2)\varphi_N^{\ell}(\underset{\sim}{r}_1).$$ II.36

The spectroscopic amplitude, $d^{j\ell\frac{1}{2}}$, is called the "spectroscopic fac-

tor" and is usually denoted by $s^{j\ell}$.

If, on the other hand, we require $\alpha = \beta$ in Equation II.22a and use

the result in expression II.11, we obtain

$$\left\{ \sum_{\substack{\{n_i\ell_i j_i\} \\ \ell_{12}\alpha_x}} C^{(A)}_{\{n_i\ell_i j_i\}\ell_{12}\alpha_x j} \begin{bmatrix} \ell_{12} & \ell_3 & \ell \\ 0 & \frac{1}{2} & \frac{1}{2} \\ \ell_{12} & j_3 & j \end{bmatrix} \begin{bmatrix} \ell_1 & \ell_2 & \ell_{12} \\ \frac{1}{2} & \frac{1}{2} & 0 \\ j_1 & j_2 & \ell_{12} \end{bmatrix} \frac{2}{\sqrt{2}\,(1+\delta_{n_1 n_2}\delta_{\ell_1\ell_2}\delta_{j_1 j_2})} \right.$$

$$\langle 00N'\ell_{12}{:}\ell_{12}|n_1\ell_1 n_2\ell_2{:}\ell_{12}\rangle_{11}\langle 00N\ell{:}\ell|N'\ell_{12}n_3\ell_3{:}\ell\rangle_{21} \Big\} \Phi_o^o(\underset{\sim}{r}_2)\varphi_N^{\tilde{\ell}}(\underset{\sim}{r}_1)$$

II.37

where

$$2N' + \ell_{12} = 2(n_1 + n_2) + \ell_1 + \ell_2.$$

Comparing the right hand side of Equation II.36 to II.37 shows that the spectroscopic factor is given by

$$S^{j\ell} = \left\{ \quad \right\}, \quad \text{where} \left\{ \quad \right\}$$

represents the term in brackets in II.37. A number of (p, α) and (α, p) studies have deduced cluster model "spectroscopic factors" (see II.5 and II.25 for example). None of these experimental spectroscopic factors have been compared with theoretical $S^{j\ell}$ values calculated in the manner presented here.

H. The Use of Shell Model Wavefunctions

The nuclear structure information is contained in the expansion coefficients $C^{(A)}$. In order to test shell model wavefunctions, a prescription for calculating these coefficients must be devised. We will do this by introducing an intermediate state expansion so that reduced matrix elements for two nucleon configurations and single nucleon configurations may be used. This method has the advantages of using the output of existing shell model codes (codes for calculating three nucleon overlaps have not been written as yet) and of allowing us to separate the two neutrons for easy anti-symmeterization as we have done. In addition, this method is intuitively pleasing since it divides the problem into two nucleon transfer and single nucleon transfer.

The expansion coefficients defined in Equation II.3 are given by

$$C^{(A)}_{\{n_i \ell_i j_i\} j_{12} \alpha_x j} = \left\langle \left[\varphi^{I_B} \left\{ A \; \varphi^{j_1} \varphi^{j_2})^{j_{12}} \varphi^{j_3} \right\}^j \right]^{I_A} \Big| \varphi^{I_A} \right\rangle .$$ II.38

A p-n formalism has been used and we have anti-symmeterized according-
ingly. However, the shell model wavefunctions which we wish to use
for the calculation of $C^{(A)}$ are derived in the isospin formalism. It is
necessary, therefore, to begin by converting the right hand side of
Equation II.38 to the appropriate form for the isospin formalism. We do
this by expanding the three nucleon wavefunction

$$\left\{ A \left(\varphi^{j_1 \frac{1}{2}}_{-\frac{1}{2}} \varphi^{j_2 \frac{1}{2}}_{-\frac{1}{2}} \right)^{j_{12} 1}_{-\frac{1}{2}} \varphi^{j_3 \frac{1}{2}}_{\frac{1}{2}} \right\} = -\sqrt{2/3} \left\{ A \left(\varphi^{j_1 \frac{1}{2}} \varphi^{j_2 \frac{1}{2}} \right)^1 \varphi^{j_3 \frac{1}{2}} \right\}^{j \frac{1}{2}}$$

$$+ \sqrt{1/3} \left\{ A \left(\varphi^{j_1 \frac{1}{2}} \varphi^{j_2 \frac{1}{2}} \right)^1 \varphi^{j_3 \frac{1}{2}} \right\}^{j \; 3/2} .$$ II.39

Even though neither term on the right hand side is anti-symmetric, the
total must be since it is an expansion of an anti-symmetric wavefunc-
tion with a complete basis set. The right hand side also has the dis-
pleasing feature of having a term that has an isospin coupling of 3/2.
This is because our p-n formalism triton wavefunction does not have
good isospin.

It is desirable to work with reduced matrix elements so as to
simplify the algebra. The following definition is useful in this regard.

$$\langle (\varphi^{k_1} \varphi^{k_2})^k | \varphi^k \rangle = \frac{(-1)^{2k_2}}{\sqrt{2k+1}} (\varphi^{k_1} || \varphi^{k_2} || \varphi^k) .$$ II.40

Inserting Equations II.39 and II.40 into II.38 gives

$$C^{(A)}_{\{n_i\ell_ij_i\}j_{12}\alpha_Xj} = \frac{(-1)^{2j}}{\sqrt{2I_A+1}}\left[-\sqrt{2/3}\left(\varphi^{I_BT_B}_{N_B}\|A\left\{\left(\varphi^{j_1\frac{1}{2}}\varphi^{j_2\frac{1}{2}}\right)^{j_{12}1}\varphi^{j_3}\right\}^{j\frac{1}{2}}\|\varphi^{I_AT_A}_{N_A}\right)\right.$$

$$\left.+\sqrt{1/3}\left(\varphi^{I_BT_B}_{N_B}\|A\left\{\left(\varphi^{j_1\frac{1}{2}}\varphi^{j_2\frac{1}{2}}\right)^{j_{12}1}\varphi^{j_3\frac{1}{2}}\right\}^{j\,3/2}\|\varphi^{I_AT_A}_{N_A}\right)\right]. \qquad \text{II.41}$$

Here the reduced matrix elements are reduced in spin only. The Wigner Eckhart theorem can be applied to reduce them in isospin as well.

$$C^{(A)}_{\{n_i\ell_ij_i\}j_{12}\alpha_Xj} = \frac{(-1)^{2j}}{\sqrt{2I_A+1}}\left[-\sqrt{2/3}\,(-1)^{T_B-N_B}\begin{pmatrix}T_B & \frac{1}{2} & T_A\\-N_B & -\frac{1}{2} & N_A\end{pmatrix}\left(\varphi^{I_BT_B}\right.\right.$$

$$\cdot\left\{A_{\left(\varphi^{j_1\frac{1}{2}}\varphi^{j_2\frac{1}{2}}\right)^{j_{12}1}\varphi^{j_3\frac{1}{2}}}\right\}^{j\frac{1}{2}}\|\|\varphi^{I_AT_A}\right)\sqrt{1/3}\,(-1)^{T_B-N_B}\begin{pmatrix}T_B & 3/2 & T_A\\-N_B & -\frac{1}{2} & N_A\end{pmatrix}$$

$$\left.\left(\varphi^{I_BT_B}\|\|\left\{A\left(\varphi^{j_1\frac{1}{2}}\varphi^{j_2\frac{1}{2}}\right)^{j_{12}1}\varphi^{j_3\frac{1}{2}}\right\}^{j\,3/2}\|\|\varphi^{I_AT_A}\right)\right]. \qquad \text{II.42}$$

These reduced matrix elements can be expanded using the relation

$$\left(\varphi^J\|[T^{k_1}\times T^{k_2}]^k\|\varphi^{J'}\right) = (-1)^{J+k+J'}\sqrt{2k+1}\sum_{\gamma J''}\begin{Bmatrix}k_1 & k_2 & k\\J' & J & J''\end{Bmatrix}$$

$$\cdot\left(\varphi^J\|T^{k_1}\|\varphi^{J''}_\gamma\right)\left(\varphi^{J''}_\gamma\|T^{k_2}\|\varphi^{J'}\right) \qquad \text{II.43}$$

where γ represents other quantum numbers which may be needed to describe the intermediate states. The resulting expression for $C^{(A)}$ is

$$C^{(A)}_{\{n_i\ell_ij_i\}j_{12}\alpha_Xj} = \frac{(-1)^{I_A+j+I_B}}{\sqrt{2I_A+1}}\sqrt{\frac{2j+1}{2T_A+1}}\frac{2}{\sqrt{3}}\sum_{\substack{J'T'\\\gamma}}\left[(-1)^{2T_A}(T_BN_B\tfrac{1}{2}-\tfrac{1}{2}|T_AN_A)\right.$$

$$\cdot\begin{Bmatrix}1 & \frac{1}{2} & \frac{1}{2}\\T_A & T_B & T'\end{Bmatrix}+(-1)^{2T_A+1}(T_BN_B\tfrac{3}{2}-\tfrac{1}{2}|T_AN_A)\begin{Bmatrix}1 & \frac{1}{2} & \frac{3}{2}\\T_B & T_B & T'\end{Bmatrix}\right]\times$$

$$\times \begin{Bmatrix} j_{12} & j_3 & j \\ I_A & I_B & J' \end{Bmatrix} \left(\varphi^{I_B T_B} \parallel \mathcal{A} \left(\varphi^{j_1 \frac{1}{2}} \varphi^{j_2 \frac{1}{2}} \right)^{j_{12} 1} \parallel \varphi_\gamma^{J' T'} \right) \left(\varphi_\gamma^{J' T'} \parallel \varphi^{j_3 \frac{1}{2}} \parallel \varphi^{I_A T_A} \right).$$

II.44

This is the result we desire since it is really these reduced matrix elements that the shell model overlap codes provide. Notice that only even values are allowed for the two nucleon coupling if the target has a ground state spin of zero. This is so because the two nucleons are in an isospin one state and a relative s state. Thus the sum over J' is only over the values 0, 2, 4, ...

I. Sample Calculations

Figure II.4 shows a comparison of three methods of calculating three nucleon form factors. The microscopic Woods-Saxon form factor was calculated assuming each was bound by 8 MeV. The oscillator form factor was calculated assuming a size parameter of .226 fm^{-2} (see below). A hankel tail was matched to the oscillator form factor to give the correct asymptotic behavior. The mass three cluster form factor was calculated using a Woods-Saxon well and the triton separation energy from ^{52}Cr. The two form factors have similar shapes, although they differ a bit near the nuclear surface. The mass three cluster form factor has its nodes pushed out further than the other two form factors and does not display an accentuated last maximum. In addition, the cluster form factor does not have the same tail as the microscopic Woods-Saxon form factor.

Figure II.4

Form factors for $^{53}Cr(p,\alpha)^{49}V$ going to the $7/2^-$ ground state of ^{49}V.
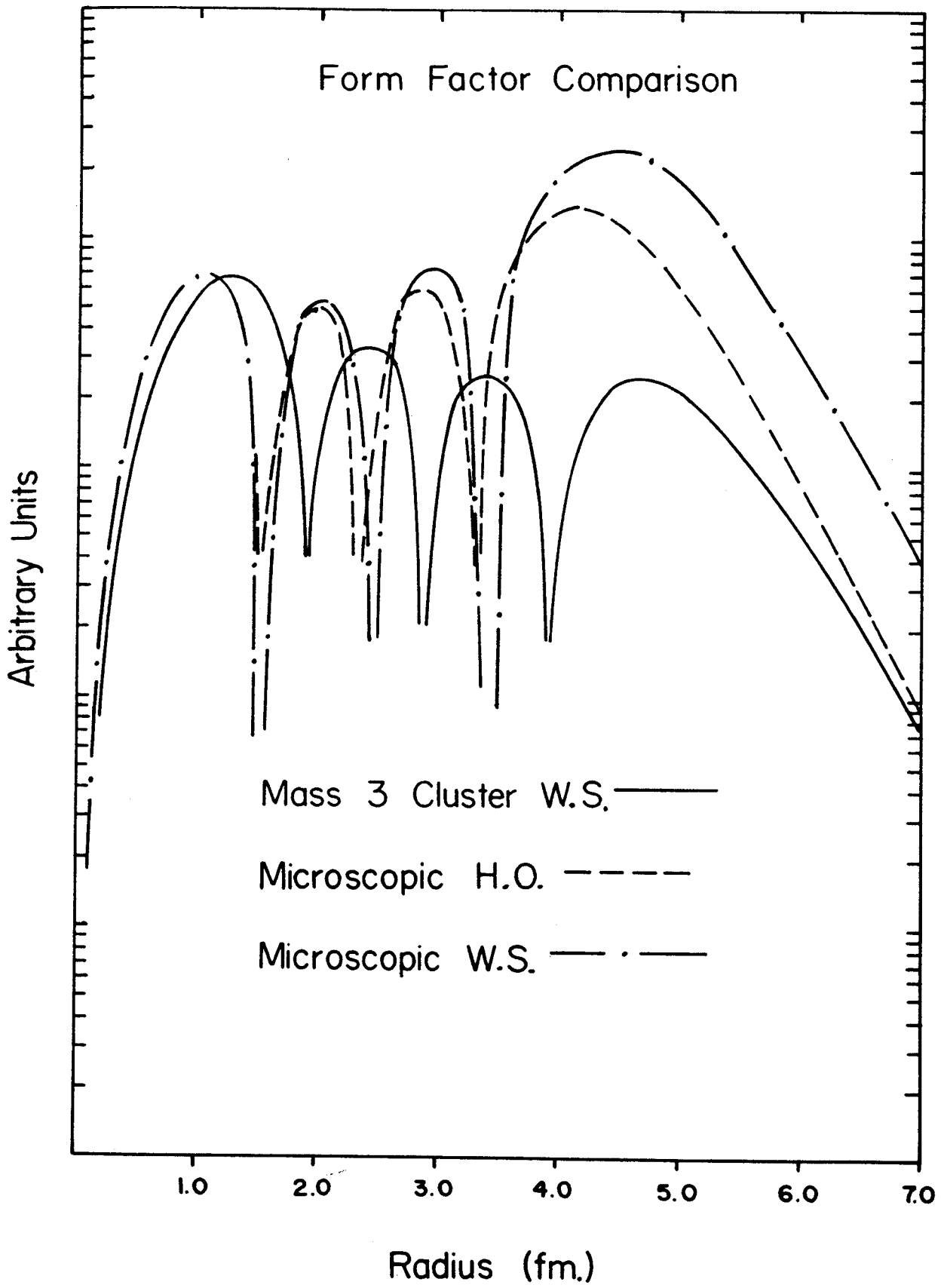
Figure II.4

Zero range DWBA calculations for the form factors in Figure II.4 are shown in Figure II.5. Even though the cluster form factor is different, the predicted angular distribution is similar to both microscopic calculations. The optical parameters for all the DWBA calculations which we present are given in Table II.2.

TABLE II.2

OPTICAL PARAMETERS

Particle	V_e	r_r	a_r	V_{so} a)	r_{so}	a_{so}	V_I	r_I	o_I	W_s a)
p	-43.22	1.22	.72	-25.0	1.01	.75	-5.0	1.32	.52	12.6
α	196.0	1.22	.72				-16.0	1.82	.38	

[a] As input for DWUCK72 (II.27)—e.g., includes factor of 4.0.

The effect of different neutron orbitals is shown in Figures II.6 and II.7. The $(1p3/2)^2 0f7/2$ and $(0f7/2)^3$ form factors differ in much the same way that the cluster form factor and the $(0f7/2)^3$ form factor differ. The angular distributions are similar again, but the $(1p3/2)^2 0f7/2$ transfer is predicted to have ten times more cross section. This feature can be tested by examining the $7/2^-$ states in $^{54,56}Fe(p,\alpha)^{51,53}Mn$ reactions.

The form factors which are shown in Figures II.4 and II.6 are for a particular choice of the α-particle size. We have used 1.63 fm for the root mean square radius of the α-particle. This value was measured by electron scattering (II.26).

Figure II.5

Zero range DWBA calculations for the $7/2^-$ form factors shown in Figure II.4. $E_p = 35$ MeV.

DWBA Calculations

Mass 3 Cluster ——————

Microscopic W.S. —— · ——

Microscopic H.O. — — — —

$d\sigma/d\Omega$ (Arbitrary Units)

C.M. Angle (degrees)
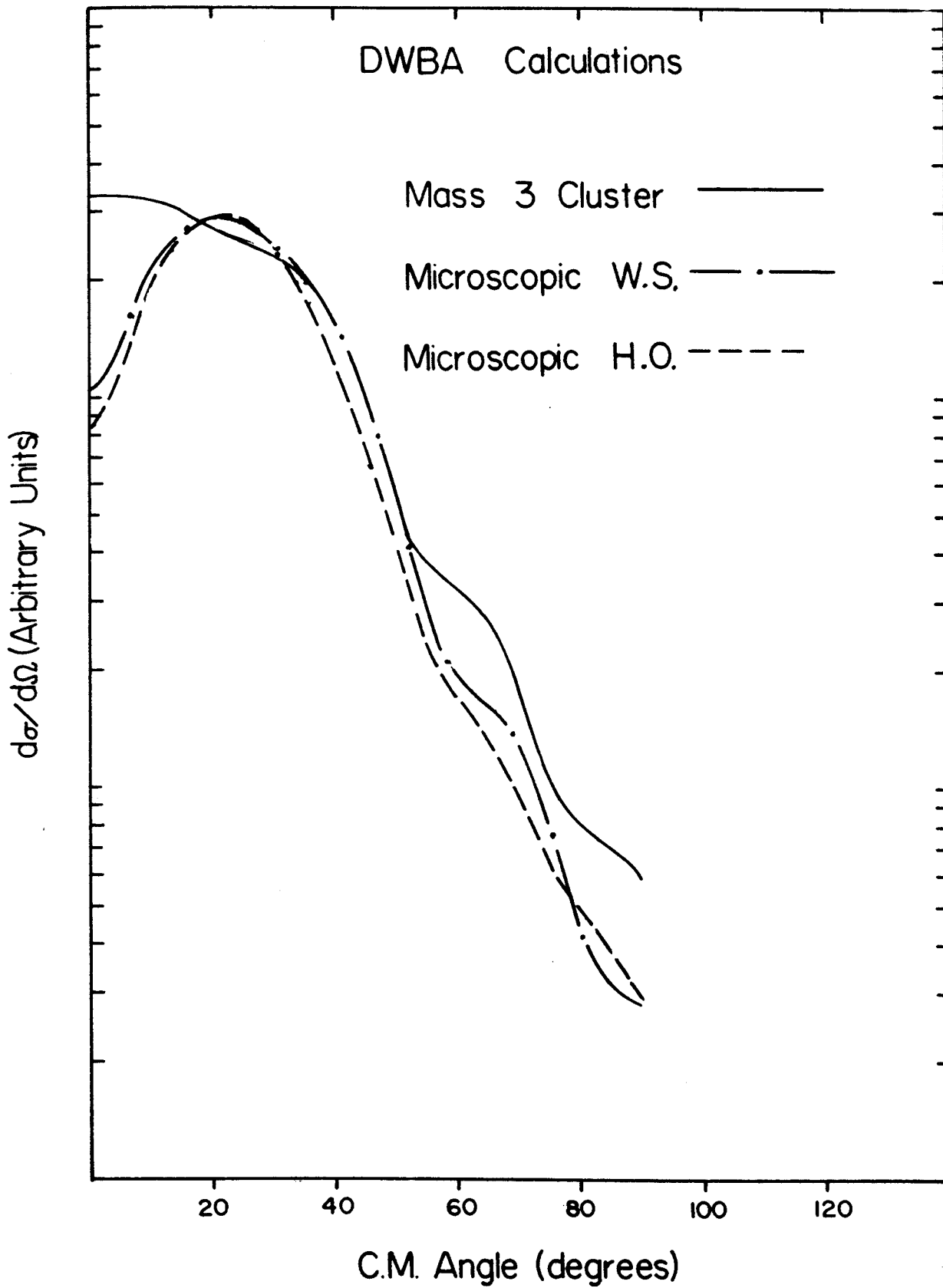
Figure II.5

Figure II.6

Microscopic form factors for a seniority one $7/2^-$ transfer in the $^{52}Cr(p,\alpha)^{49}V$ reaction—Woods-Saxon potential.
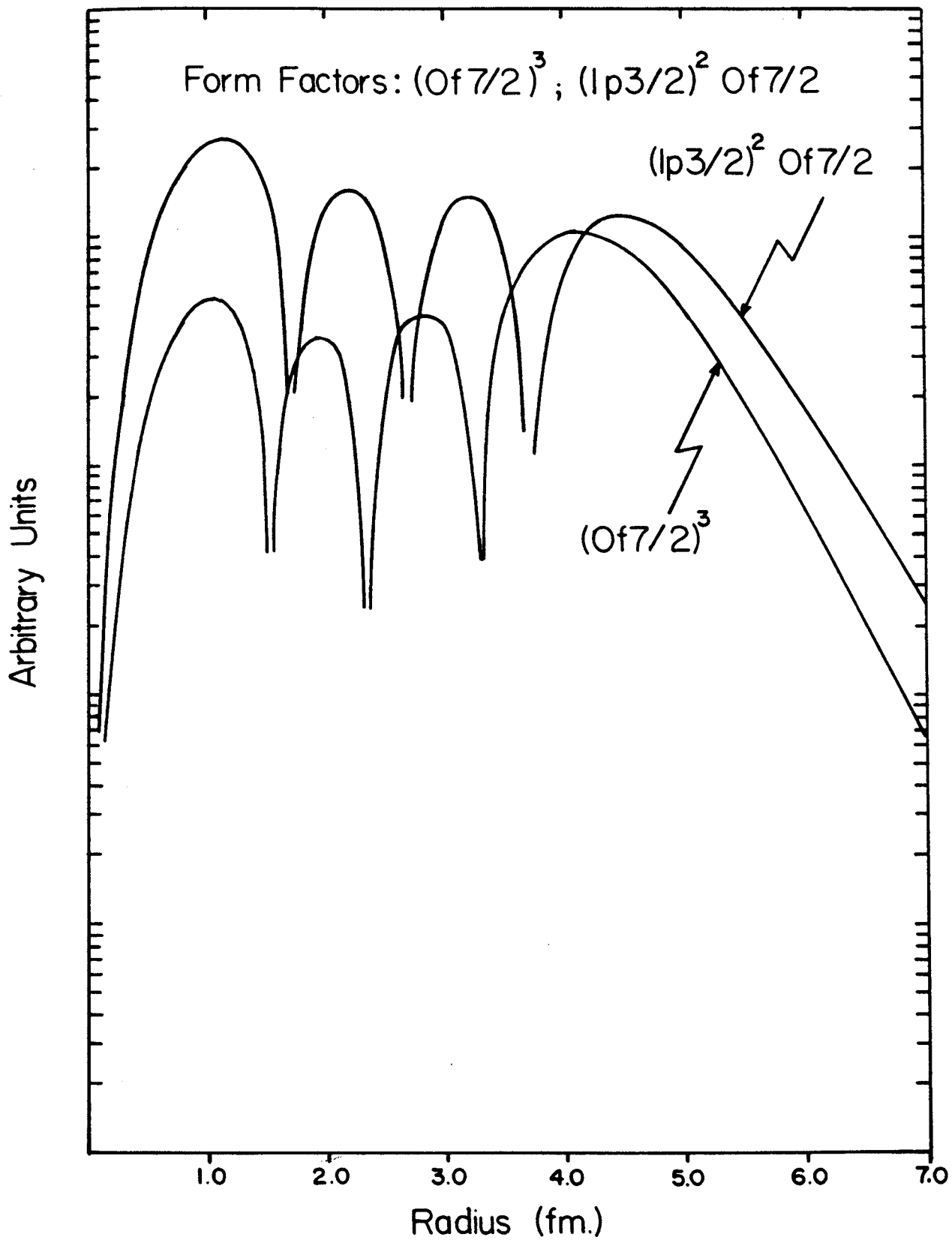
Figure II.6

Figure II.7

DWBA calculations for the form factors shown in Figure II.6. $E_p = 35$ MeV.
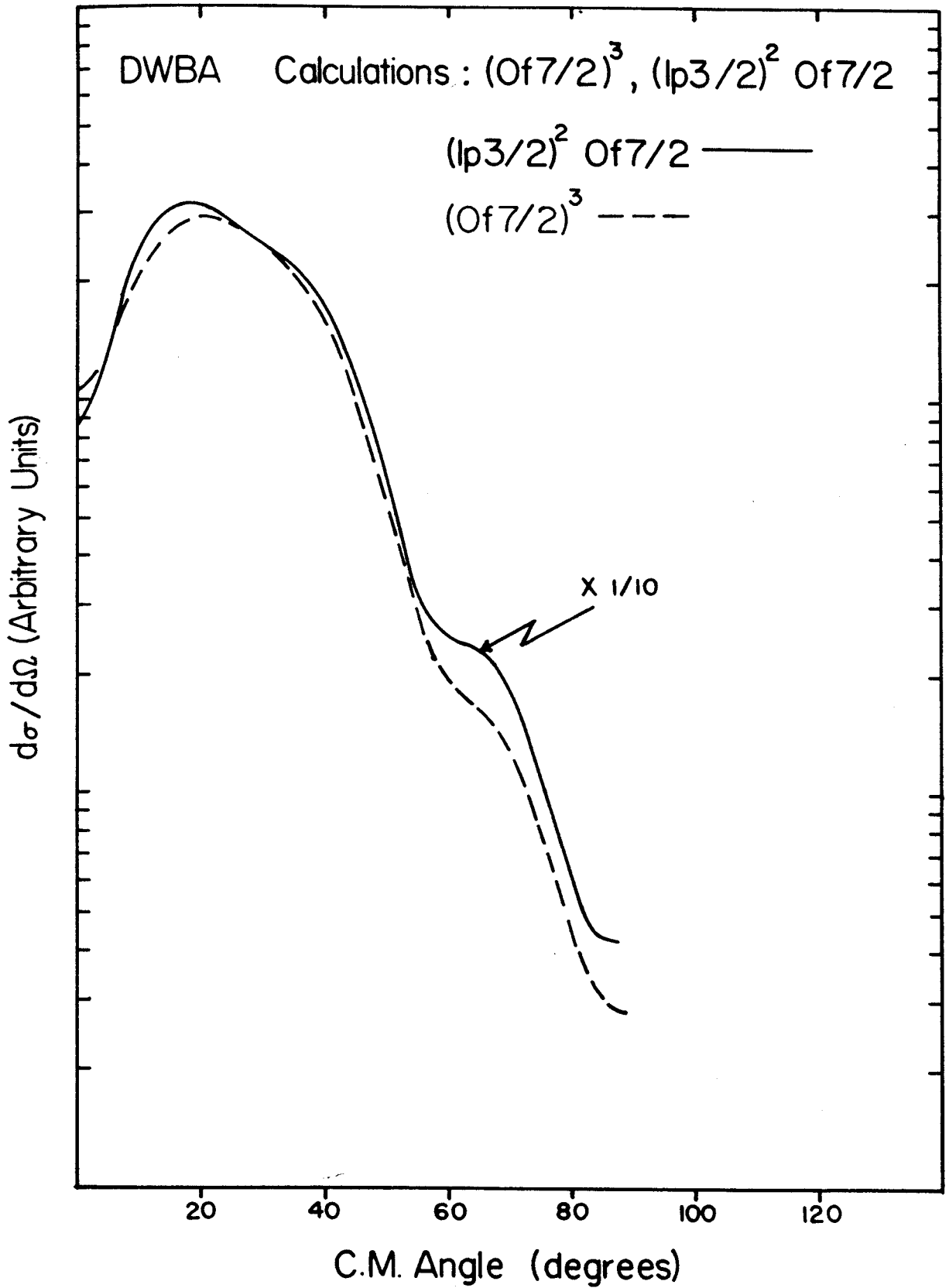
Figure II.7

To perform the Woods-Saxon form factor calculation, it is necessary to determine the n-n separation and the proton—di-neutron separation from the α-particle radius. The appropriate r.m.s. separations turn out to be

$$\Delta_{n-n} = 1.537 \text{ fm}$$

$$\Delta_{p-(nn)} = 1.331 \text{ fm.}$$

For the harmonic oscillator calculation, it is necessary to find the relation between β and the α-particle radius. The α-particle wavefunction is

$$\varphi = e^{-\beta/2 \sum_{i=1}^{4} (\underset{\sim}{r}_i - \underset{\sim}{R}_{CM})^2}.$$

The sum may be transformed to internal coordinates only by

$$\sum_{i=1}^{4} (\underset{\sim}{r}_i - \underset{\sim}{R}_{CM})^2 = \frac{1}{2} r_{12}^2 + \frac{2}{3} r_{123}^2 + \frac{3}{4} r_2^2.$$

Earlier we used the variables $\underset{\sim}{\rho}_{12}$ and $\underset{\sim}{\rho}_{123}$. These variables are now seen to be

$$\underset{\sim}{\rho}_{12} = \frac{1}{\sqrt{2}} \underset{\sim}{r}_{12}; \quad \underset{\sim}{\rho}_{123} = \sqrt{2/3}\, \underset{\sim}{r}_{123}; \quad \underset{\sim}{\rho}_{1234} = \frac{\sqrt{3}}{2} \underset{\sim}{r}_2.$$

The definition of the r.m.s. radius is

$$\Delta_\alpha^2 = \frac{1}{4} \frac{\int_o^\infty e^{-\beta(\rho_{12}^2 + \rho_{123}^2 + \rho_{1234}^2)} (\rho_{12}^2 + \rho_{123}^2 + \rho_{1234}^2)\, \rho_{12}\rho_{123}\rho_{1234} d\rho_{12} d\rho_{123} d\rho_{1234}}{\int_o^\infty e^{-\beta(\rho_{12}^2 + \rho_{123}^2 + \rho_{1234}^2)} \rho_{12}^2\rho_{123}^2\rho_{1234}^2 d\rho_{12} d\rho_{123} d\rho_{1234}}.$$

If the integrals are carried out, the expression for β is

$$\beta = \frac{9}{8} \frac{1}{\Delta_\alpha^2} = .42 \text{ fm}^{-2}.$$

The nuclear wavefunction also requires a size parameter. For the Woods-Saxon well the usual $A^{\frac{1}{3}}$ prescription was used with $r_0 = 1.22$ fm and a diffuseness of .72 fm. The size parameter for the harmonic oscillator can be determined from the electron scattering r.m.s. radius measurements with the relation

$$\langle R^2 \rangle = \frac{1}{Z\alpha} \sum_{n\ell} N_{n\ell} (2n + 2\ell + 3/2)$$

which follows from the virial theorem. The sum is over protons only and $N_{n\ell}$ is the proton occupation number for the $n\ell$-orbit. The center of mass motion is neglected in deriving this relation. Therefore, it cannot be expected to give accurate results for light nuclei. For example, the size parameter for the α-particle that was calculated exactly is 33 percent smaller than that which is arrived at if the above relation is used. Typical size parameters for the periodic table are given in Table II.3.

TABLE II.3

TYPICAL OSCILLATOR SIZE PARAMETERS

Nucleus	Radius (fm)[a]	$\alpha(\text{fm}^{-2})$
^{16}O	2.718	.3046
^{40}Ca	3.482	.2474
^{58}Ni	3.764	.2420
^{90}Zr	4.265	.2062
^{208}Pb	5.498	.1900

[a] Radius parameters are electron scattering results from Reference II.26.

The difference between the size parameters, α and β, is a measure of the importance of the 1s, 2s, 3s, . . . internal triton states. A table of structure factors which show the effect for two nucleon transfer has been published by Glendenning (II.28). Similarly, a three nucleon structure factor may be defined by

$$
S^{j\ell}_{\nu_1} = \begin{bmatrix} \ell_{12} & \ell_3 & \ell \\ 0 & \frac{1}{2} & \frac{1}{2} \\ \ell_{12} & j_3 & j \end{bmatrix} \begin{bmatrix} \ell_1 & \ell_2 & \ell_{12} \\ \frac{1}{2} & \frac{1}{2} & 0 \\ j_1 & j_2 & \ell_{12} \end{bmatrix} \frac{2}{\sqrt{2(1+\delta_{n_1 n_2}\delta_{\ell_1 \ell_2}\delta_{j_1 j_2})}} \sum_{\nu_2 \nu_3}
$$

$$
\cdot \langle (N'-\nu_2)\ell_{12}\nu_2 0:\ell_{12}| n_1 \ell_1 n_2 \ell_2:\ell_{12}\rangle_{11}
$$

$$
\cdot \langle \nu_1 \ell \nu_3 0:\ell | (N'-\nu_2)\ell_{12} n_3 \ell_3:\ell \rangle_{21} \left(2^{3/2} \left(\frac{\beta}{\pi}\right)^{9/4} A_{\nu_2 \nu_3} \right)
$$

where $A_{\nu_2 \nu_3}$ is given by Equation II.26. The form factor is given by

$$
f^\ell(\underset{\sim}{r}_1) = \sum_{\nu_1} S^{j\ell}_{\nu_1} \varphi^\ell_{\nu_1}(\sqrt{3\alpha}\,\underset{\sim}{r}_1).
$$

Table II.4 is a set of structure factors for all $(0f7/2)^3$ configurations. In general the structure factors increase as the number of nodes in the radial wavefunction increases. They decrease as the intermediate coupling value increases if $j = \ell + \frac{1}{2}$, but have the opposite behavior if $j = \ell - \frac{1}{2}$. An alternation in the magnitude of the structure factors is also apparent. For example, the $19/2^-$ transition has a larger structure factor than the $17/2^-$ transition. Similarly the $15/2^-$ structure factors are larger than the $13/2^-$ values.

The actual strength of a pure configuration is dependent on the reaction kinematics. Examination of the structure factors is not

TABLE II.4

STRUCTURE FACTORS × 10,000

Alpha = .22600   Beta = .42000

	NN = 0	JN = 7/2⁻	NN = 0	JN = 7/2⁻	NP = 0 JP = 7/2⁻
J = 1/2⁻ L12	N = 0	1	2	3	4
4	.04432081	- .37335992	1.40971470	-2.55520630	1.81403637
J = 3/2⁻ L12	N = 0	1	2	3	4
2	.05071824	- .42725194	1.61319733	-2.92403316	2.07588196
4	.02648672	- .22312492	.84246475	-1.52702618	1.08409405
J = 5/2⁻ L12	N = 0	1	2	3	4
2	- .10100371	.47564608	- .95509964	.72021532	
4	- .14313543	.67405242	-1.35350132	1.02063847	
6	- .19930810	.93858087	-1.88467598	1.42118263	
J = 7/2⁻ L12	N = 0	1	2	3	4
0	- .47428691	2.23350811	-4.48489952	3.38194180	
2	- .25250876	1.18911266	-2.38774586	1.80053425	
4	- .16630810	.78317738	-1.57262421	1.18587303	
6	- .09965408	.46929067	- .94233823	.71059209	

TABLE II.4—Continued

Alpha = .22600   Beta = .42000   NN = 0   JN = 7/2⁻   NN = 0   JN = 7/2⁻   NN = 0   NP = 0   JP = 7/2⁻

J = 9/2⁻ L12	N = 0	1	2	3	4
2	.34184670	-.89296818	.76775187		
4	.46310407	-1.20971489	1.04008293		
6	.52943254	-1.38297749	1.18905067		

J = 11/2⁻ L12	N 3 0	1	2	3	4
2	1.43004799	-3.73355565	3.21173964		
4	.83368152	-2.17773438	1.87236309		
6	.52943254	-1.38297749	1.18904972		

J = 13/2⁻ L12	N = 0	1	2	3	4
4	-1.23404598	1.40946102			
6	-1.44575977	1.65126896			

J = 15/2⁻ L12	N = 0	1	2	3	4
4	-4.31916428	4.93311787			
6	-2.34239483	2.67635591			

TABLE II.4—$\underline{\text{Continued}}$

Alpha = .22600	Beta = .42000	NN = 0	JN = 7/2$^-$	NN = 0	JN = 7/2$^-$	NN = 0	JN = 7/2$^-$	NP = 0	JP = 7/2^0
			1		2		3		4

J = 17/2$^-$
L12 | N = 0   3.41528320

6 |

J = 19/2$^-$
L12 | N   0   11.06678200

6 |

sufficient to investigate cross section ratios of transfers that have different angular momentum characteristics. Peak cross sections for the $(0f7/2)^3$ configurations are tabulated in Table II.5.

TABLE II.5

MAXIMUM CROSS SECTIONS FOR $(0f7/2)^3$ CONFIGURATIONS*

J^π	$\ell_{12} =$ 0	2	4	6
$1/2^-$			(.283)1.132	
$3/2^-$		(.398).796	(.107).214	
$5/2^-$		(.057).076	(.114).152	(2.18).291
$7/2^-$	(1.0) 1.0	(.283).283	(.122).122	(.044).044
$9/2^-$		(.059).047	(.109).087	(.142).114
$11/2^-$		(.602).401	(.206).137	(.083).055
$13/2^-$			(.052).030	(.071).041
$15/2^-$			(.092).346	(.203).102
$17/2^-$				(.005).029
$19/2^-$				(.698).279

( ) = σ_{DWUCK}.

No ( ) = $\sigma_{DWUCK}/(2J+1)$.

*All values relative to the $J^\pi = 7/2^-$; $\ell_{12} = 0$ maximum cross section.

These values are the results of zero range calculations using $(0f7/2)^3$ Woods-Saxon form factors. The $7/2^-$ seniority one transfer has been normalized to one and all other values are relative to it. The peak cross sections were taken to be the largest value irrespective of the angle at which it occurred. The exact values may not have much

meaning when comparing calculations with different angular momentum values because of the large angular momentum mismatch. However, the fact that the $j_>$ member always has more cross section than the $j_<$ member of a spin-orbit pair is general. In addition, the same intermediate coupling dependence that was noted for the structure factors is again evident.

The effect of the orbital spins on the cross section is demonstrated in Figure II.7 where the $(1p3/2)^2 0f7/2$ seniority transfer was seen to have ten times the predicted cross section of that of the $(0f7/2)^3$ seniority transfer. This effect can be understood as being the result of a larger "S" component in the relative wavefunction for two nucleons in low spin orbitals than for two nucleons in high spin orbitals. The $^{208}Pb(p,\alpha)^{205}Tl$ and $^{208}Pb(\alpha,p)^{211}Bi$ reactions should be ideal reactions with which to test this feature. Since the (p,α) reaction picks particles out of low spin orbitals, the cross sections to ^{205}Tl should be large. The states in ^{211}Bi will be mostly three particles in orbits with spins of 9/2 and should not be easily excited.

The center of mass motion becomes important when comparing cross sections of states in different final nuclei. This is especially important for light nuclei. The center of mass correction is displayed for a $(0d5/2)^3$ seniority one transfer from ^{24}Mg in Figure II.8. Primarily the center of mass correction is a multiplicative factor, even though it could change the shape slightly. Slight shape changes are

Figure II. 8

Center of mass correction for a $5/2^+$ seniority one transfer in the $^{24}Mg(p,\alpha)^{21}Na$ reaction. The top two curves show the absolute magnitudes, while the bottom two curves have been shifted to emphasize the shape differences introduced by the correction.
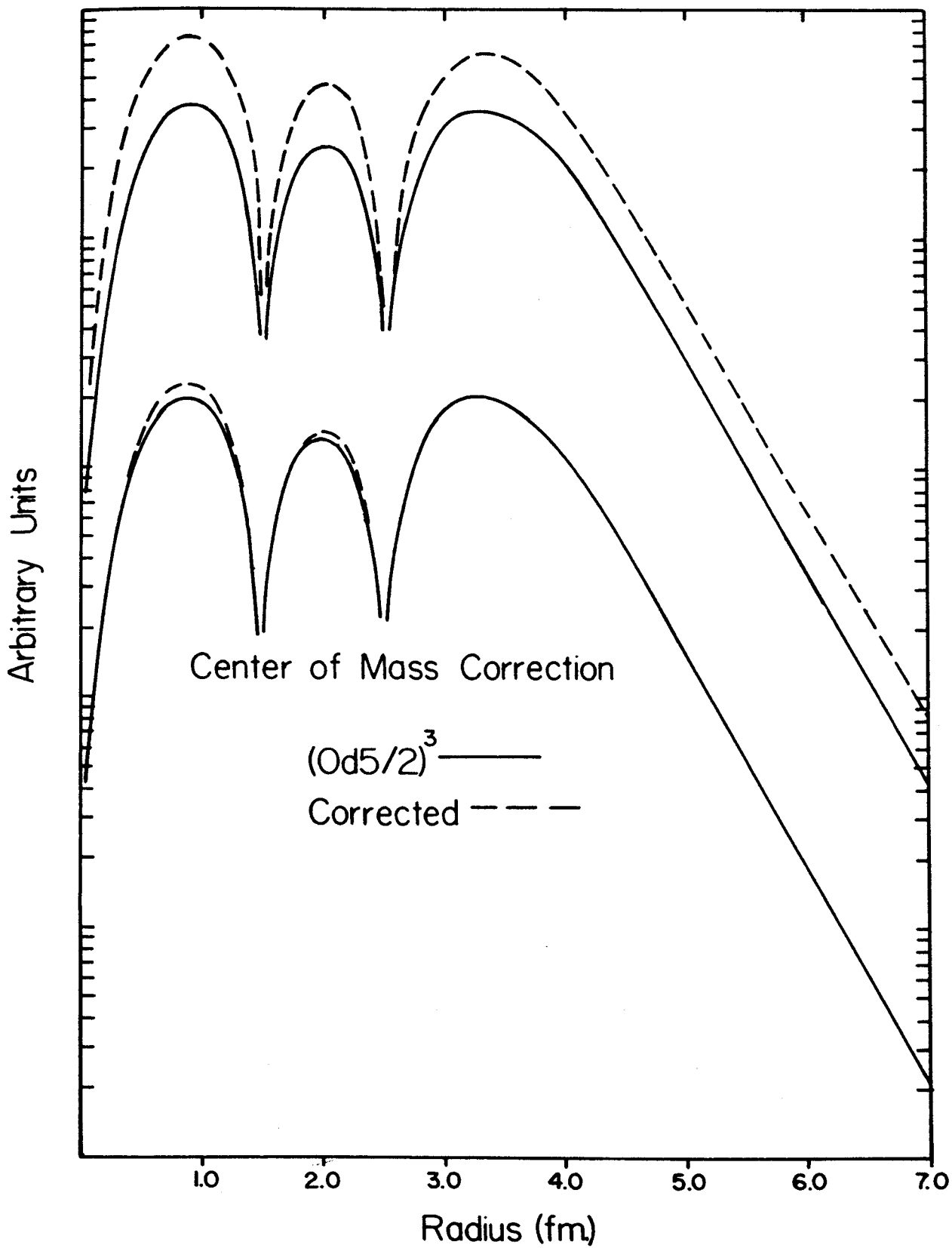
Figure II. 8

evident on the first two maxima. For this case the cluster multiplicative factor $(A/(A-3))^{N+\ell/2}$ is sufficient correction. Since the shape change is small, it seems reasonable to apply this correction to all form factor models.

If the size parameter for the α-particle is equal to the size parameter of the target potential well in the oscillator model, then the triton internal state must be a 0s state. In this instance, the structure factors are all zero except the one with the largest number of radial nodes. The radial shape becomes the same as that of a mass three particle in a harmonic oscillator well with a size parameter given by 3α. A $(0f7/2)^3$ calculation where both α and β were taken to be .226 fm is compared with the Woods-Saxon mass three cluster form factor in Figure II.9. These two form factors are rather similar. Since the differences are small, it seems reasonable to calculate mass three cluster spectroscopic factors microscopically by the prescription given in Section G.

I. The DWBA and the (p,α) Reaction

Multi-particle transfer reactions are difficult to handle with the DWBA because of the large mass transfer and, hence, the large momentum transfer. Such circumstances give rise to finite range effects which often cannot be accounted for using the zero range approximation. Most important of these effects is the recoil which is left out of the zero range approximation because the projectile, picked up cluster,

Figure II.9

Cluster form factors for a $7/2^-$ transfer in the $^{52}Cr(p,\alpha)^{49}V$ reaction.
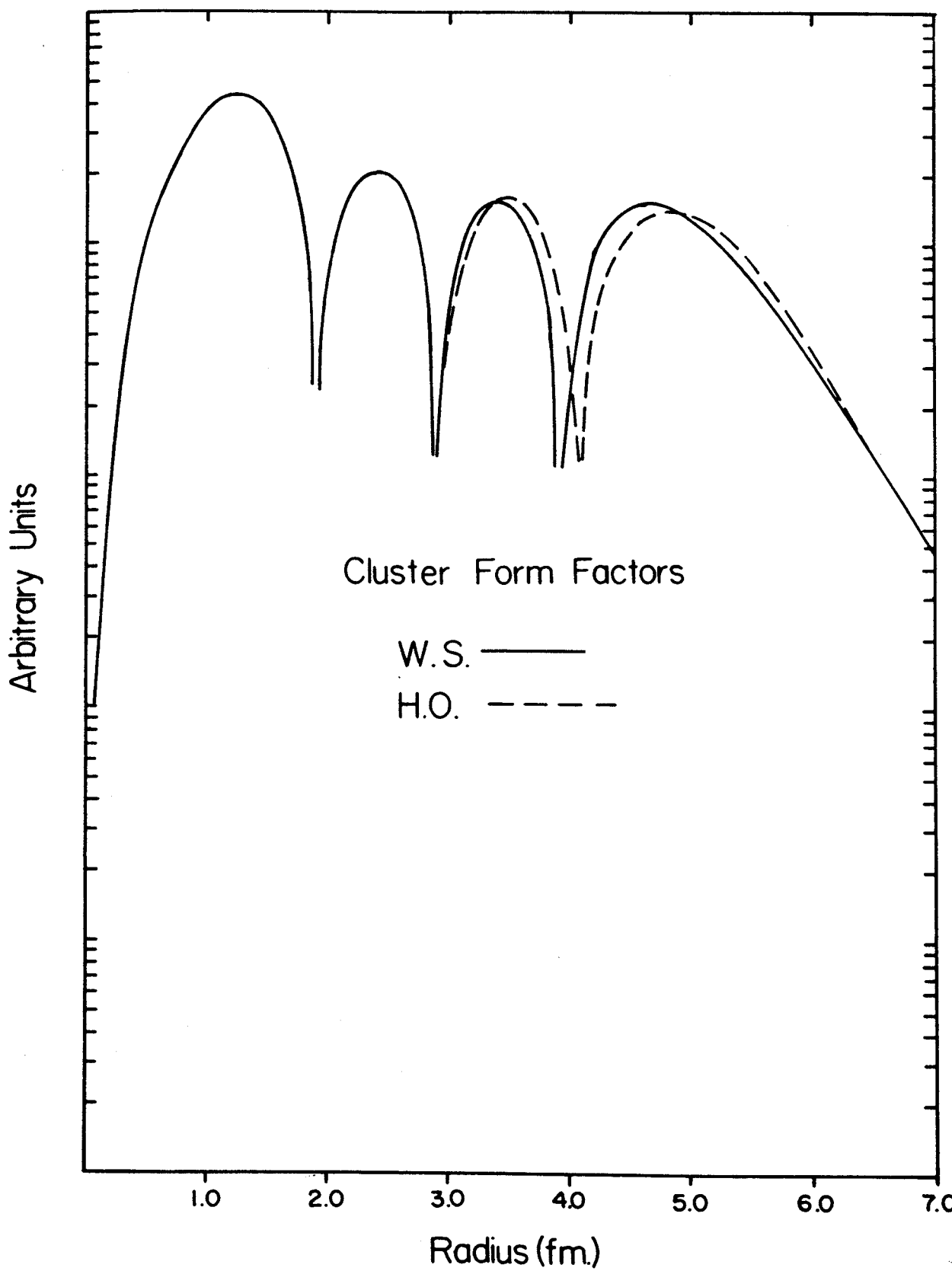
Figure II.9

and ejectile all move on the same line in the zero range theory. In addition, a large angular momentum mismatch can cause great difficulty since both the shapes and magnitudes of the angular distributions are sensitive to the optical parameters, which are poorly determinted for composite particles, when the mismatch is severe.

The finite range effects for the (p,α) reaction have been studied previously by Drisko and Satchler (II.29). They found very little shape dependence for the one case that they reported. We have performed exact finite range calculations using the code LOLA (II.30) for a number of transitions. No spin-orbit potential is allowed in this code so the comparison to zero range calculations done with DWUCK72 (II.27) must be done without spin-orbit coupling in the proton optical parameters. The results of an $\ell = 3$ calculation using the microscopic Woods-Saxon $(0f7/2)^3$ form factor from Figure II.4 is shown in Figure II.10. There do not appear to be strong shape changes that can be attributed to finite range effects. This is very fortunate since the spin-orbit coupling is necessary to reproduce the j-dependence that has been observed. The lack of finite range dependence may be attributed to the choice of optical parameters. To first order the largest finite range effect is to reduce the contribution of the nuclear interior to the transition matrix element. To some extent this may also be accomplished by a judicious choice of the optical parameters. It has been noted previously for the (d,α) reaction that finite range

Figure II.10

A comparison of an exact finite range DWBA calculation and a zero range DWBA calculation. The microscopic Woods-Saxon model form factor shown in Figure II.4 was used in both calculations. The calculations were done without spin-orbit coupling in the proton channel. $E_p = 35$ MeV.

DWBA : Finite Range vs. Zero Range

$^{52}Cr(p, \alpha)^{49}V$ L = 3

Z.R. - - -
F. R. ———

$d\sigma/d\Omega$ (Arbitrary Units)

C.M. Angle (degrees)
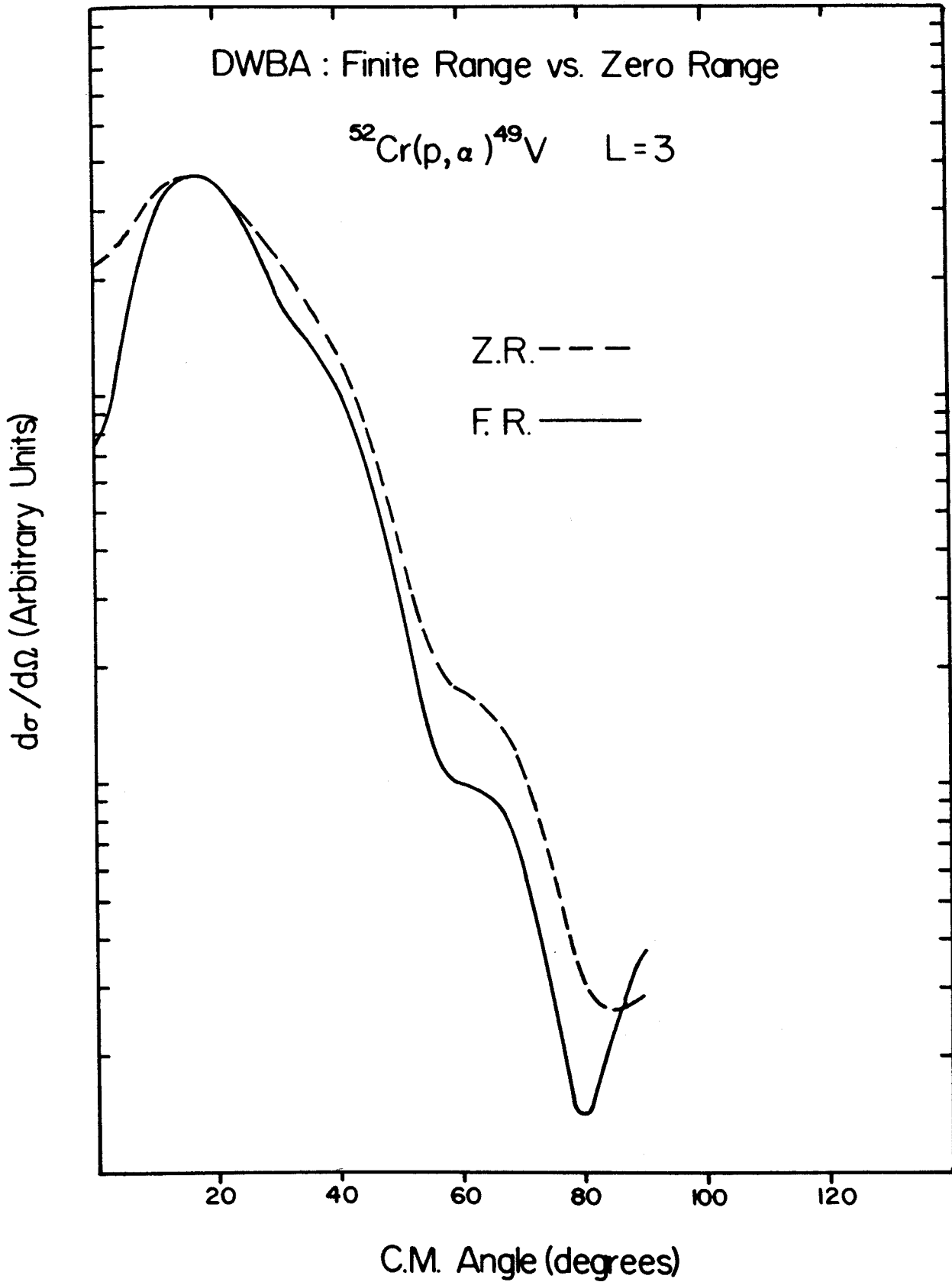
Figure II.10

effects are minimized if the "well matched" optical potentials are chosen (II.31). The optical parameters which we have used have the same geometry and have real well depths of about 50 MeV for the proton channel and about 200 MeV for the α-particle potential. These are the well matching conditions.

The angular momentum mismatch may be illustrated in a number of ways. A classical approximation which is frequently used is to assume that the reaction takes place at the nuclear surface and that the ejectile is emitted at 0°. Under this assumption the classical change in angular momentum is

$$\Delta \ell = \left| \frac{r\,(p_p - p_{\alpha'})}{\hbar} \right| .$$

For the ^{52}Cr case which we have been considering, $\Delta \ell$ is about 6. For the (p, α) reaction on Te, where the Q-value is more positive and the radius is larger, $\Delta \ell$ may go as high as 9 or 10. Since most ℓ-transfers are between 0 and 5, they do not meet the angular momentum requirements and are suppressed. Classically they would not occur at all.

A quantum mechanical way of looking at this effect is to examine the elastic scattering reflection coefficients. Most of the reaction cross section comes from a few partial waves near the one which has $|\eta_L| \cong .5$. A plot of the reflection coefficients vs. L is displayed in Figure II.11. The gap at $|\eta_L| \cong .5$ between the two curves is about

Figure II. 11

Reflection coefficients for proton and α-particle elastic scattering.

Figure II.11

$8\hbar$. In other words, this picture predicts an even larger angular
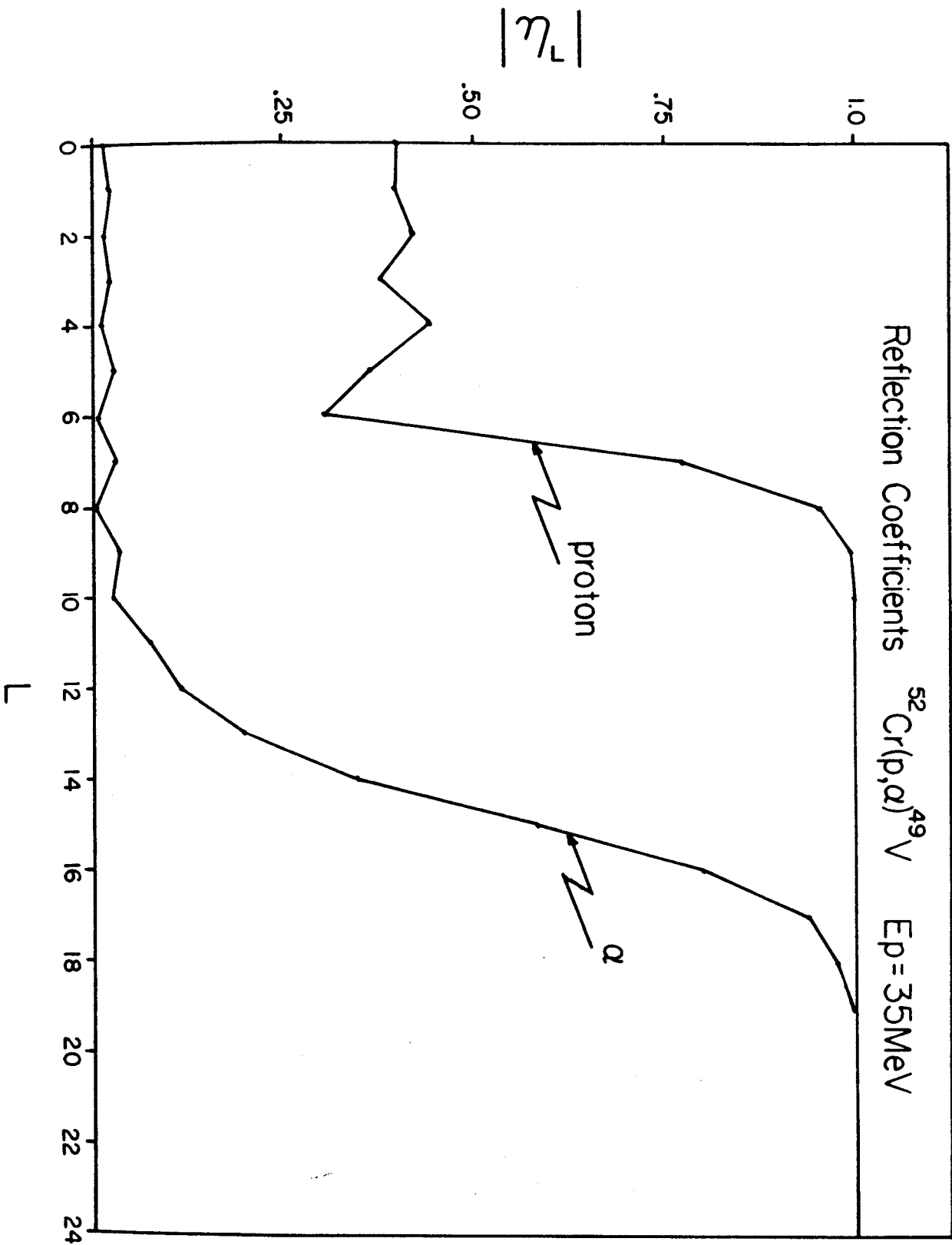
momentum transfer is favored.

Another point is apparent in Figure II.11. The partial waves

with L less than 11 for the α-particle are completely absorbed. Hence,

they do not contribute to the elastic scattering. A study of 40 MeV

α-scattering from Ni has shown that the lowest 14 partial waves can

be ignored without changing the elastic scattering calculations by more

than a few percent (II.32). If these partial waves turn out to dominate

the (p,α) cross section, the DWBA may be sensitive to changes in the

optical parameters and the nuclear interior.

The magnitude of the contribution of the individual α-particle

partial waves to the cross section can be determined by examining the

radial integrals. This has been done by Stock et al. (II.33) for the

$(^3\text{He},\alpha)$ reaction. It is better to go one step further and look at the

quantity

$$
A_{L_\alpha} = \left| \sum_{J_p L_p} i^{L_\alpha - L_p - \ell} (L_p 0 s_p \tfrac{1}{2} | J_p \tfrac{1}{2})(L_\alpha (\tfrac{1}{2}-m) jm | J_p \tfrac{1}{2})(2L_\alpha + 1) \right.
$$

$$
\left. \cdot (L_\alpha 0 \ell 0 | L_p 0)\sqrt{2(2j+1)(2L_\alpha+1)(2L_p+1)} \begin{Bmatrix} L_\alpha & 0 & L_\alpha \\ \ell & \tfrac{1}{2} & j \\ L_p & \tfrac{1}{2} & J_p \end{Bmatrix} I^{\ell s j}_{J_p L_p L_\alpha L_\alpha} \right|.
$$

The radial integrals are

$$
I^{\ell s j}_{J_p L_p L_\alpha L_\alpha} = \int \chi^*_{L_\alpha L_\alpha}(r_\alpha) f^{\ell s j}(r_1) \chi_{J_p L_p}(r_p) dr_p dr_\alpha.
$$

The quantity A includes all the radial matrix elements that go with the

L_α partial wave. Previous workers have chosen to examine only one

term of this sum. For the sake of calculation, m can be taken to be 1/2. Figure II.12 is a graph of A vs. L_α for a few angular momentum transfers. The two different curves in each box are for the two different j values that are associated with the ℓ-transfer.

The first thing to notice is that essentially all the important L_α values are the ones that are poorly determined by elastic scattering. The only exception is the $\ell = 9$ transfer.

Perhaps the most striking feature of these plots is the difference between the $1/2^-$ and $3/2^-$ curves. It is not surprising that the DWBA predicts these transfers to have very different angular distributions. The $1/2^-$ transfer is dominated by the sixth and seventh partial waves, while the $3/2^-$ transition is spread over a much larger group of partial waves. The radial matrix elements are the same for these two transfers since they do not know about the j-value unless the form factor depends on j. However, some of these radial matrix elements do not contribute to the sum for the $1/2^-$ transfer because they do not satisfy the selection rule implied by

$$(L_\alpha 0 \tfrac{1}{2} \tfrac{1}{2} | J_p \tfrac{1}{2}).$$

The possible values for L_p are $L_\alpha + 1$ and $L_\alpha - 1$. The possible values of J_p are $L_p + \tfrac{1}{2}$ and $L_p - \tfrac{1}{2}$. If J_p is $L_p - \tfrac{1}{2}$, then all the radial integrals with $L_p = L_\alpha - 1$ will not be allowed since this implies that $J_p = L_p - 3/2$. Similarly for $J_p = L_p + \tfrac{1}{2}$, the set of radial matrix elements with $L_p = L_\alpha + 1$ cannot contribute. For the $3/2^-$ transfer all the radial integrals will contribute to the sum.

Figure II.12

A plot of $|A_{L_\alpha}|$ vs. L_α. $|A_{L_\alpha}|$ is proportional to the contribution of the L_α partial wave to the cross section. The calculations are for the $^{52}Cr(p,\alpha)^{49}V$ reaction at $E_p = 35$ MeV.
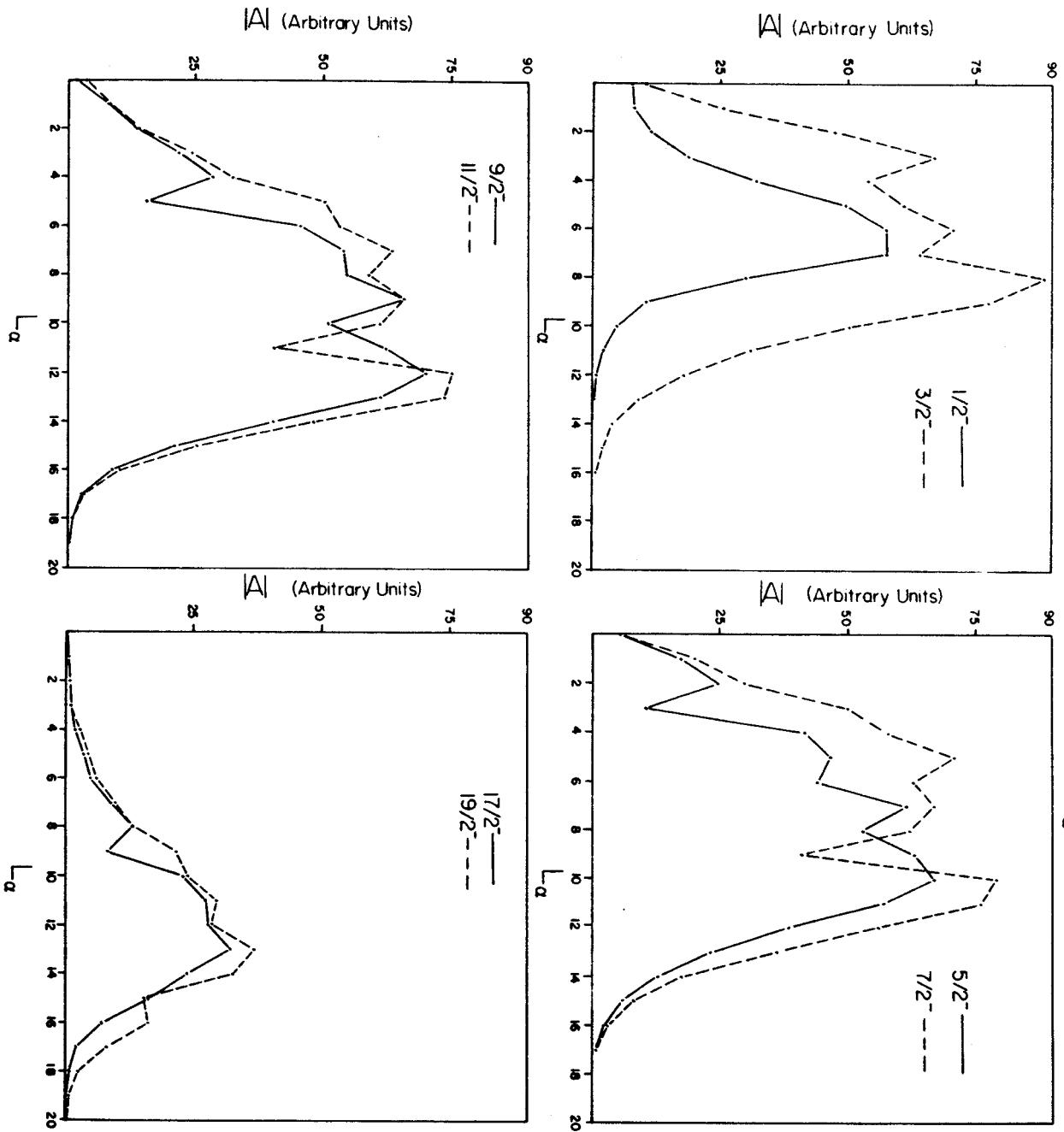
Figure II.12

The j-dependence which is so apparent in the $\ell = 1$ graph is much more subtle for the other three cases in Figure II.12. This is because many partial waves contribute to each term. Even though one less proton partial wave is involved in the $j_<$ sum, there are still enough partial waves involved to give a broad distribution of strength.

This would seem to indicate that the j-dependence may be the result of simple angular momentum selection rules. To test this hypothesis the sign of the spin-orbit potential in the proton channel can be changed. Since the sharply peaked distribution for the $1/2^-$ transfer is basically the result of angular momentum selection rules changing the sign of the potential should not change this distribution much. Therefore, the angular distribution should not change. Figure II.13 shows the angular distributions for the $1/2^-$ and $3/2^-$ transfers when the spin-orbit sign is reversed. The angular distributions are nearly reversed. The oscillations are nearly gone in the $1/2^-$ curve where the $3/2^-$ curve now has peaks and valleys which were not previously apparent. Therefore, the j-dependence is not caused by the number of radial matrix elements that are allowed.

The only other effect that the spin-orbit potential has is to change the shape of the proton optical potential. The effect is something like increasing the radius of the real volume term for the $j_>$ member and decreasing the radius for the $j_<$ member. The j-dependence can be investigated by turning off the spin-orbit force and changing the radius

Figure II.13

DWBA calculations for the ^{52}Cr(p,α)^{49}V reaction with the wrong sign for the spin-orbit potential in the proton channel. E_p = 35 MeV.

L=1 DWBA   Wrong Sign for V_{SO}

1/2

3/2

Arbitrary Units

C.M. Angle (degrees)
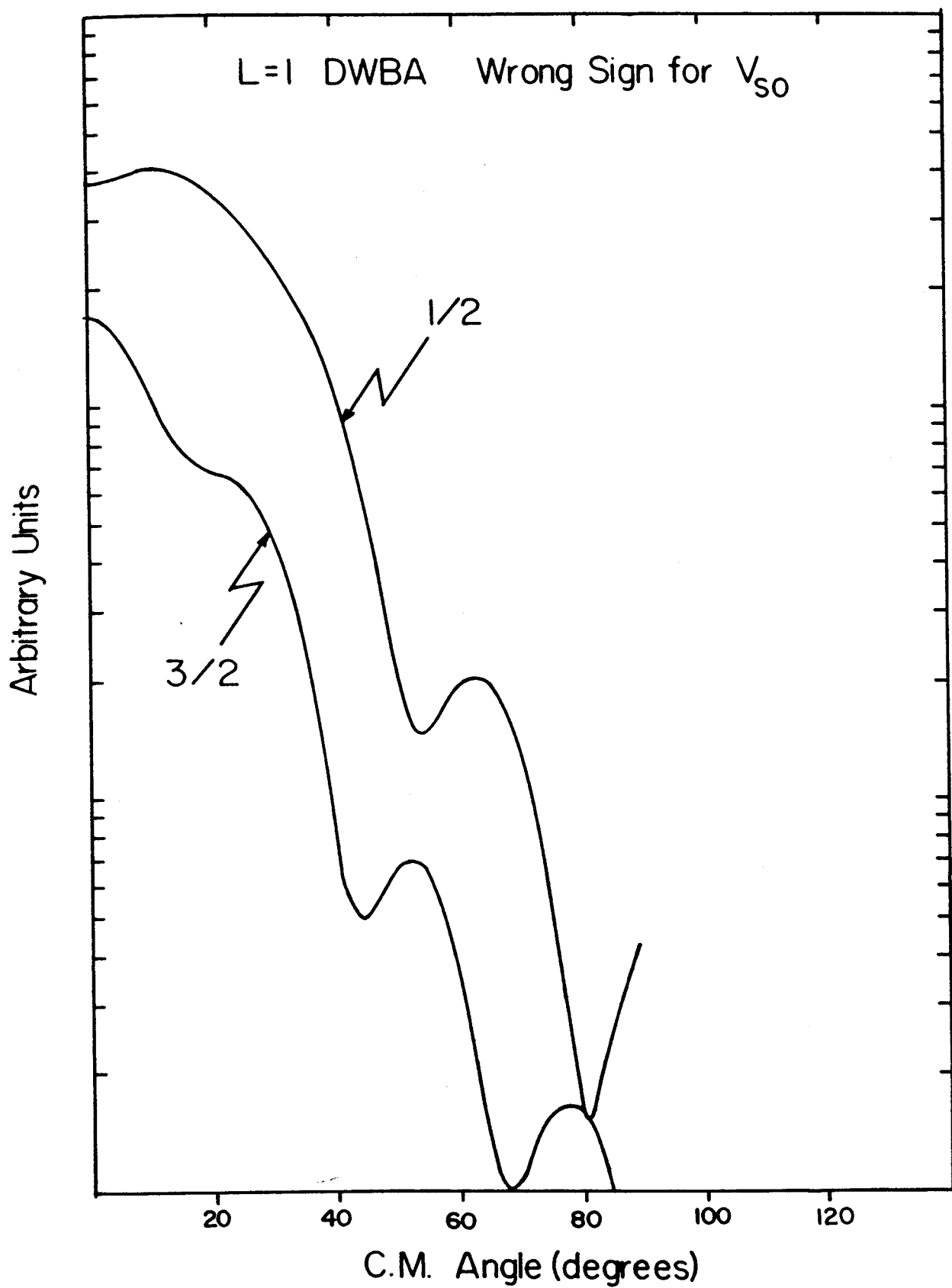
Figure II.13

of the real well in the proton channel. The results of this procedure are shown for an $\ell = 1$ transition in Figure II.14. The $1/2^-$ structure is apparent for small radii, while the washed out $3/2^-$ shape appears for larger radius parameters. This appears to be the source of the j-dependence.

j-dependence still remains a puzzle, even though we seem to have isolated the source. The above discussion seems to imply that there should be a larger j-dependence for the (p,d) reaction than is observed. It seems clear that the α-particle must play an important role in the j-dependence in the (p,α) reaction while the deuteron is less important to j-dependence in the (p,d) reaction. Qualitatively this may be understood, if the α-particles come from the nuclear surface, since changing the proton optical potentials in the way that we have causes the region of high proton flux on the back surface of the nucleus to change rapidly across the surface.

K. Conclusions

Two methods of calculating microscopic form factors for the (p,α) and (α,p) reactions have been found to produce consistent results. When hankel tails are matched to form factors calculated using harmonic oscillator wavefunctions, the form factors have been shown to be nearly equivalent.

The correction for the center of mass motion has been carried out on the harmonic oscillator model. This correction is mainly a

Figure II. 14

DWBA calculations for the $^{52}Cr(p,\alpha)^{49}V$ reaction without the spin-orbit potential in the proton channel. The real well radius of the proton optical potential is varied to mock-up the effect of V_{SO}. $E_p = 35$ MeV.
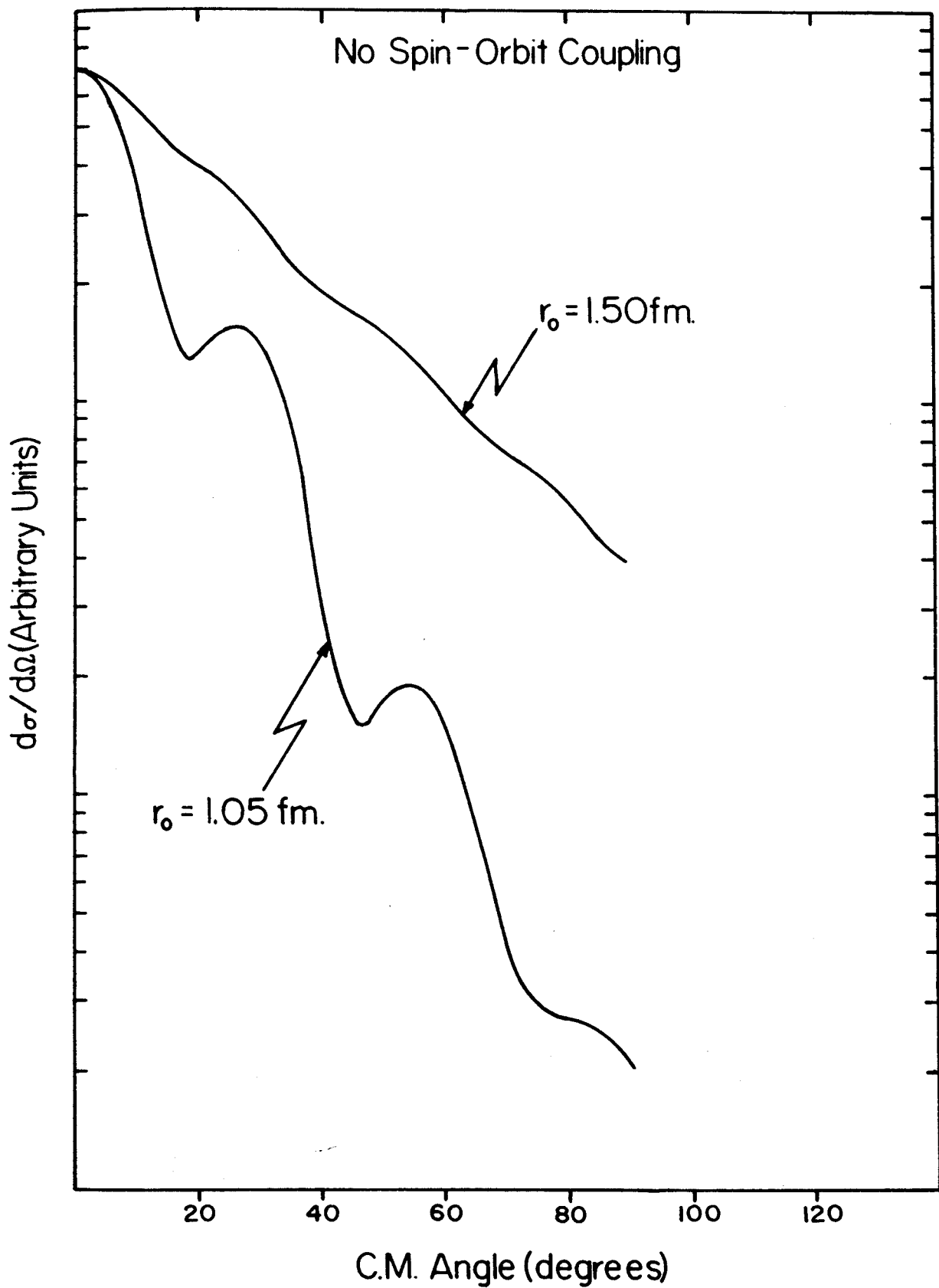
Figure II.14

multiplicative factor. Hence, we conclude that a reasonable form factor can be corrected by multiplying by $(A/(A-3))^{N+\ell/2}$ where N is the number of nodes in the form factor.

It has also been shown that a mass three cluster spectroscopic factors can be calculated microscopically using the harmonic oscillator model. The form factor for a mass three particle in an oscillator potential has been found to be similar to that of a mass three particle in a Woods-Saxon well if a hankel tail is matched to the oscillator form factor. We conclude that spectroscopic factors calculated by using either cluster form factor model can be calculated microscopically by the method given in section six.

The cross section of pure configurations on the angular momentum coupling has been investigated. It has been found that the $j_>$ member of a spin-orbit pair is always predicted to have more yield, if coherence is neglected.

The use of zero range DWBA has been tested and found to be adequate. Finite range calculations indicated that angular distribution shapes are not affected by finite range effects.

Angular momentum matching has been studied. The (p,α) and (α,p) reactions have been found to be severely mismatched so that detailed fits are not expected to be good and sensitivity to optical parameters is expected.

Finally the cause of j-dependence has been investigated. It appears that j-dependence is not a result of differences in the number of partial waves that contribute to the $j_<$ and $j_>$ transitions. The j-dependence seems to come from the change in shape of the real well in the proton optical potential which is caused by the spin-orbit force.

REFERENCES FOR CHAPTER II

II.1   R. Sherr, Proceedings of the Conference on Direct Interactions and Nuclear Reaction Mechanisms, University of Padua, edited by E. Clementel and C. Villi (1962), 205.

II.2   J. A. Nolen, Jr., Ph.D. thesis, Princeton University (1965), unpublished.

II.3   J. A. Nolen, Jr., C. M. Glashausser, and M. E. Rickey, Phys. Lett. 21 (1966), 705.

II.4   L. L. Lee, Jr., A. Marinov, C. Mayer-Boricke, J. P. Schiffer, R. H. Bassel, R. M. Drisko, and G. R. Satchler, Phys. Rev. Lett. 14 (1965), 261.

II.5   R. J. Petersen and H. Rudolph, Nucl. Phys. A241 (1974), 253.

II.6   Michel Vergnes, Georges Rotbard, Jacques Kalifa, and Genevieve Berrier-Ronsin, Phys. Rev. C10 (1974), 1156.

II.7   Yong Sook Park, H. D. Jones, and D. E. Bainum, Phys. Rev. C7 (1973), 445.

II.8   R. K. Bhowmik, R. G. Markham, M. A. M. Shahabuddin, and J. A. Nolen, Jr., Bull. Am. Phys. Soc. 20 (1975), 1164, private communication.

II.9   D. F. Bayman, Nuclear Spectroscopy with Direct Reactions II, Argonne National Lab. Report ANL-6878 (1964), 335.

II.10   R. O. Ginaven, Ph.D. thesis, Massachusetts Institute of Technology (1966).

II.11   H. J. Mang, UCRL-8931 Lawrence Radiation Lab. Report (1959).

II.12   R. O. Ginaven and A. M. Bernstein, Nucl. Phys. A154 (1970), 417.

II.13   S. H. Suck and W. R. Coker, Nucl. Phys. <u>A176</u> (1971), 89.

II.14   Tetsuo Kammuri and Hiroshi Yoshida, Nucl. Phys. <u>A137</u> (1969), 641.

II.15   J. D. McCullen, B. F. Bayman, and Larry Zamick, Princeton University Technical Report NYO-9891 (1964).

II.16   J. W. Smits, F. Iachello, R. H. Siemsen, and A. van der Woude, Phys. Lett. <u>53B</u> (1974), 337.

II.17   J. W. Smits and R. H. Siemsen, Nucl. Phys. <u>A261</u> (1976), 385.

II.18   W. R. Falk, Phys. Rev. <u>C8</u> (1973), 1757.

II.19   W. R. Falk, A. Djaloeis, and D. Ingham, Nucl. Phys. <u>A252</u> (1975), 452.

II.20   Y. F. Smirnov, Nucl. Phys. <u>27</u> (1961), 177.

II.21   B. F. Bayman and A. Kallio, Phys. Rev. <u>156</u> (1967), 1121.

II.22   Taro Tamura, Physics Reports <u>14C</u>, 2.

II.23   R. G. Markham, private communication.

II.24   M. Ichimura, A. Arima, E. C. Hilbert, and T. Terawasa, Nucl. Phys. <u>A204</u> (1973), 225.

II.25   C. R. Dingham, K. van der Borg, R. J. de Meijer, and A. van der Woude, Bull. Am. Phys. Soc. (April 1976).

II.26   C. W. de Jager, H. de Vries, and C. de Vries, Nuclear Data Tables <u>14</u> (1974), 489.

II.27   P. D. Kunz, unpublished.

II.28   N. K. Glendenning, Nuclear Data Tables.

II.29   R. M. Drisko and G. R. Satchler, Phys. Lett. <u>9</u> (1964), 342.

II.30   R. de Vries, unpublished.

II.31   R. M. Del Vechio and W. W. Daehnick, Phys. Rev. <u>C6</u> (1972), 2095.

II.32   R. M. Drisko, G. R. Satchler, and R. H. Bassel, Phys. Lett.
        $\underline{5}$ (1963), 347.

II.33   R. Stock, R. Bock, P. David, H. H. Duhm, and T. Tamura,
        Nucl. Phys. $\underline{A104}$ (1967), 136.

CHAPTER III

EXPERIMENTAL CONSIDERATIONS

The (p,α) reaction presents a number of experimental problems.
The bombarding energy must be sufficient to insure that the reaction
proceeds by direct pick-up. In addition, it is desirable to be looking
at α-particles that are much more energetic than the boil-off and decay
α-particles so as to not be hindered by background from these
processes. Sherr et al. (III.1) have found that proton energies above
17 MeV are sufficient to observe direct reaction α-particles for nuclei
in the nickel region.

The density of final states is frequently very high. An energy
resolution of 20 keV FWHM, or better, is desirable to resolve a
reasonable number of states.

Typical cross sections are of the order of 10μb/sr. The strongest
peaks may be as large as 200μb/sr., while many weak transitions may
be observed at the 1μb/sr. level. In order to observe such small cross
sections, a system to cleanly identify the α-particles in the midst of a
sea of other reaction products is required.

The 35 MeV proton beam was chosen because it satisfies the
experimental requirements and because it is a reliable beam for the

M.S.U. cyclotron to produce. 35 MeV is sufficiently above the
Coulomb barrier, even for lead, to insure that boil-off α-particles are
not a problem. Many high resolution (p,p') experiments have been
performed in the last couple of years using this beam. Energy resolu-
tion as good as 1.5 keV FWHM has been obtained with this beam in
test situations. The cyclotron and beam line settings for this high
quality beam are highly reproducible. Furthermore, beam currents of 2
to 3 μA on target are obtained with relative ease at this energy.

An Enge split pole magnetic spectrograph is an ideal instrument
for studying low cross section reactions with good energy resolution.
The spectrograph aperture may be as large as 1.2 msr. without
degrading the resolution to worse than about 5 keV FWHM at 30 MeV
particle energy. The small cross sections require the largest possible
solid angles and the highest possible beam currents.

The (p,α) reaction is a bit more difficult to study with a spectro-
graph than most reactions because protons and α-particles have the
same magnetic rigidity (m/q^2) causing protons and α-particles of the
same energy to be focused at the same place in the focal plane of the
spectrograph. Most (p,α) reactions have Q-values near zero, some
slightly negative and others a bit positive. Thus the region of the
focal plane which contains the α-particle spectrum is riddled with
strong proton groups. In addition, there is a continuum of lower
energy deuterons and tritons in the same region. The focal plane

detector must be able to cleanly identify α-particles while rejecting protons at a high rate.

Photographic emulsions may be used in the focal plane. These emulsions may be purchased with various sensitivities. Since α-particles are highly-ionizing, while protons leave a minimum ionization, insensitive emulsions are called for. Ilford K,1 emulsions (III.2) were used for this purpose. These emulsions have a low enough sensitivity that protons and deuterons pass through without leaving a track. Unfortunately, it was found that tritons did leave tracks that could not be distinguished from the α-particle tracks. It may be that Ilford K,0 emulsions are better for this purpose.

Photographic emulsions have the advantage of being the highest resolution detectors available. In addition, they do not require expensive electronics to operate. However, they must be scanned with off-line microscopes. This process usually takes a number of months for a complete angular distribution. In addition, the triton background can obscure very weak peaks. Therefore, a livetime counting system is desirable.

Most of the spectra taken for this work were recorded with the focal plane counter developed by Markham and Robertson (III.3). Figure III.1 shows a cross sectional view of this counter, while Figure III.2 shows a top view of the front chamber. The ionization track left by the particle is multiplied at the anode wires. Charge is

Figure III.1

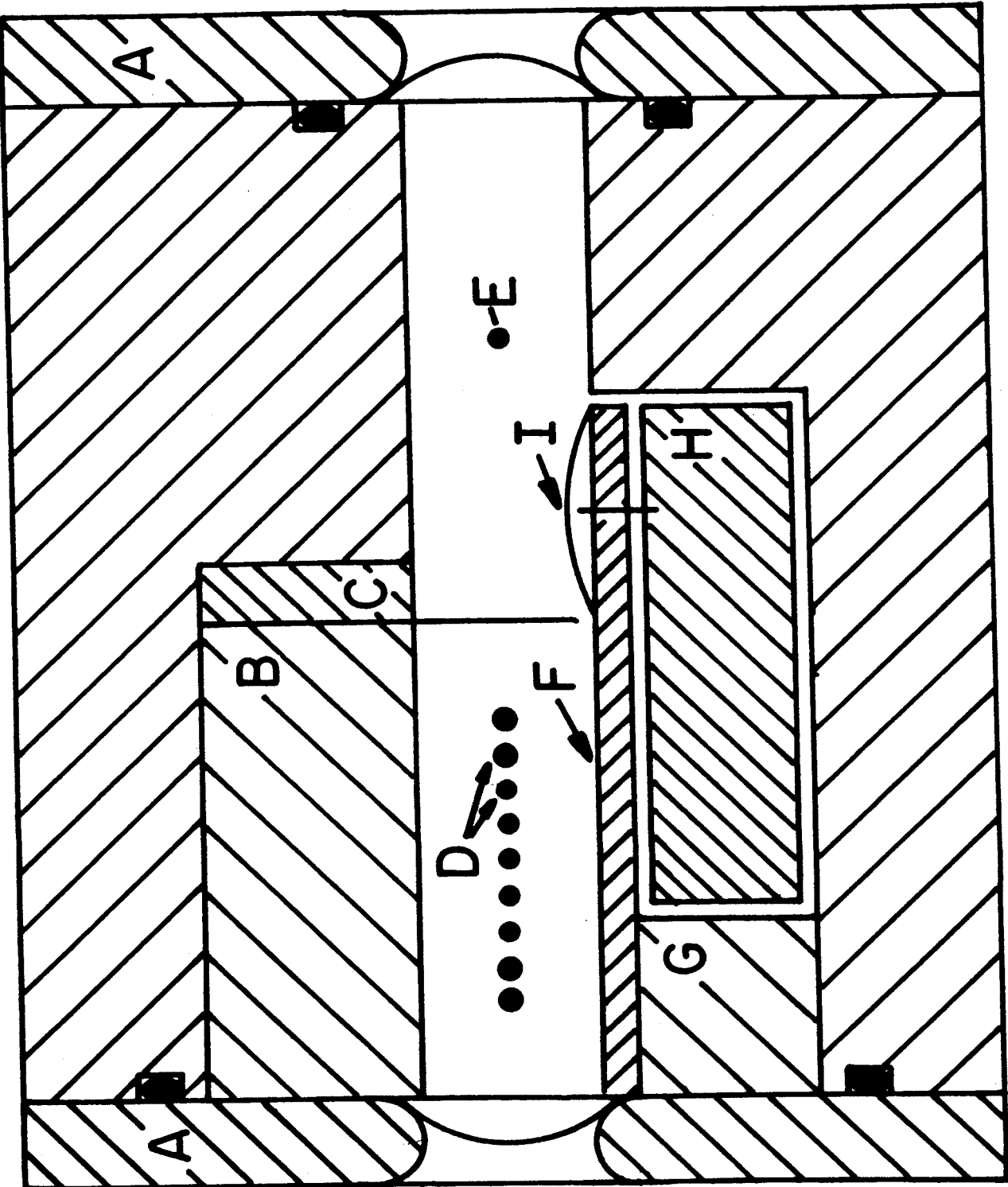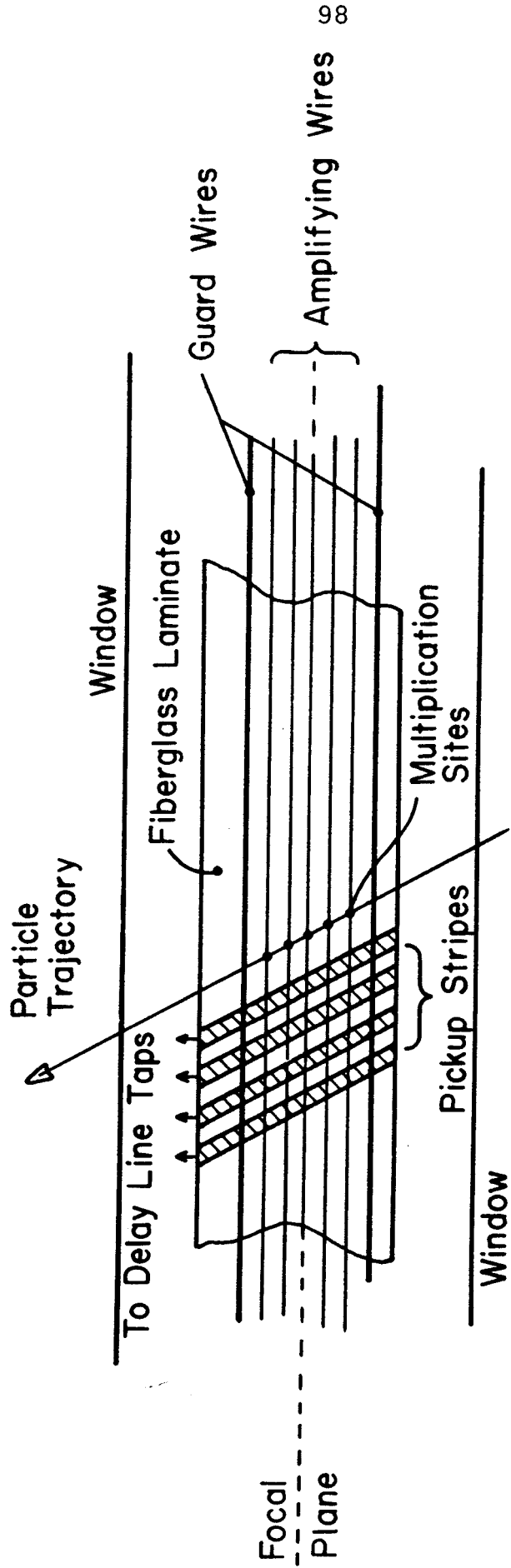Cross sectional view of the focal plane counter.

Figure III.1

Figure III.2

Top view of the focal plane counter.

SCHEMATIC (Plan View) OF "WASHBOARD" COUNTER

Figure III.2

induced on the cathode pick-up stripes below. The induced charge is collected by a delay line. The signal from one end of the delay line is used to start a time to amplitude converter, while the signal from the other end of the delay line is delayed for a period which is longer than the total delay of the delay line and then used to stop the TAC. The resulting pulseheight is the position of the track. The second chamber contains a conventional single wire proportional counter. The signal from this wire is proportional to the energy loss of the particles that pass through the chamber. The α-particles may be identified because they have a larger energy loss than protons, deuterons, tritons, or ^{3}He ions. Further restrictions are necessary to eliminate all the protons. Because of the tremendous number of protons, there are an intolerable number that have the same energy loss as an α-particle even though the probability of such events is very low. The added restriction is obtained by using a plastic scintillator as a third counter mounted behind the exit window of the proportional counter. The anode signal from the photomultiplier can be used to start a TAC which is subsequently stopped by the cyclotron r.f. The resulting signal is a measure of the flight time of the particle through the spectrograph. The time-of-flight requirement easily distinguishes protons from α-particles. Very clean spectra can be obtained if the energy loss and the time-of-flight requirements are used simultaneously. The system count rate is limited by the proton rejection rate if the elastics are on the counter.

The targets need to be $\lesssim 100\,\mu g/cm^2$ thick in order to keep the energy loss of the α-particles from degrading the energy resolution. The targets were made by reducing metal oxides and evaporating the liberated metal. The vapor was condensed on $20\,\mu g/cm^2$ carbon foils.

The details of each experiment are presented in the fourth and fifth chapters.

REFERENCES FOR CHAPTER III

III.1   R. Sherr, Proceedings of the Conference on Direct Interactions and Nuclear Reaction Mechanisms, University of Padua, edited by E. Clementel and C. Villi.

III.2   Ilford Nuclear Research, Ilford Limited, Ilford Essex, England.

III.3   R. G. Markham and R. G. H. Robertson, Nucl. Inst. and Meth. 129 (1975), 131.

CHAPTER IV

FEATURES OF THE $^{52}Cr(p,\alpha)^{49}V$ REACTION

A. Introduction

The (p,α) and (α,p) reactions may prove to be very useful spectro

scopic tools. The qualitative features of these reactions are not well

documented, with the exception of j-dependence for $\ell = 1$ transfers

(IV.1, IV.2, IV.3, IV.4). In this chapter the qualitative features of the

(p,α) reaction as seen in the $^{52}Cr(p,\alpha)^{49}V$ reaction are investigated.

Since three nucleons are transferred, it is possible to study final nuclei

that are not accessible by other pick-up reactions either because the

targets for these reactions are unstable or difficult to make. Final

nuclei in this class are ^{47}V (IV.5, IV.6), ^{51}Mn (IV.6, IV.7, IV.8),

^{55}Co (IV.6, IV.9), and ^{119}Te (IV.10). To understand the spectra of

these unknown nuclei, it is necessary to document the properties of the

(p,α) reaction on nuclei that have been previously studied with simpler

reactions. The $^{52}Cr(p,\alpha)^{49}V$ reaction is a good choice for such a study

in the 0f7/2 shell because ^{49}V has been studied by a number of others

(IV.11, IV.12, IV.13, IV.14, IV.15, IV.16, IV.17, IV.18, IV.19, IV.5).

Previous work in this mass region at beam energies above 17 MeV

has shown that the simple proton hole states that are populated in

102

single proton pick-up reactions dominate the (p,α) spectra (see Reference IV.2, for example). These states seem to be described reasonably well with seniority-one wavefunctions (IV.2). Therefore, we should expect the ^{49}V spectrum to display strong peaks for the 7/2$^-$ ground state and the 3/2$^+$ and 1/2$^+$ sd-shell proton hole states.

In addition to the T = 3/2 proton hole states, the T = 5/2 analogs of the neutron hole states in ^{49}Ti should also be populated. These states are not isospin allowed in the ^{50}Cr(d,^{3}He)^{49}V or ^{50}Cr(t,α)^{49}V reactions. Experimental observation of analog states with the (p,α) reaction has not been previously demonstrated except for some tentative assignments by Bardin and Rickey (IV.20) using Ti isotope targets.

Multi-particle transfer reactions offer the chance to study high spin states. For some time now the (α,xnγ) reactions have been used to populate such states. Recently heavy ion induced reactions such as (^{19}F,p2nγ) have been used to find high spin states such as the 12$^+$ in ^{44}Ti (IV.21). If two 0f7/2 neutrons and a 0f7/2 proton are picked up via the (p,α) reaction, it is possible to reach final states via J$^\pi$ transfers of up to 19/2$^-$. The (p,α) reaction on ^{51}V could, in principle, then, directly populate the 12$^+$ in ^{48}Ti. If the proton comes from the 0d3/2 orbit, 15/2$^+$ is the maximum J$^\pi$ transfer. A study of the ^{90,92,94,96}Zr(p,α) reactions has concentrated on this aspect of the reaction. Spins up to 15/2$^-$ were observed in that work (IV.22). The maximum coupling of (0d5/2)^3, which is 13/2$^+$, has been observed in ^{23}Na(p,α)^{20}Ne, ^{12}C(α,p)^{15}N, and ^{16}O(α,p)^{19}F (IV.23, IV.24, IV.25).

Lee et al. (IV.1) have shown that the j-dependence is a result of spin-orbit coupling in the proton optical potential. The j-dependence for the $J^\pi = 1/2^-$, $3/2^-$ spin-orbit pair is reproduced by DWBA calculations using mass three cluster form factors (for example, see Reference IV.22). The reliability of j-dependence for higher ℓ-values is still an open question. Studies of the $\ell = 2$ and 3 transfers are confusing (IV.4, IV.26). Much of this confusion is apparently the result of important structure effects in the sd-shell. A study of the ^{24,26}Mg$(p,\alpha)^{21,23}$Na reactions shows that the angular distributions for states with the same J^π values sometimes have very different shapes (IV.27). It would seem that j-dependence will only be a useful tool if the shapes of the angular distributions are insensitive to the detailed structures of the states. This may be the case for targets that are heavier than those in the sd-shell.

The most common method of using the DWBA to predict the shapes of angular distributions for (p,α) and (α,p) studies has been to do zero-range calculations which employ mass three cluster form factors. These calculations can fit the data reasonably well in many cases. In regions where nuclear structure does not affect the shapes of the angular distributions, it may be possible to use these calculations to make J^π assignments (IV.22, IV.28).

Recently a few microscopic reaction models have been developed (see Chapter II and IV.24, IV.29, IV.30, IV.31). Such models may

make it possible to predict both shapes and magnitudes of the angular

distributions even when nuclear structure effects are important, pro-

vided detailed wavefunctions are available.

In the sections to follow we will look into the general features

of the data, try to evaluate the reliability of the $\ell = 2$ and 3

j-dependence for this case, check the use of the DWBA using cluster

form factors, and test DWBA calculations based on the microscopic

form factors described in Chapter II.

B. Experimental Method and Data

The 35 MeV proton beam from the Michigan State University

isochronous cyclotron was used to bombard an isotopically enriched

^{52}Cr target. The reaction products were momentum analyzed in an

Enge split pole spectrograph and detected with the delay line counter

developed by Markham and Robertson (IV.32). Position and energy loss

information were taken from this counter, while a plastic scintillator

placed behind the counter was used to obtain particle time-of-flight

information relative to the cyclotron r.f. structure. The α-particles

were cleanly identified by their energy loss in the counter and their

time-of-flight. An over-all energy resolution of 20 KeV FWHM was

obtained with this system.

The target thicknesses were typically 20 to 40 $\mu g/cm^2$. The

thicknesses were measured by comparing proton elastic scattering on

the second maximum of the elastic scattering angular distribution to

the results of optical model predictions. Targets $\lesssim 100\,\mu g/cm^2$ were necessary to keep the energy loss of the α-particles to a minimum. However, the thermal coefficient of expansion of Cr presented a further constraint on the target thickness. The targets were made by reducing $^{52}Cr_2O_3$ with tantalum and simultaneously evaporating the liberated Cr. The Cr was deposited on $20\,\mu g/cm^2$ carbon foils. When the target reached a thickness of $\sim 50\,\mu g/cm^2$, the backing would break thereby imposing an upper limit on the target thickness obtainable by this technique.

Because of the thin targets, large solid angles and high beam currents were necessary. For the most part, a solid angle of 2.0 msr. and a beam current of $2.5\,\mu A$ were used.

A few spectra were also recorded on photographic emulsions in order to obtain more precise values for the excitation energies and better resolution. One of these spectra is shown in Figure IV.1. The resolution is about 10 keV FWHM. The three strong peaks are the $7/2^-$ ground state, the $3/2^+$ proton hole state at 0.748 MeV, and the 1.646 MeV, $1/2^+$ proton hole state. In addition, there is a tall peak due to the 1.95 MeV $5/2^+$ hole state in ^{29}P which is the result of ^{32}S impurity in the target. The wide peak near channel 1650 is the ^{13}N ground state, which is kinematically out of focus.

A log plot of the same spectrum is shown in Figure IV.2. It is immediately evident that there are a great number of weaker states in

Figure IV. 1

The ^{52}Cr(p,α)^{49}V spectrum at 16° plotted on a linear scale. The spectrum was recorded on a photographic emulsion.
$E_p = 35$ MeV; FWHM $\sim$ 10 keV.

Figure IV.1

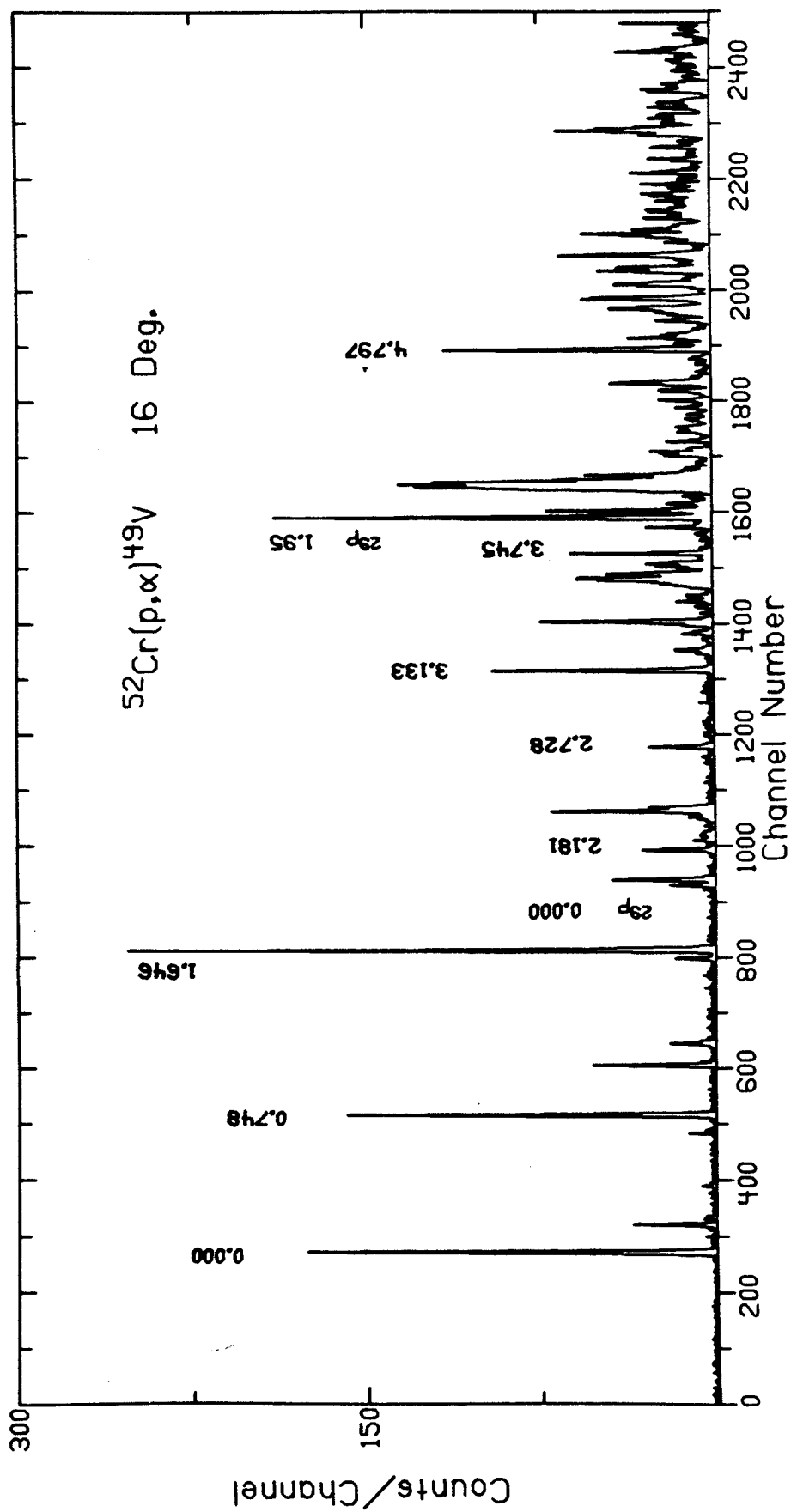Figure IV. 2

The same spectrum as Figure IV. 1 but plotted on a log scale.

$^{52}Cr(p,\alpha)^{49}V$ 16 Deg.

0.000
0.748
1.646
2.181
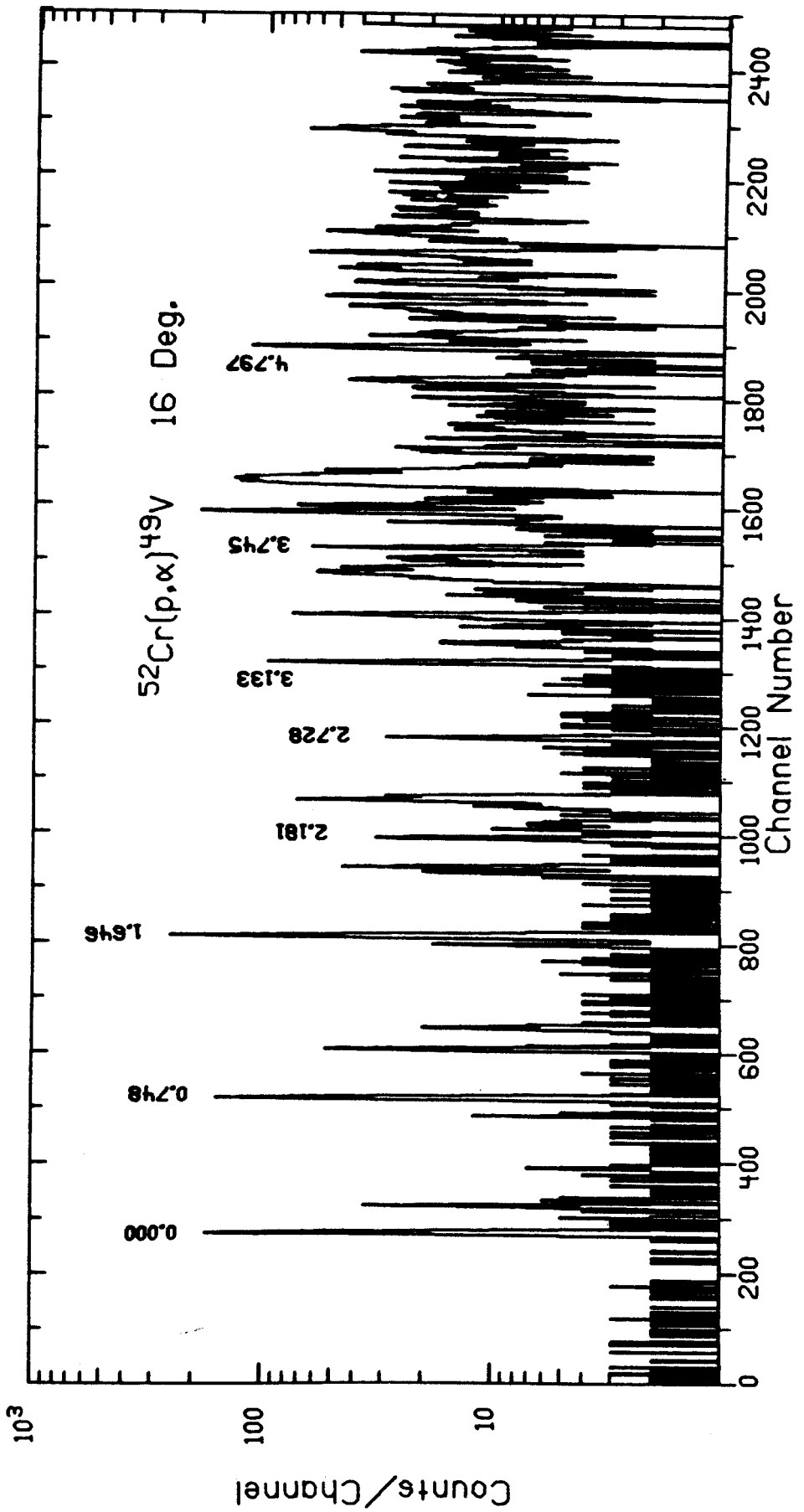2.728
3.133
3.745
4.797

Channel Number

Counts/Channel

Figure IV.2

addition to the proton hole states. The background counts are probably

triton tracks on the plate that could not be distinguished from the

α-particle tracks. Ilford K,1 emulsions (IV.37) were used for this work.

These emulsions are insensitive to the inelastic proton groups which

struck the plate, but discrimination against tritons was not possible.

A spectrum taken at the same angle with the counter system is

shown in Figure IV.3. This spectrum is much cleaner because the tri-

tons cannot satisfy the time-of-flight requirement. In this case the

resolution is about 20 keV FWHM.

In order to look for the $T = 5/2$ proton hole states, the spectro-

graph field was adjusted so that the high rho end of the counter was

located at approximately 4 MeV excitation energy. This allowed for

about one and a half MeV of overlap with the lower excitation spectra.

Typical spectra for the high excitation region are displayed in

Figure IV.4. At forward angles the break-up of ^{9}B, made by the

^{12}C$(p,\alpha)^9$B reaction, causes a large background as can be seen in the

top half of Figure IV.4. The bottom half of Figure IV.4 contains the

55-degree spectrum where the ^{9}B has kinematically shifted out of the

way. The three sharp peaks are the $7/2^-$, $1/2^+$, and $3/2^+$ $T = 5/2$

analogs of states in ^{49}Ti. The excitation energies of these levels are

compared with the corresponding levels in ^{49}Ti in Table IV.1.

Figure IV.3

The ^{52}Cr$(p,\alpha)^{49}$V spectrum at 16° recorded with the counter system.
E_p = 35 MeV; FWHM ~ 20 keV.
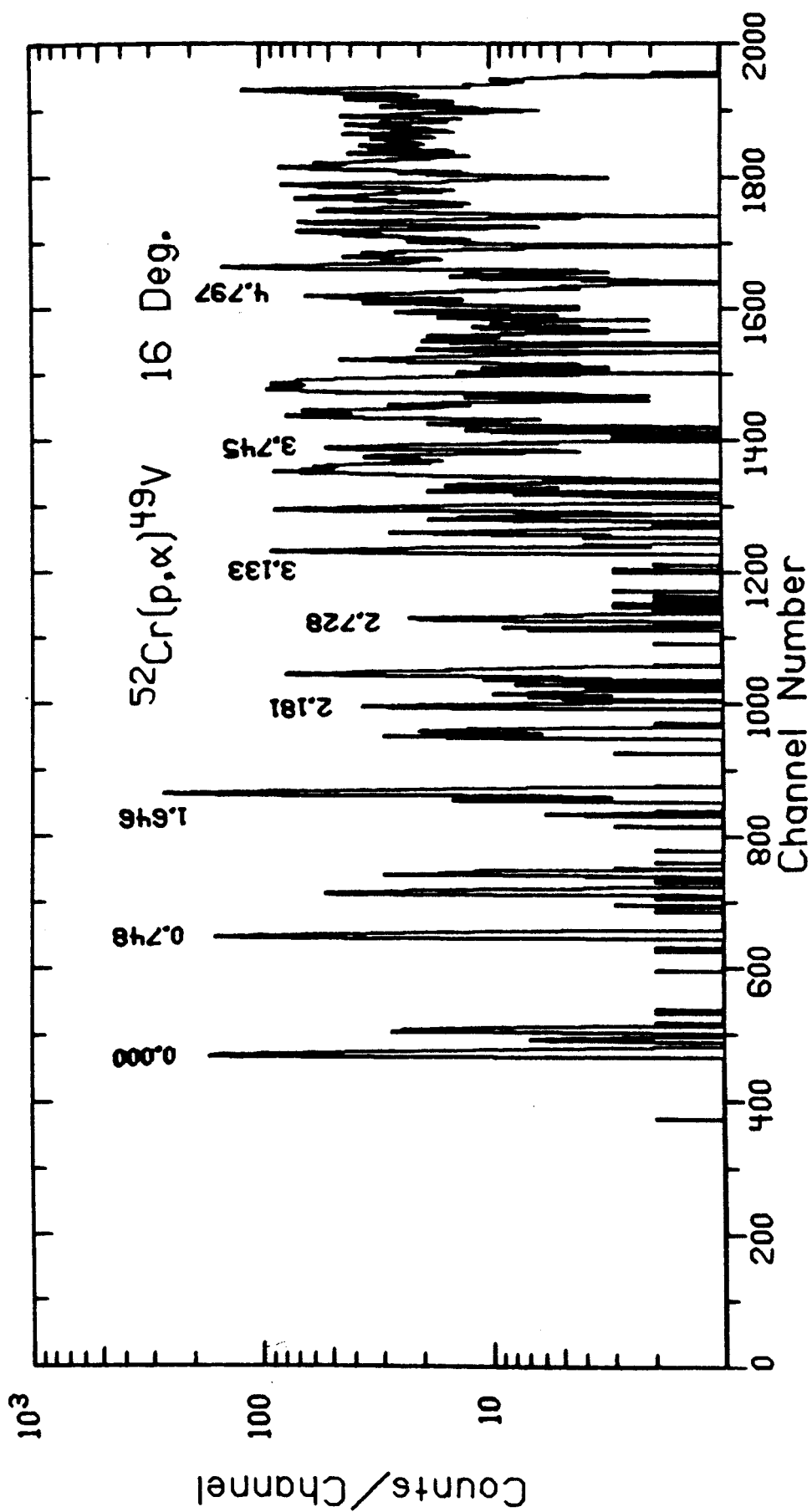
Figure IV.3

Figure IV.4

High excitation spectra showing the $T = 5/2$ proton hole states in ^{49}V.
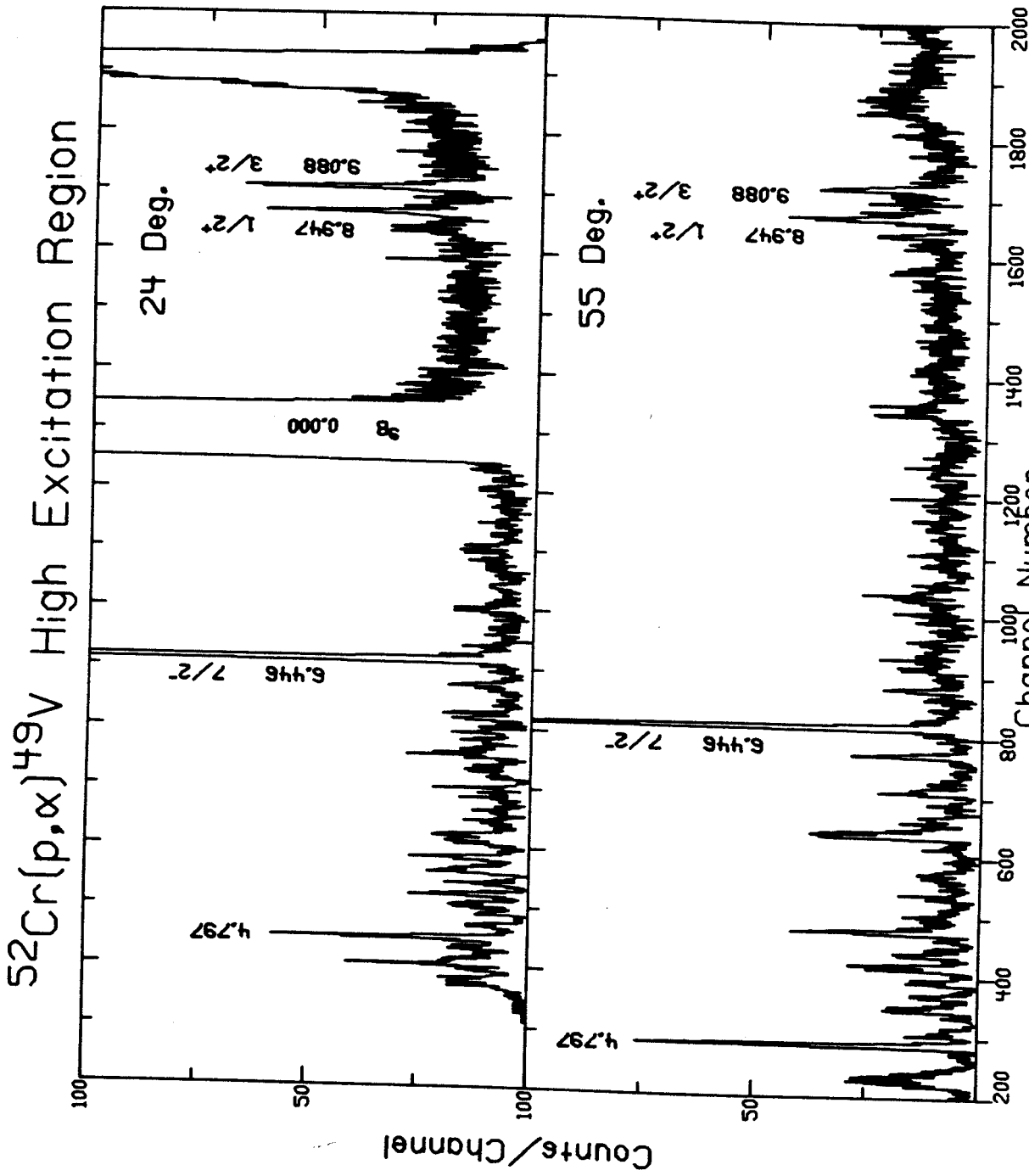
Figure IV.4

TABLE IV.1

T = 5/2 ENERGIES

^{49}V	Excitation	E_c	Differential	^{49}Ti (MeV)
$7/2^-$	$6.446 \pm .020$	$7.848 \pm .03$	---	0.000
$1/2^+$	$8.947 \pm .025$	$7.848 \pm .03$	$2.50 \pm .010$	2.50
$3/2^+$	$9.088 \pm .025$	$7.830 \pm .03$	$2.642 \pm .010$	2.66

NOTE: $E_c/Z_< = .357$ for $7/2^-$.

Candidates for high spin states can be identified by looking for large peaks in the back angle spectra. Figure IV.5 is the 60-degree spectrum. Peaks due to levels which have lower spins become weak as the angle increases, while the higher spin states have relatively flat angular distributions. The peak at 4.797 MeV is a good candidate for a high spin state. In the spectrum at 12 degrees (Figure IV.1), it is comparable in yield to many other states, while at 60 degrees it is the strongest peak.

The angular distributions that have been obtained are displayed in Figures IV.6, IV.7, IV.8. The high spin type of angular distribution is evident for the 4.797 MeV level. This angular distribution is even seen to rise in the low angles as the angle increases.

C. Comparison with Other Experiments

A summary of the energy levels observed in this experiment is presented in Table IV.2. The table also contains a summary of the data

Figure IV.5

The ^{52}Cr(p,α)^{49}V spectrum at 60° showing candidates for high spin states at 3.612, 3.745, and 4.797 MeV.
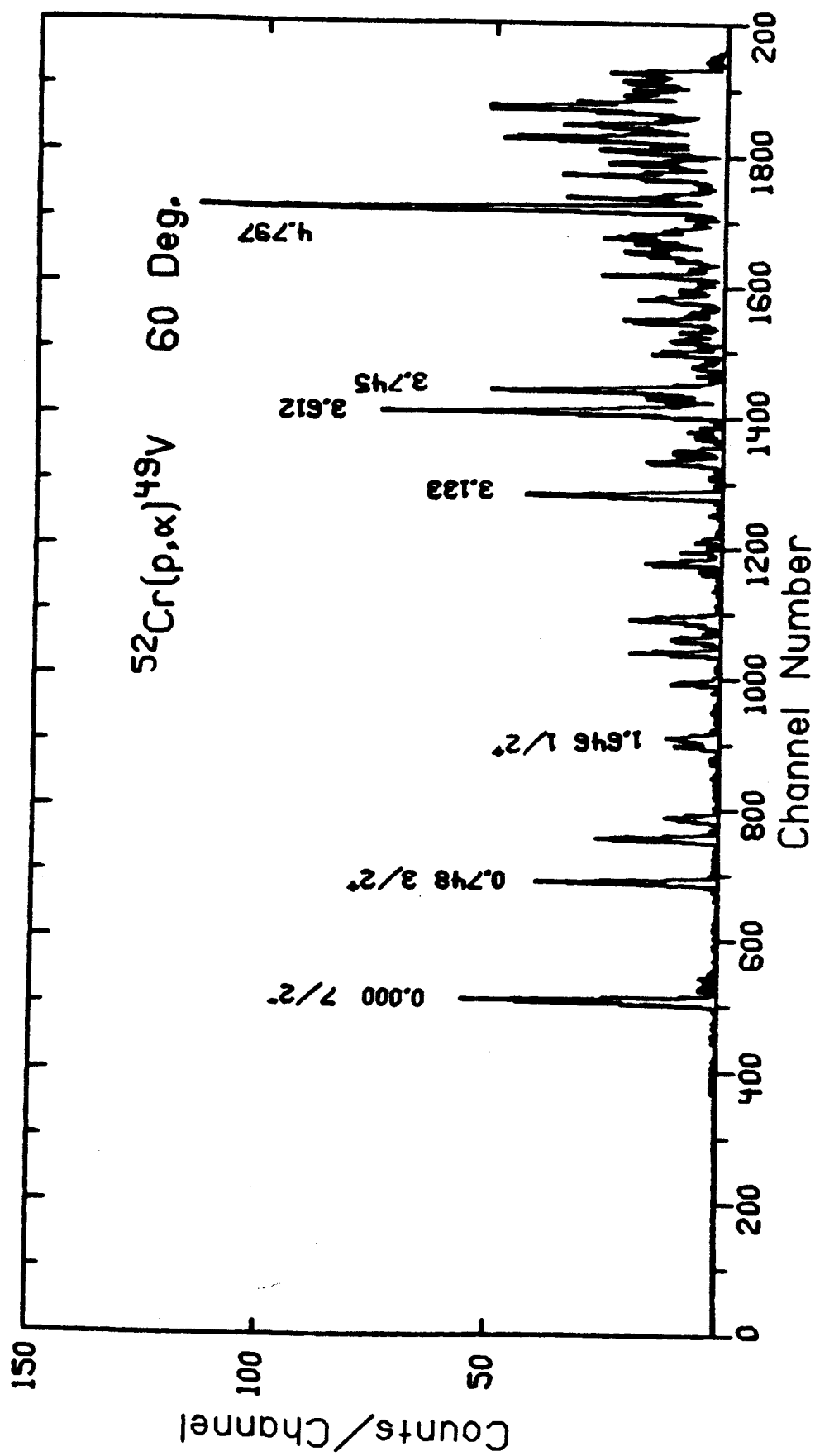
Figure IV.5

Figure IV.6

^{52}Cr(p,α)^{49}V angular distributions.

^{52}Cr(p,α)^{49}V Ep=35MeV

Figure IV.6

Figure IV.7

^{52}Cr(p,α)^{49}V angular distributions.

$^{52}Cr(p,\alpha)^{49}V$ Ep=35MeV
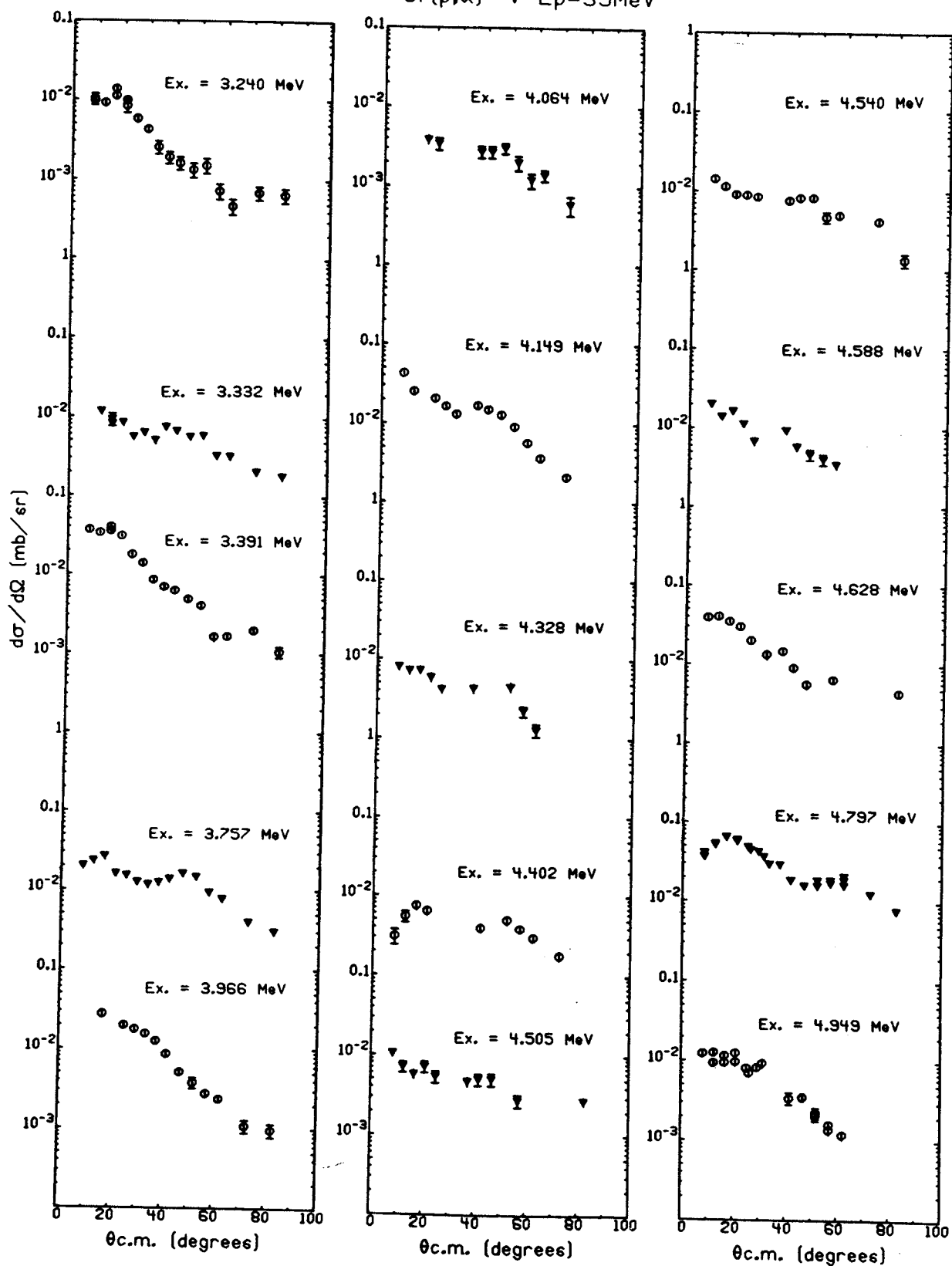
Figure IV.7

Figure IV. 8

^{52}Cr(p, α)^{49}V angular distributions.
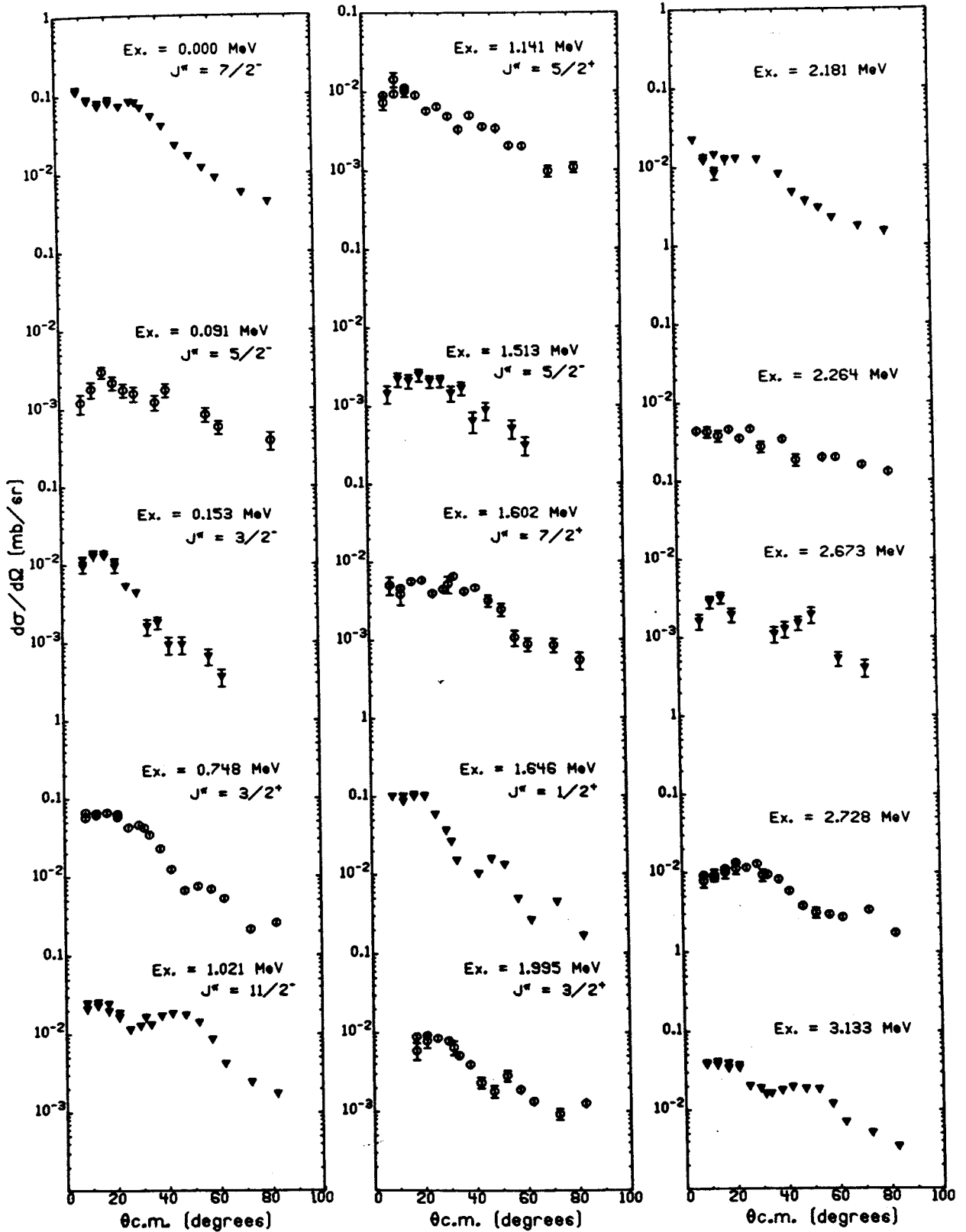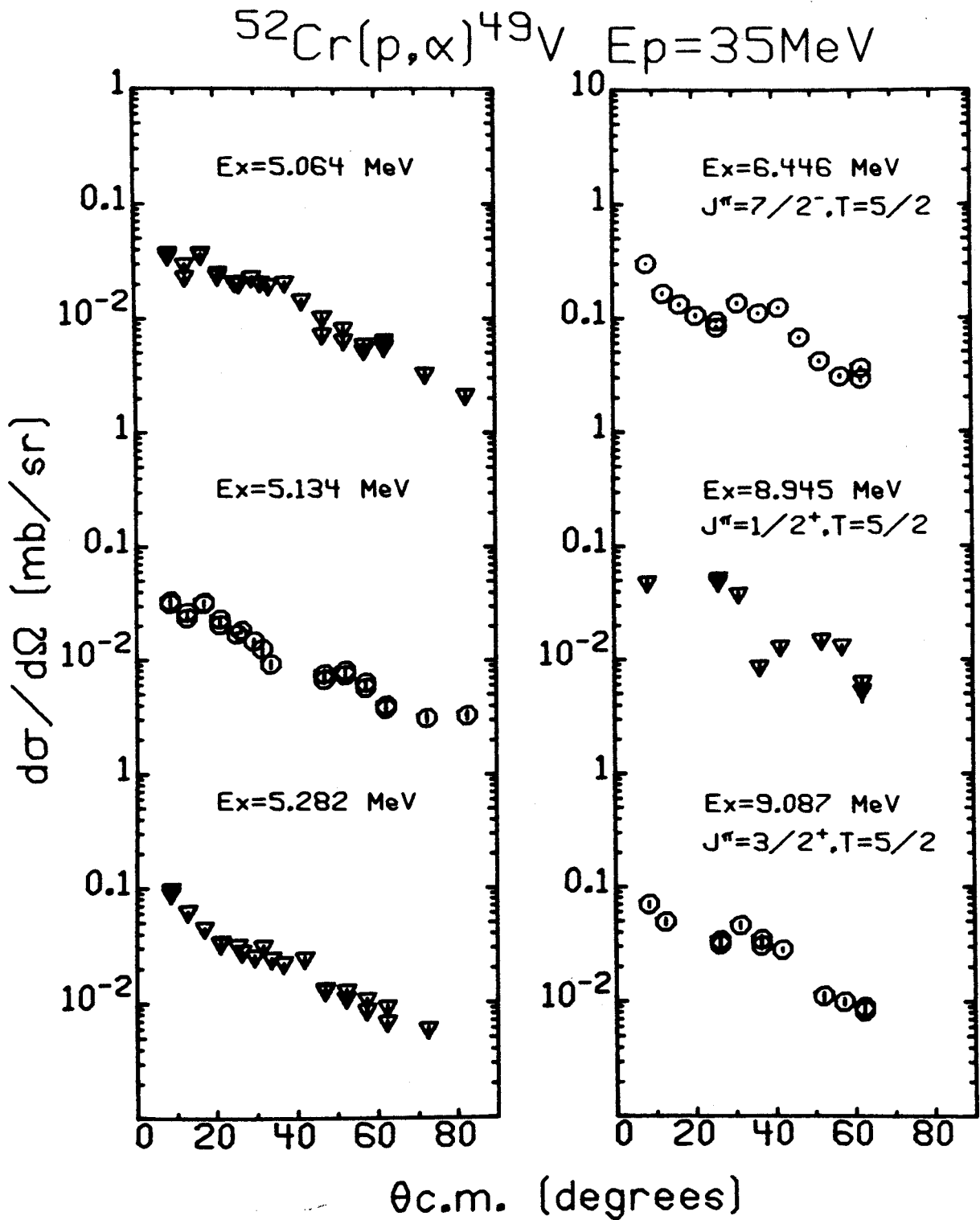
Figure IV. 8

TABLE IV.2

LEVELS OF ^{49}V

(p,α)[a]	(p,t)[b]	(t,α)[c]	$(^3He,d)$[c]	(p,γ)[d]	$(\alpha,p\gamma)$[e]	J^π
0.000	0.000	0.000	0.000			$7/2^-$
0.091	0.091	0.090	0.092	0.091	0.091	$5/2^-$
0.153	0.153	0.153	0.155	0.153	0.153	$3/2^-$
0.748		0.752	0.750	0.747	0.748	$3/2^+$
1.021	1.020	1.025	1.025	1.021	1.022	$11/2^-$
1.141				1.140	1.141	$5/2^+$
	1.154	[1.148]		1.155	1.155	$9/2^-$
1.513	1.516	1.531(?)		1.514	1.515	$5/2^-$
1.602					1.603	$7/2^+$
				1.644	1.643	$(1/2^-)$
1.646					1.646	1.2^+
	1.662		1.672	1.661	1.661	$3/2^-$
				1.770(?)		
				1.796(?)		
1.995		1.999		1.996	1.995	$3/2^+$
[2.181]		[2.189]	[2.193]		2.179	$9/2^+$
	2.183				2.183	$7/2^-$
			2.204			
2.235	2.235	2.241		2.235	2.235	$5/2^-$
[2.265]	[2.263]	[2.266]			2.263	$15/2^-$
					2.265	$3/2^-$
			2.279			
2.308	2.306	2.314	2.317	2.309	2.310	$9/2^-$
2.354	2.350	2.358			2.353	$9/2^-$
		[2.394]		2.388	2.388	$5/2^+$
2.406	2.404				2.408	$7/2^-$
2.673	2.666	2.681			2.671	
2.728	2.727	2.736			2.728	$(15/2^-)$
					2.741	
	2.786				2.786	$(9/2,11/2)^-$
	2.811	2.812		2.808	2.811	
	2.861				2.861	
	3.020				3.017	
[3.133]	[3.136]	[3.132]	[3.137]		3.1334	
					3.1337	
			3.152			
3.241	3.241	3.248	3.248	3.237		$7/2^-$
					3.259	
	3.305					
3.330	3.332					

TABLE IV.2—<u>Continued</u>

$(p,\alpha)^{a)}$	$(p,t)^{b)}$	$(t,\alpha)^{c)}$	$(^3He,d)^{c)}$	$(p,\gamma)^{d)}$	$(\alpha,p\dot{\gamma})^{e)}$	J^{π}
3.346	3.347	3.345			3.342	
3.391	3.398	3.388	3.401	3.390		
	3.479					
3.499						
3.525	3.534					
3.612	3.609					$\geqq(11/2^-)^{a)}$
	3.624					
3.639	3.649					
3.673	[3.685]					
3.694						
	3.720					
3.745		3.748		3.744		$\geqq(9/2^+)^{a)}$
	3.757	3.763		3.757		
	3.795					
	3.825			3.816		
3.838				3.840		
3.882	3.886					
	3.910			3.914		
3.934		3.929	3.922			
3.965	3.975	3.976				
4.004		4.005	4.012	4.006		
	4.048	4.042				
4.064						
	4.098	4.090				
			4.135	4.127		
4.149		4.152				
	4.165					
	4.209					
			4.224			
			4.253	4.250		
4.268*	4.277	4.280				
	4.305					
4.326						
4.375			4.375	4.373		
4.400		4.402				
4.436			4.448(?)			
4.470						
4.501		4.511	4.502	4.498		
4.538						
4.588		4.588	4.587	4.590		
			4.599			
4.628*				4.639		
		4.646	4.645			

TABLE IV.2—<u>Continued</u>

(p,α) [a]	(p,t) [b]	(t,α) [c]	$(^3 He,d)$ [c]	(p,γ) [d]	$(\alpha,p\gamma)$ [e]	J^π
4.662						
		4.680				
4.755		4.743				
4.797						$(> 11/2)$ [a]
4.830		4.848				
4.863			4.852			
4.885						
4.949		4.959	4.945			
4.988						
5.101		5.018	5.017			
5.134			5.130			
5.204		5.216	5.212			
5.282		5.285				
5.347		5.355				
		5.375	5.370			
5.387						
5.411						
6.446						$7/2, T=5/2$ [a]
8.945						$1/2^+, T=5/2$ [a]
9.087						$3/2^+, T=5/2$ [a]

NOTE: Errors are ±.003 MeV for states below 3 MeV, ±.006 MeV for states above 3 MeV, and ±.025 MeV for the $T=5/2$ states

[a] This experiment.

[b] Reference IV.11.

[c] Reference IV.12.

[d] Reference IV.19.

[e] Reference IV.16.

* The peak is an unresolved doublet. Its width is too large to be a single peak.

[ ] Energy corresponds to a known multiplet that cannot be resolved.

(?) Placement is unsure.

in the literature. The column of J^π values is a consensus of the litera-
ture. Although most J^π assignments are from the previous work, our
results are consistent with those assignments. The assignments
explicitly made in this work are the tentative "high spin" assignments
and the J^π, T assignments for the three analog states.

To begin the discussion of Table IV.2, consider the columns
labeled (p,α) and (p,t). Beginning at the top of the (p,t) column and
working down, it is seen that the 0.748 MeV state is the first one not
seen in the (p,t) reaction. This is the $3/2^+$ state due to a proton hole
in the 0d3/2 orbit. The next level not observed in the (p,t) reaction is
the 1.141 MeV, $5/2^+$ state. Furthermore the 1.602 MeV, $7/2^+$ and
1.646 MeV, $1/2^+$ levels are not observed in the (p,t) data. All these
levels are seen in the (p,α) experiment. A summary of the levels seen
in the (p,α) data that are not in the (p,t) data is given in Table IV.3.
Table IV.3 contains every known positive parity state in ^{49}V except the
2.179 MeV, $9/2^+$ which cannot be resolved from the 2.183 MeV, $7/2^-$
state. Furthermore there are no known negative parity levels in this
list. This comparison indicates that parity assignments can be made
with reasonable certainty by such a comparison.

Reversing the comparison shows that there are levels seen in the
(p,t) experiment that are not seen in the (p,α) spectra. The first of
these is the 1.661 MeV, $3/2^-$ state. In addition, all the $5/2^-$ levels
are so weak in the (p,α) reaction as to be virtually absent. If the (t,α)
results are included in the comparison, it is found that there are levels

TABLE IV.3

LEVELS SEEN IN $^{52}Cr(p,\alpha)^{49}V$ THAT ARE NOT IN $^{51}V(p,t)^{49}V^{a)}$

Excitation Energy	J^{π}
1.748	$3/2^{+}$
1.141	$5/2^{+}$
1.602	$7/2^{+}$
1.646	$1/2^{+}$
1.995	$3/2^{+}$
2.388	$5/2^{+}$

[a] Reference IV.11.

excited by the (t,α) reaction that are not in the (p,α) column. Some of these levels are in both the (p,t) and (t,α) data, but not in the (p,α) column. Behavior of this nature can only be explained by a microscopic model which contains the coherent sum over all the di-neutron couplings and all the three nucleon configurations. Table IV.4 is a summary of the missing levels in the (p,α) data.

$(\alpha,p\gamma)$ research has resulted in a $15/2^{-}$ assignment for the levels at 2.263 MeV and 2.728 MeV. Unfortunately, $17/2^{-}$ and $19/2^{-}$ levels have not been found by gamma-ray spectroscopy. In the case of positive parity, the highest definite J^{π} assignment is $9/2^{+}$. The two $15/2^{-}$ levels are observed very weakly. The angular distributions are found in Figure IV.6.

Although the high spin levels which are observed here have not been previously reported in α-induced gamma-ray coincidence

TABLE IV. 4

LEVELS SEEN IN EITHER ^{51}V(p,t)^{49}V[a] OR ^{50}Cr(t,α)^{49}V[b]
NOT OBSERVED IN ^{52}Cr(p,α)^{49}V

Excitation Energy	J^π
1.154*	$1/2^-$
1.662*	$3/2^-$
2.786*	$(9/2, 11/2)^-$
2.811**	$(5/2, 7/2)^-$
2.861*	$13/2^-$
3.020*	$(3/2, 7/2)^-$
3.305*	
3.479*	$7/2^-$
3.624*	
3.720*	
3.825*	
3.910*	
4.048**	
4.098**	
4.165*	
4.209*	
4.305*	

[a]Reference IV.11.

[b]Reference IV.12.

*Seen in (p,t) data.

**Seen in (p,t) and (t,α) data.

experiments, we can be reasonably sure that the 3.612 MeV level has

(-) parity and the 3.745 MeV state is a positive parity state. Neither

of these assignments is unambiguous since the 3.612 MeV peak is too

broad at forward angles to be a single state and the 3.745 MeV level

has been reported in the (t,α) and (p,γ) data, indicating a low spin

state at this energy. The parity of the 4.797 MeV level cannot be dis-

cussed since the (p,t) data does not extend to this excitation. Neither

the 3.612 MeV state nor the 4.797 MeV state are particularly close to

the MBZ (IV.33) predictions for high spin negative parity states. The

predicted energies for $15/2^-$ levels are 2.575 MeV, 3.544 MeV, 4.083

MeV, and 4.964 MeV. The predicted excitation for the first $15/2^-$ is

nearly 300 keV too high, while the second one is over-predicted by

about 800 keV. It is not surprising that our high spin candidates are

not near the MBZ predictions given the poor results for the known $15/2^-$

levels. The MBZ predictions for the two $19/2^-$ levels with the largest

"triton" components are 4.331 MeV and 5.143 MeV.

D. j-Dependence

The striking j-dependence for $\ell = 1$ transitions was not observed

in this experiment because the only known $1/2^-$ level is obscured by

the $1/2^+$ proton hole state. The $3/2^-$ level at 0.153 MeV excitation

does exhibit the usual featureless exponential fall-off.

Two $3/2^+$ and two $5/2^+$ states have been observed. The $5/2^+$

state at 2.386 MeV cannot be resolved sufficiently well to obtain its

angular distribution. The three $\ell = 2$ angular distributions are shown in Figure IV.9. The $3/2^+$ distributions have similar shapes. The $5/2^+$ is rather featureless. There is no strong j-dependence in this case, though the angular distributions are different. There is not enough data to determine if the difference is due to j-dependence or is the result of structure effects. Additional data in this mass region is necessary to document the stability of the $\ell = 2$ j-dependence.

The spin-orbit pair with $\ell = 3$ is observed. Three $5/2^-$ levels are populated weakly. The cross section is less than $1 \mu b/sr$ at many points. The 0.091 MeV and 1.513 MeV levels were strong enough to obtain angular distributions. The angular distributions for these two levels appear to be different. The lowest $5/2^-$ level in many nuclei in this mass region is known to be primarily a seniority three proton state (IV.33, IV.34) and, hence, should not be populated in this experiment. Its weak population may indicate a more complicated reaction mechanism. The angular distribution for the 0.091 MeV state is flat. The angular distribution of the 1.513 MeV level is probably more representative of a $5/2^-$ angular distribution. $7/2^-$ states are observed at 0.000 MeV, 3.241 MeV and y.446 MeV excitation. Figure IV.10 shows all the $\ell = 3$ angular distributions. The angular distribution for the 3.241 MeV level is very different from the other $7/2^-$ levels. The $7/2^-$ assignment for this state is unambiguous since it is based on the $\ell = 0$ angular distribution observed in the $^{51}V(p,t)^{49}V$ reaction (IV.11). Either

Figure IV.9

^{52}Cr(p,α)^{49}V L=2 angular distributions.

$^{52}Cr(p,\alpha)^{49}V$ $L=2$

Ex=0.748 MeV
$J^{\pi}=3/2^+$

Ex=1.995 MeV
$J^{\pi}=3/2^+$

Ex=1.141 MeV
$J^{\pi}=5/2^+$

$d\sigma/d\Omega$ [mb/sr]

θc.m. (degrees)
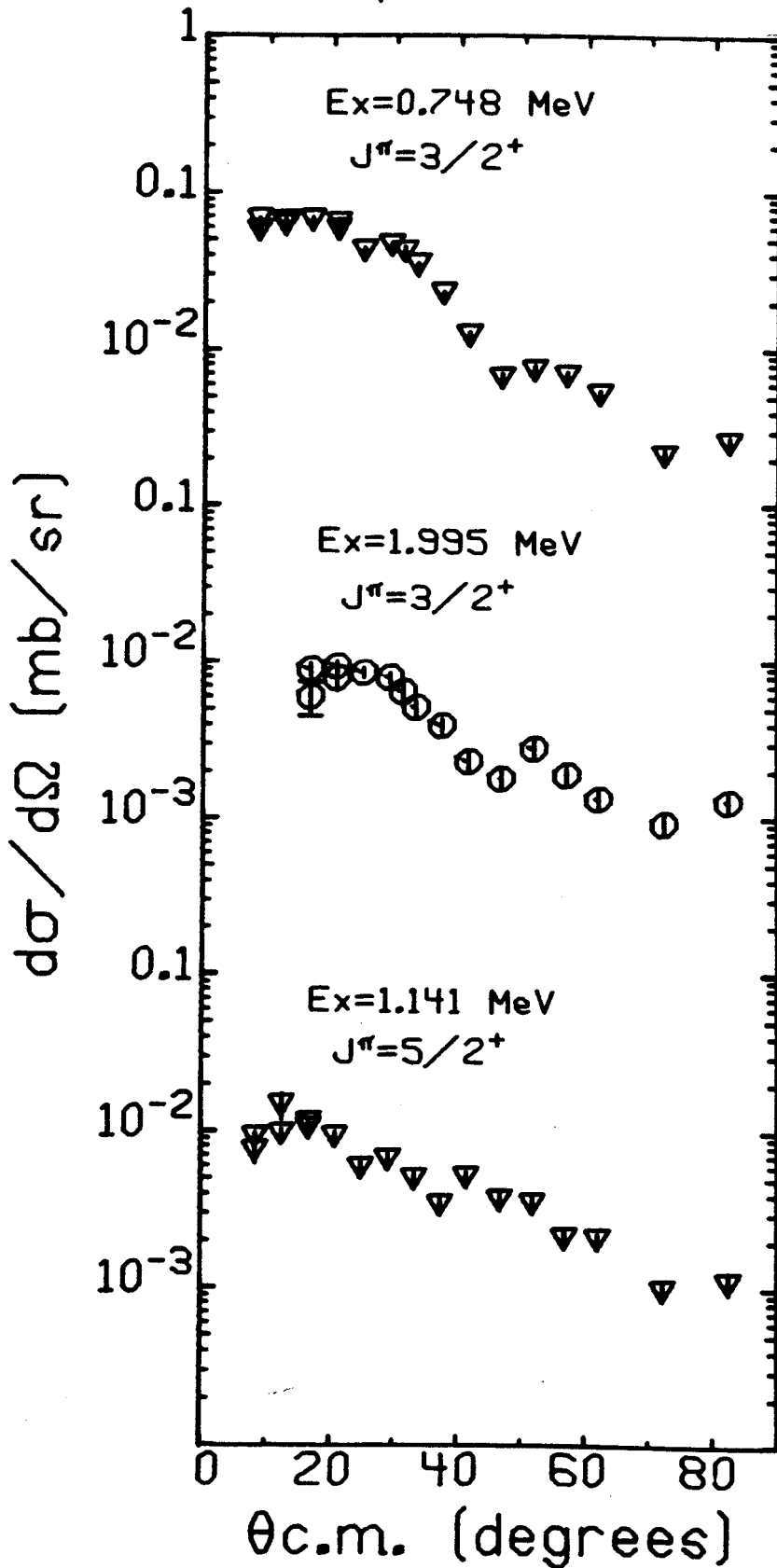
Figure IV.9

Figure IV. 10

^{52}Cr(p,α)^{49}V L=3 angular distributions.
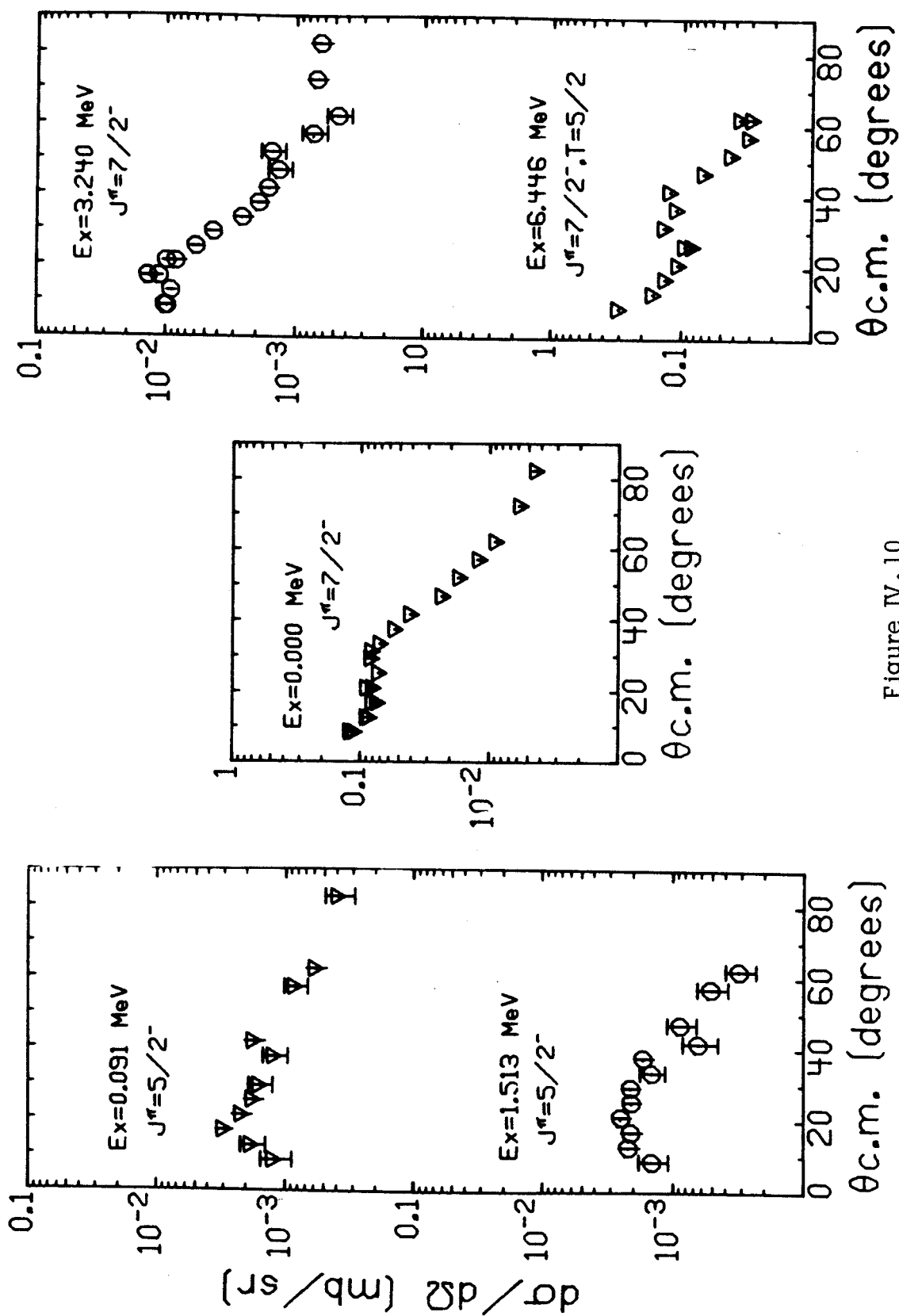
$^{52}Cr(p,\alpha)^{49}V$ L=3

Figure IV.10

this is an unresolved doublet or this is a case where structure effects can be as strong as j-dependence. If the abnormal angular distribution is neglected, the j-dependence appears to be manifested in the forward angles. The $5/2^-$ tends to go down as the angle decreases, while the $7/2^-$ rises. Two other $7/2^-$ states are also populated. Unfortunately, they are members of close doublets.

Only one $\ell = 4$ transfer is resolved. This leads to the $7/2^+$ state at 1.602 MeV. The $9/2^+$ level at 2.179 MeV may be populated, but cannot be resolved from the $7/2^-$ state at 2.183 MeV.

There are known $9/2^-$ and $11/2^-$ levels in the first two MeV of excitation. The $11/2^-$ is observed, but there is no evidence for the $9/2^-$. Another $9/2^-$ state located at 2.354 MeV is barely visible in some spectra.

Both j-values that go with $\ell = 7$ have been previously identified. The two known $15/2^-$ states are weakly populated. The $13/2^-$ level at 2.861 MeV is not seen in this experiment.

There have not been any previous spin assignments for states to be reached by $\ell = 6, 8,$ or 9 transfers.

An alternation of strength is clearly evident for negative parity states. For a given ℓ-transfer, the $j_>$ member is the strongest. This is in qualitative agreement with the structure factors presented in Table II.4 and the calculated peak cross sections found in Table II.5.

In conclusion there appears to be some evidence for subtle j-dependence in the $\ell = 2, 3$ transfers. This j-dependence may not

be a very reliable tool in this mass region, since structure differences may cause similar changes in the angular distributions.

E. DWBA Calculations—Cluster Form Factors

It has been shown that zero-range DWBA calculations can be used to obtain reasonable fits to (p,α) angular distributions (see, for example, References IV.22, IV.28, IV.36). In addition, finite range effects have been found to produce only minor changes in the shapes of the DWBA calculations (see Figure II.10). Mass-3 cluster form factors have been used frequently for these calculations because they are easy to generate. In addition, most researchers have found the radius and diffuseness parameters of the bound state well to be useful variables. These are usually varied to obtain the best overall fit to all the known levels. A wide variety of these parameters have been used (see References IV.28, IV.36). Many different sets of α-particle optical potentials have been tried also. These vary from shallow real wells of about 50 MeV depth to deep wells of 200 MeV depth. For the most part, the choice of α-optical potential determines the values of the bound state well parameters that will best fit the data.

A simple, consistent, method of generating reasonable calculations is needed. We have, therefore, set out to find a general procedure that can be used to get first-order fits reliably.

Since angular momentum matching is a problem for the (p,α) reaction, it seems reasonable to try the "well matching" procedure for

choosing the optical potentials and the bound state parameters. This procedure has been suggested by Dodd and Greider (IV.37) and by Stock et al. (IV.38) for reactions that are poorly matched. The method has been successfully applied to the (d,α) reaction (IV.39).

The proton optical potentials were taken from Bechetti and Greenlees second best set (IV.40). This is the set with a 1.22 fm. radius parameter. The α-particle optical potential was taken to be a set with roughly 200 MeV real well depth. The well matching procedure requires that the radius and diffuseness of all the real potentials be the same. α-scattering data of Fernandez and Blair (IV.41) were refit to find an optical potential that met the well matching requirement. Since the α-elastic scattering could not be reproduced as well with a radius parameter of 1.17 fm. as with the 1.22 fm. choice, the second preferred proton set was taken. By this prescription the bound state wavefunction should be calculated in a well with $r_0 = 1.22$ fm. and a diffuseness of .72 fm. to agree with the other potentials. The well depth should ideally be about 150 MeV. However, the depth was allowed to vary to reproduce the triton separation energy. For the most part the appropriate depth was between 120 MeV and 140 MeV. The optical potentials are given in Table IV.5.

The fits that are obtained to the known energy levels using this procedure are shown in Figure IV.11. In general they are satisfactory. The forward angle behavior of the $7/2^-$ calculation does not increase

TABLE IV.5

OPTICAL POTENTIALS[a]

	V	r_o	a	V_{so}	r_{so}	a_{so}	W	r_{oi}	a_i	W_{sf}
Proton	43.22	1.22	.72	-25.0	1.01	.75	-5.0	1.32	.52	12.60
α	196.34	1.22	.72				-15.72	1.76	.42	

[a] V_{so} and W_{sf} include the factor of 4 necessary for using the code DWUCK45.

as the angle decreases, but the data does. The dip in the $11/2^-$ calculation comes at too small an angle. The "well matching" procedure has also been used in studies of Te(p,α) and ^{44}Ca(p,α)^{41}K with similar results (see Reference IV.10 and Chapter V).

Most of the searching on the bound state that has been done by other researchers has resulted in smaller diffuseness parameters than were used above. If the diffuseness is decreased to .65 fm., the $7/2^-$ calculation has the correct forward angle behavior. In other words, the forward angles are sensitive to the diffuseness. The fits obtained with this choice are shown in Figure IV.12. Smaller diffuseness values were also investigated. In general smaller values were found to produce more pronounced oscillations.

Sensitivity of this kind is a characteristic of reactions that suffer from a severe angular momentum mismatch. The semi-classical matching value for the ground state Q-value is about six. The angular

Figure IV.11

Cluster model DWBA calculations. The real well geometrical parameters were $r_o = 1.22$ fm. and $a = .72$ fm.
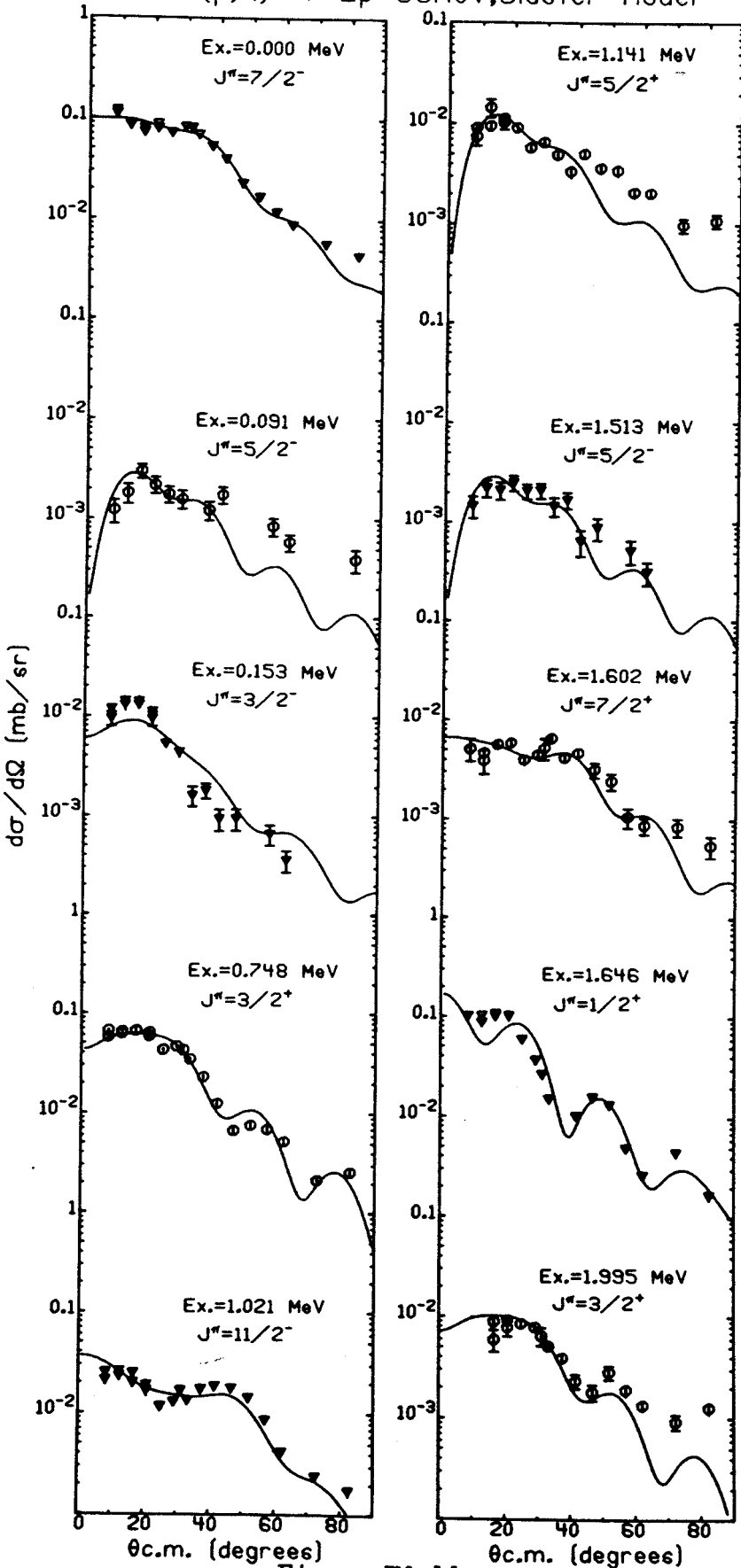
Figure IV.11

Figure IV.12

Cluster model DWBA calculations. The real well geometrical parame-
ters were $r_o = 1.22$ fm. and $a = .65$ fm.

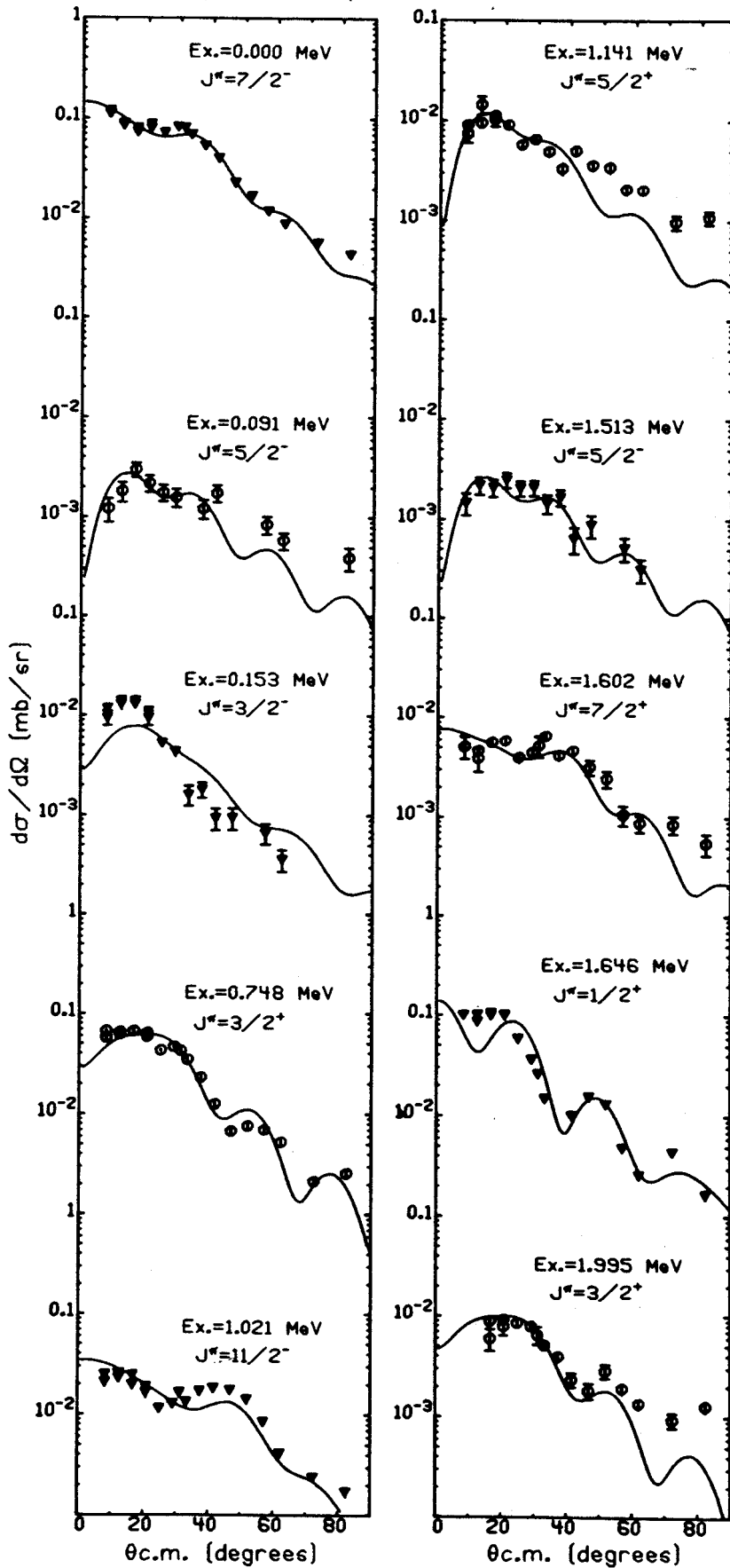^{52}Cr(p,α)^{49}V Ep=35MeV;Cluster Model

Figure IV.12

momentum characteristics of the DWBA have been discussed previously in Chapter II.

Angular momentum mismatch also implies that predicted strengths can vary strongly with excitation energy. The higher the excitation energy the lower the angular momentum matching value. In general, the better the match the larger the cross section. Even though cluster model calculations are not particularly useful when comparing the strengths of individual transitions, their energy dependence is meaningful. Figure IV.13 shows a comparison of DWBA calculations assuming no excitation to a set calculated with 5 MeV excitation. When calculating the excited levels it is important to make both the Q-value and the binding energy more negative. No strong dependence on excitation energy is observed, though there are some small changes in predicted shapes. It is interesting to note that the change in shape for the $7/2^-$ forward angle behavior is similar to what is actually observed for the 6.446 MeV state.

In general the normalization of cluster model calculations to the data does not yield a number which is easily related to nuclear wavefunctions. In certain cases, however, two states may be described by the same p-n formalism wavefunction. These states differ in their isospin quantum number. This is illustrated in Figure IV.14 for the $7/2^-$ ground state of ^{49}V and the $T = 5/2$, $7/2^-$ state in ^{49}V. Since the wavefunctions are the same, the spectroscopic factors are identical and the ratio of the $T_>$ normalization to the $T_<$ normalization becomes

Figure IV.13

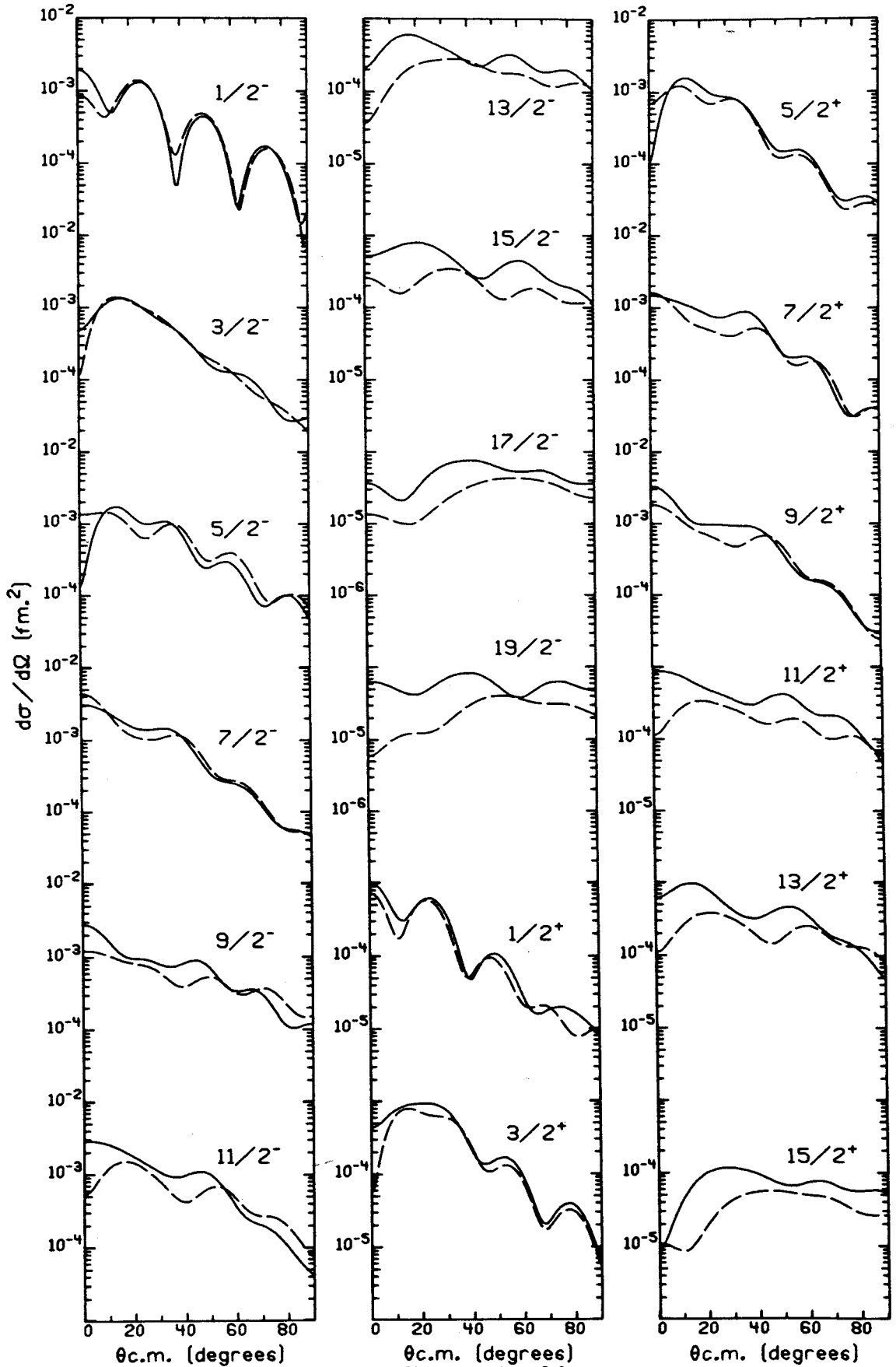Q-value dependence of cluster model DWBA calculations.

Q-Value Dependence

Q= - 2.590
Q= - 7.590

Figure IV.13

Figure IV. 14

Wavefunctions for analogs of ^{49}V hole states.

^{49}V 7/2$^-$ (T=3/2

p   n

xxx |ooxxxxxx of 7/2

^{49}Ti 7/2$^-$ (T=5/2) $\xrightarrow{T<}$ ^{49}V 7/2$^-$ (T=5/2)

p   n   p   n

xx |oxxxxxxx f $_{7/2}$ xxx |ooxxxxxx   f $_{7/2}$

^{49}V 3/2$^+$ (T=3/2)

p | n   p | n

a xxxx |ooxxxxxx f $_{7/2}$ + b xxx |oxxxxxxx f $_{7/2}$
      o| |o
         d $_{3/2}$ d $_{3/2}$

^{49}Ti 3/2$^+$ (T=5/2)

p | n   p | n

α xx |xxxxxxxx f $_{7/2}$ + β xxx |oxxxxxxx f $_{7/2}$
     |o   d $_{3/2}$ o| d $_{3/2}$

^{49}V 3/2$^+$ (T=5/2)

p | n   p | n

γ xxxx |ooxxxxxx f $_{7/2}$ + δ xxx |oxxxxxxx f $_{7/2}$
      o| d $_{3/2}$ |o   d $_{3/2}$
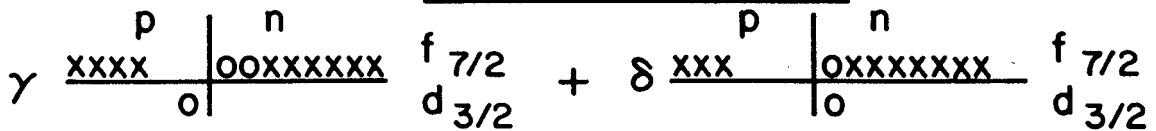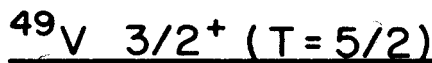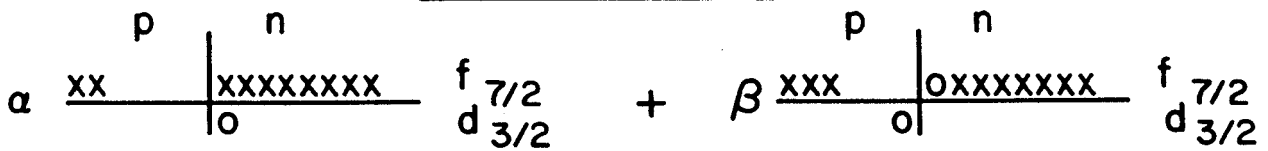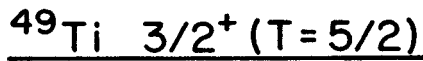
Figure IV.14

$1/(2T+1)$ which is the ratio of the isospin Clebsch-Gordon coefficients squared, where T is the isospin of the target. This ratio is independent of the form factor model since the microscopic wavefunctions are the same. Since the Q-value dependence of the form factor is most easily handled with the cluster model, we will use this model for the comparison. For the ^{52}Cr target, the expected ratio is .2, while the ratio deduced from the fit to the $7/2^-$ state at 6.446 MeV shown in Figure IV.15 is 2.41. This kind of analysis cannot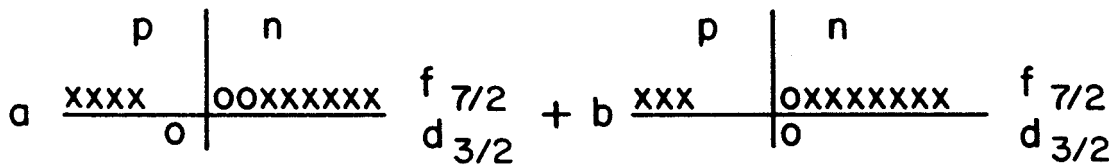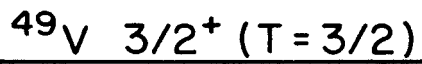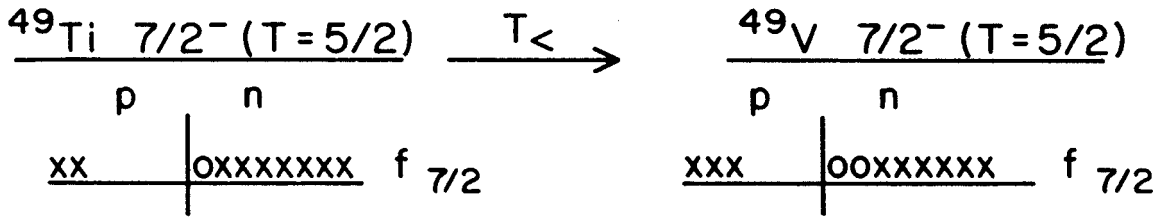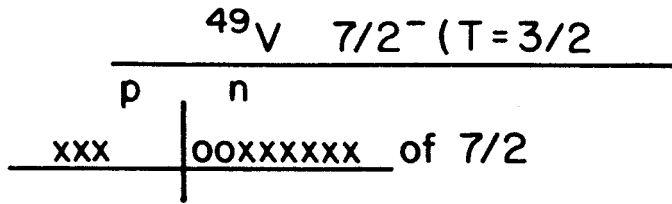 be applied to the $3/2^+$ and $1/2^+$ states, since the assumption of equal spectroscopic factors is not valid as is illustrated in Figure IV.14.

A similar enhancement of analog states in the (p,d) reactions has been observed (IV.43). The effect has been explained via coupled channels calculations which may be approximated by using the same well depth for the analog calculation as for the $T_<$ calculation and allowing the bound state radius to vary to reproduce the correct binding energy (IV.44). It remains to be seen if this approach will work for the (p,α) reaction.

F.   DWBA Calculations—Microscopic Form Factors

The cluster model is useful for studying the effects of optical potentials and the bound state well shape. However, the relative strengths of states are difficult to predict with such a model.

A microscopic model is necessary to predict the relative strengths of states from shell model wavefunctions. Any microscopic form factor

Figure IV. 15

Cluster model DWBA calculations for the $T = 5/2$ states.

Figure IV.15
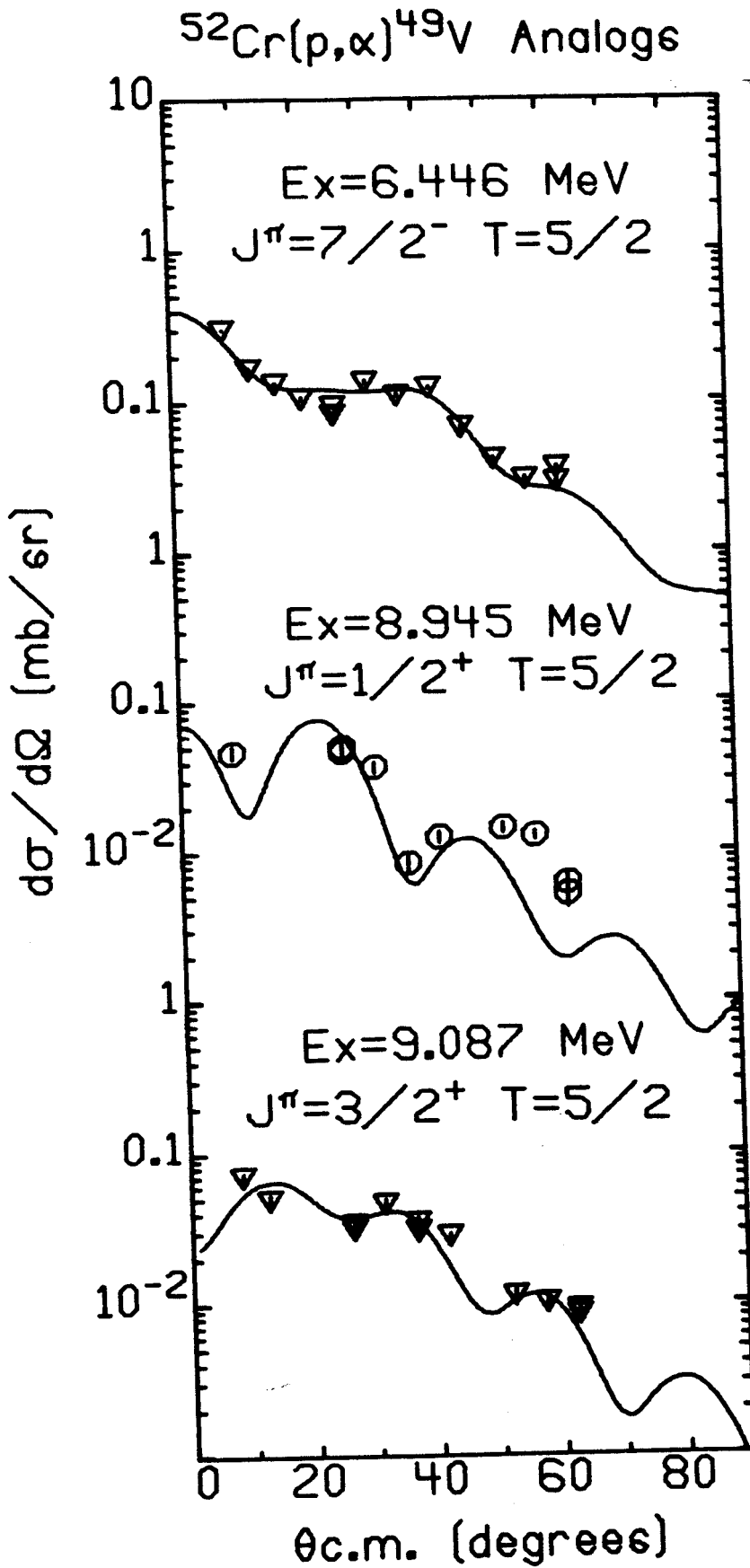
will not have the shape flexibility that the cluster form factor has.
Therefore, it is necessary to choose the "well matched" optical param-
eters, since they are the least sensitive to form factor shapes.

A microscopic model which uses single particle wavefunctions
generated in a Woods-Saxon well has been developed previously
(Chapter II). The two neutrons are coupled together to make a di-
neutron using the two nucleon form factor method of Bayman and Kallio
(IV.35). The di-neutron is then treated as a mass two particle and
coupled to the proton to make a triton in a 0s internal state by a modi-
fication of the two nucleon technique.

DWBA calculations using these form factors are shown in
Figure IV.16. The fits are comparable to the cluster fits shown in
Figure IV.12.

The calculation of strengths requires detailed spectroscopic
amplitudes from shell model wavefunctions. However, the hole states
may be described by simple seniority one transfers. We assume that
the two neutrons are coupled to zero angular momentum. The j-transfer
for the hole states is the proton total angular momentum. This assump-
tion makes the relative strengths for the $7/2^-$, $3/2^+$, and $1/2^+$ proton
hole states the same as would be expected for the $^{50}Cr(d, ^3He)^{49}V$
reaction. The hole state relative spectroscopic factors are given in
Table IV.6. The agreement with the expected values is very good, thus
the simple seniority one assumption seems to be reasonable for these
states.

Figure IV.16

Microscopic model DWBA calculations. The form factors were calcu-
lated for $(0f7/2)^3$, $(0f7/2)^2 0d3/2$, and $(0f7/2)^2 1s1/2$ configurations.

^{52}Cr(p,α)^{49}V Ep=35MeV;Microscopic Model
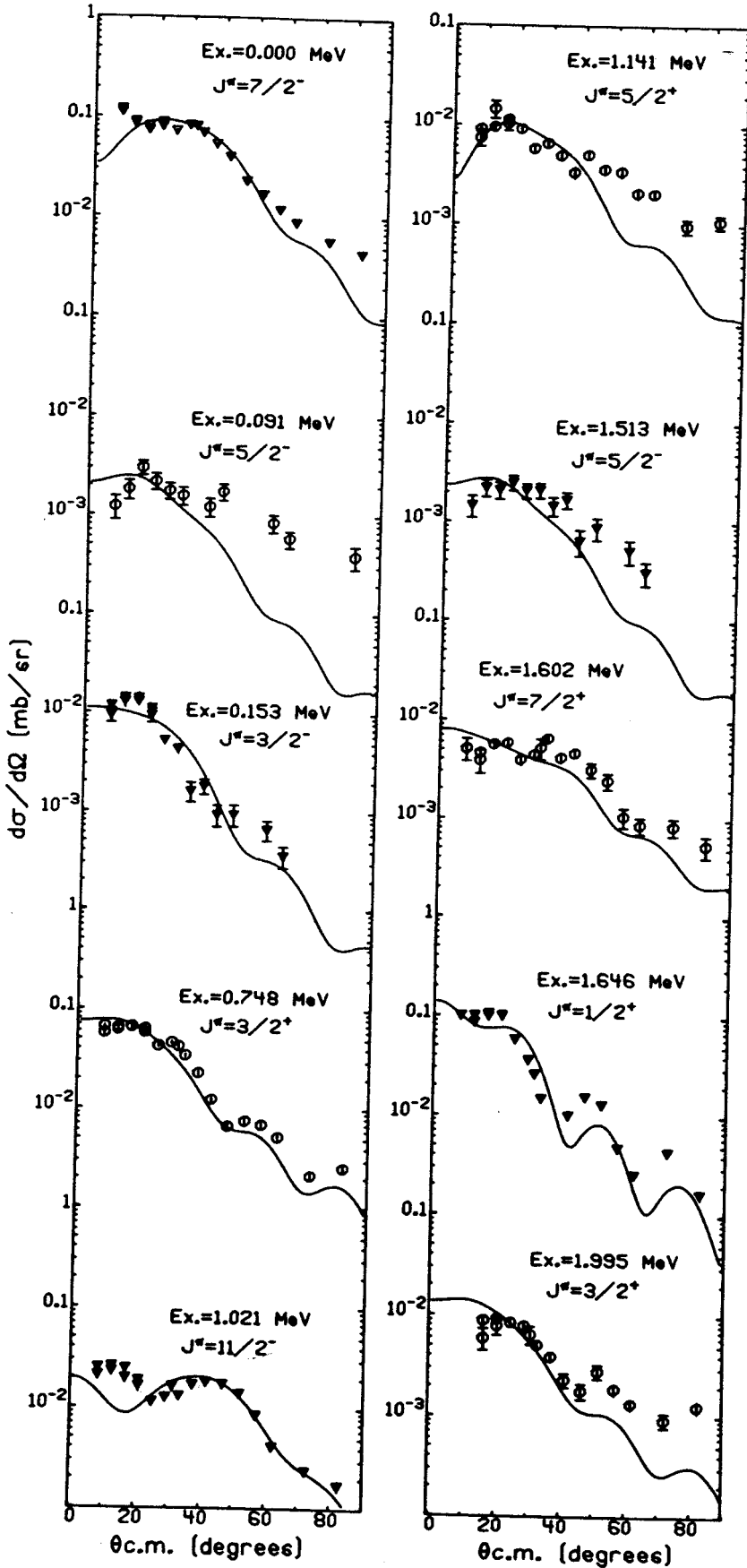
Figure IV.16

TABLE IV.6

RELATIVE SPECTROSCOPIC FACTORS

Excitation Energy	J^π	Theory	Measured
0.000	$7/2^-$	1.0	1.0^*
0.748	$3/2^+$	1.0	.84
1.646	$1/2^+$	.5	.54

*Normalized to one. All other values relative to this.

The same ratios should be expected for the $T = 5/2$ proton hole states. Analysis similar to that given in the last paragraph shows that the model does not work for these levels. The seniority one assumption apparently is not a good one for these levels.

Although the angular distributions of the high spin states may not be reliably predicted, the microscopic model can be used to predict the likelihood of observing a $19/2^-$ level. Comparing the calculations shows that the ground state prediction is 48 times stronger than the $19/2^-$ at 12°. At 70° the $19/2^-$ is expected to be 6 times stronger than the $7/2^-$ seniority one transfer. Although these numbers may be off by a factor of 2 or so, qualitatively this is what is observed for the level at 4.797 MeV.

The peak cross sections from microscopic model calculations for $(0f7/2)^3$ configurations have been given in Table II.5. A qualitative feature of this table is that the $j_>$ member of a given ℓ-transfer is

always larger than the $j_<$ member. This is exactly the trend that was notice for the negative parity states in the j-dependence discussion.

G. Conclusions

The proton hole states have been found to dominate the $^{52}Cr(p,\alpha)^{49}V$ spectra at forward angles. This observation agrees with others that have studied the (p,α) reaction in the fp-shell.

Many weak transitions are observed with average differential $\sim 10\,\mu b/sr$.

The (p,α) reaction has been shown to have some degree of selectivity. A number of levels that are observed in $^{51}V(p,t)^{49}V$ were not observed in the (p,α) spectra. Turning this comparison around has proven to be a useful tool for finding positive parity states, none of which appear in the (p,t) spectra.

Large peaks in the back angle spectra have been observed. These states are candidates for high spin states. The likely spins are $19/2^-$, $15/2^-$, or $15/2^+$ for these levels.

Little evidence for j-dependence for $\ell = 2$ and $\ell = 3$ transfers has been found. If j-dependence exists, it is subtle and at a level that structure effects can be equally important.

DWBA calculations using cluster form factors have been shown to reproduce the shapes of the angular distributions of the known levels reasonably well.

DWBA calculations for the $T = 5/2$ proton hole states are unable to reproduce the ratio of $T = 5/2$ strength to $T = 3/2$ strength expected by analogy to single nucleon transfer. All the $T = 5/2$ strengths are too large.

Microscopic form factors have been tested. DWBA calculations using these form factors have been shown to reproduce the shapes of the angular distributions with quality slightly inferior to the cluster model fits. Relative spectroscopic factors for the $T = 3/2$ proton hole states have been derived from the microscopic calculations and are found to be in agreement with assuming seniority one wavefunctions. However, similar calculations for the $T = 5/2$ proton hole states do not work.

Finally a qualitative feature of j-dependent strength is observed in the data. The $j_>$ member of the $\ell = 1, 3, 5$ transfers is always observed to be stronger than the $j_<$ member. The microscopic model based on $(0f7/2)^3$ pure configurations also reproduces this qualitative effect.

REFERENCES FOR CHAPTER IV

IV.1   L. L. Lee, Jr., A. Mainov, C. Mayer-Boricke, J. P. Schiffer, R. H. Bassel, R. M. Drisko, and C. R. Satchler, Phys. Rev. Lett. $\underline{14}$ (1965), 261.

IV.2   J. A. Nolen, Jr., thesis, Princeton University (1965), unpublished.

IV.3   J. A. Nolen, Jr., C. M. Glasshauser, and M. E. Rickey, Phys. Lett. $\underline{21}$ (1966), 705.

IV.4   L. S. August, P. Shapiro, and L. R. Cooper, Phys. Rev. Lett. $\underline{23}$ (1969), 537.

IV.5   G. Brown, A. Macgregor, and R. Middleton, Nucl. Phys. $\underline{A77}$ (1966), 385.

IV.6   J. E. Finck, J. A. Nolen, Jr., R. Sherr, and P. A. Smith, private communication.

IV.7   G. Brown, S. E. Warren, and R. Middleton, Nucl. Phys. $\underline{A77}$ (1966), 365.

IV.8   R. W. Tarara, J. D. Goss, P. L. Jolivette, G. F. Neal, and C. P. Browne, Phys. Rev. $\underline{C13}$ (1976), 109.

IV.9   J. D. Goss, P. L. Jolivette, A. A. Rollefson, and C. P. Browne, Phys. Rev. $\underline{C10}$ (1974), 2641.

IV.10   R. G. Markham, R. K. Bhowmik, M. A. M. Shahabuddin, P. A. Smith, and J. A. Nolen, Jr., private communication.

IV.11   A. Saha, H. Nann, and K. K. Seth, private communication.

IV.12   D. Bachner, R. Santo, H. H. Duhm, R. Bock, and S. Hinds, Nucl. Phys. $\underline{A106}$ (1968), 577.

IV.13   N. H. Prochnow, H. W. Newson, E. G. Bilpuch, and G. E. Mitchell, Nucl. Phys. $\underline{A194}$ (1972), 353.

IV.14   Z. P. Sawa, J. Blomquist, and W. Gullholmer, Nucl. Phys. A205 (1973), 257.

IV.15   J. G. Malan, E. Barnard, J. A. M. deVilliers, J. W. Tepel, and P. Vander Merive, Nucl. Phys. A195 (1972), 596.

IV.16   B. Haas, J. Chevallier, J. Britz, and J. Styczen, Phys. Rev. C11 (1975), 1179.

IV.17   S. R. Tabor and R. W. Zurmühle, Phys. Rev. C10 (1974), 35.

IV.18   B. Haas, J. Chevallier, N. Schulz, J. Styczen, and M. Toulemoude, Phys. Rev. C11 (1975), 280.

IV.19   C. Rossi-Alvarez and C. B. Virgiani, Il Nuovo Cimento 17A (1973), 730.

IV.20   B. Bardin, thesis, University of Colorado (1964), unpublished.

IV.21   J. J. Kolata, J. W. Olness, and E. K. Warburton, Phys. Rev. C10 (1974), 1663.

IV.22   R. J. Peterson and H. Rudolph, Nucl. Phys. A241 (1975), 253.

IV.23   H. T. Fortune, P. A. Smith, J. A. Nolen, Jr., and R. G. Markham, private communication.

IV.24   W. R. Falk, A. Djaloeis, and D. Ingham, Nucl. Phys. A252 (1975), 452.

IV.25   K. VanderBorg, R. J. deMeijer, and A. vanderWoude, to be published in Nucl. Phys.

IV.26   L. S. August, P. Shapiro, L. R. Cooper, and C. D. Bond, Phys. Rev. C4 (1971), 2291.

IV.27   R. K. Bhowmik, R. G. Markham, M. A. M. Shahabuddin, P. A. Smith, and J. A. Nolen, Jr., Bull. Am. Phys. Soc. 20 (1975) 1164.

IV.28   Michel Vergnes, Georges Rotbard, Jacques Kalifa, and Genevieve Berrier-Rossin, Phys. Rev. C10 (1974), 1156.

IV.29   W. R. Falk, Phys. Rev. C8 (1973), 1757.

IV.30   J. W. Smits and R. H. Siemsen, Nucl. Phys. A261 (1976), 385.

IV.31   P. A. Smith, R. G. Markham, and J. A. Nolen, Jr., to be published.

IV.32   R. G. Markham and R. G. H. Robertson, Nucl. Instr. and Meth. 129 (1975), 131.

IV.33   J. D. McCullen, B. F. Bayman, and Larry Zamick, Princeton University Technical Report NYO-9891 (1964).

IV.34   R. Sherr, Proceedings of the Conference on Direct Interactions and Nuclear Reaction Mechanisms, University of Padua, edited by E. Clementel and C. Villi (1962), 1025.

IV.35   B. F. Bayman and A. Kallio, Phys. Rev. 156 (1967), 1121.

IV.36   Yong Sook Park, H. D. Jones, and D. E. Bairum, Phys. Rev. C7 (1973), 445.

IV.37   K. R. Greider and L. R. Dodd, Phys. Rev. 146 (1966), 671; L. R. Dodd and K. R. Greider, Phys. Rev. 146 (1966), 675.

IV.38   R. Stock, R. Boch, P. David, H. H. Duhm, and T. Tamura, Nucl. Phys. A104 (1967), 136.

IV.39   R. M. DelVechio and W. W. Daehnick, Phys. Rev. C6 (1972), 2095.

IV.40   F. D. Bechetti and G. W. Greenlees, Phys. Rev. 182 (1969), 1190.

IV.41   B. Fernandez and J. S. Blair, Phys. Rev. C1 (1970), 523.

IV.42   J. P. Schiffer, Isospin in Nuclear Physics, edited by D. H. Wilkinson.

IV.43   R. Sherr, B. F. Bayman, E. Rost, M. E. Rickey, and C. G. Hoot, Phys. Rev. 139 (1965), B1272.

IV.44   W. T. Pinkston and G. R. Satchler, Nucl. Phys. 72 (1965), 641.

IV.45   P. D. Kunz, unpublished.

CHAPTER V

THE ^{44}Ca(p,α)^{41}K REACTION

A. Introduction

The (p,α) reaction has been used to locate proton hole states in nuclei that cannot be reached by proton pick-up (V.1, V.2). For many targets it is possible to extract meaningful proton hole spectroscopic factors by assuming that these states are populated primarily by the pick-up of a zero coupled neutron pair and a proton. Relative spectroscopic factors calculated by this method have been shown to agree with the values obtained from the $(d,^3He)$ or (t,α) reactions for the ^{52}Cr(p,α)^{49}V and the ^{92}Zr(p,α)^{89}Y reactions (Chapter IV and Reference V.3). Smits et al. (V.4, V.5) have found that this "spectator model," which neglects coherent sums over three nucleon configurations and the di-neutron angular momentum, does not adequately describe the cross sections that are observed in Sn(p,α) reactions.

Previous (p,α) hole state analysis has been done on nuclei where the hole strength is concentrated in one state. A logical extension of "spectator model" analysis is to study a nucleus where proton pick-up has shown that the hole strength is divided among a number of states. If the zero coupled pair assumption is reasonable, the relative cross

sections of the fractions and the relative total spectroscopic factors

observed in the (p,α) reaction will agree with the results of the

(d,^{3}He) and (t,α) reactions.

A recent survey of the (d,^{3}He) reaction on the Ca isotopes (V.6)

has shown that the 1s1/2 proton hole strength is divided into three

states in ^{41}K. The 0d5/2 strength was found to be split among many

levels. Thus the ^{44}Ca(p,α)^{41}K reaction is a good reaction to test the

"spectator model." Work on the ^{42}Ca(p,α)^{39}K reaction by Falk (V.7)

produced good agreement for the ratio of the 1s1/2 spectroscopic fac-

tor to the 0d3/2 spectroscopic factor, deduced assuming a $(0f7/2)^2_0$

neutron configuration, with ^{40}Ca(d,^{3}He)^{39}K results (V.8). Although

this is an encouraging result, Falk also found that the 0d5/2 proton

hole strength was four to five times too large.

The beauty of the spectator model is its simplicity. However,

because of this simplicity, it can be successful only for those few

states which have large proton hole amplitudes in their wavefunction.

In general, most states observed in the (p,α) reaction are not of this

type. Microscopic models have been developed recently to describe

these more complicated transitions (Chapter II, References V.5 and

V.9). For sd-shell targets where complete shell model wavefunctions

exist, it is possible to perform the completely coherent calculations

(Chapter VI, Reference V.9). For most of the rest of the chart of the

nucleides, it is necessary to settle for qualitative agreement with pure

configuration calculations as has been done with the $^{52}Cr(p,\alpha)^{49}V$

reaction in Chapter IV. To date only neutrons from the same shell

have been considered. The low lying $7/2^-$ state in ^{41}K provides a

testing ground for mixed neutron configurations, since it can be popu-

lated directly by (0d3/2 0f7/2)0d3/2 pick-up. 2p-2h excitations in

the ^{44}Ca ground state protons provide another process for making

$7/2^-$ final states. The strength of the $7/2^-$ state in the

$^{44}Ca(d, ^3He)^{43}K$ reaction indicates that the 0f7/2 proton spectro-

scopic factor is approximately .85 (V.6). If the (p,α) spectroscopic

factor relative to the total (0d3/2 + 1s1/2) spectroscopic factor, cal-

culated assuming a spectator model, differs from (.85/5.15) = .165,

the discrepancy will be a measure of the mixed shell pick-up.

Finally, it is worth noting that very few j^π assignments have

been made for ^{41}K. A number of $3/2^+$ and $5/2^+$ final states should be

populated, thereby testing the $l = 2$ j-dependence. The j-dependence

of the (p,α) reaction may turn out to be useful for making low-spin

assignments.

B. Experimental Method and Data

A beam of 35 MeV protons was accelerated in the MSU cyclotron

and directed to a target of isotopically enriched ^{44}Ca. The reaction

products were momentum analyzed in an Enge split-pole spectrograph.

The particles were detected with the delay line counter developed by

Markham and Robertson (V.10). Position and energy loss information

were taken from this counter. Particle time-of-flight relative to the cyclotron r.f. structure was obtained from a plastic scintillator placed behind the delay line counter. The α-particles were cleanly identified by their energy loss and time-of-flight. On the average, the energy resolution obtained from this system was 20 keV FWHM.

The target was made by reducing $^{44}CaCO_3$ with Zr and simultaneously evaporating the liberated metal. The evaporant was caught on a 20 $\mu g/cm^2$ carbon foil. The target thickness was found to be 85 $\mu g/cm^2$ by comparison of 35 MeV proton elastic scattering to optical model calculations using the Bechetti and Greenlees global proton parameters (V.11).

Because of the thin target and small cross sections, a large solid angle and high beam current were necessary. The solid angle was 1.2 msr. and the typical beam current was 2.5 μA.

The spectrum taken at 12 degrees is shown in Figure V.1. The three large peaks are the $3/2^+$ ground state, the $1/2^+$ state at 0.980 MeV, and a state at 3.520 MeV which is probably a $5/2^+$ state.

The angular distributions are given in Figures V.2, V.3, and V.4. The angular distribution for the .980 MeV level displays the deep minima which are typical of a $1/2^+$ transfer. The angular distributions for the 1.590 MeV and 3.758 MeV peaks, which have been assigned to be $1/2^+$ in the $(d,^3He)$ work, also have this shape. In addition, a new candidate for $1/2^+$ assignment is found at 3.063 MeV, although the oscillatory structure is somewhat washed out.

Figure V.1.

The ^{44}Ca(p,α)^{41}K spectrum at 12 degrees.
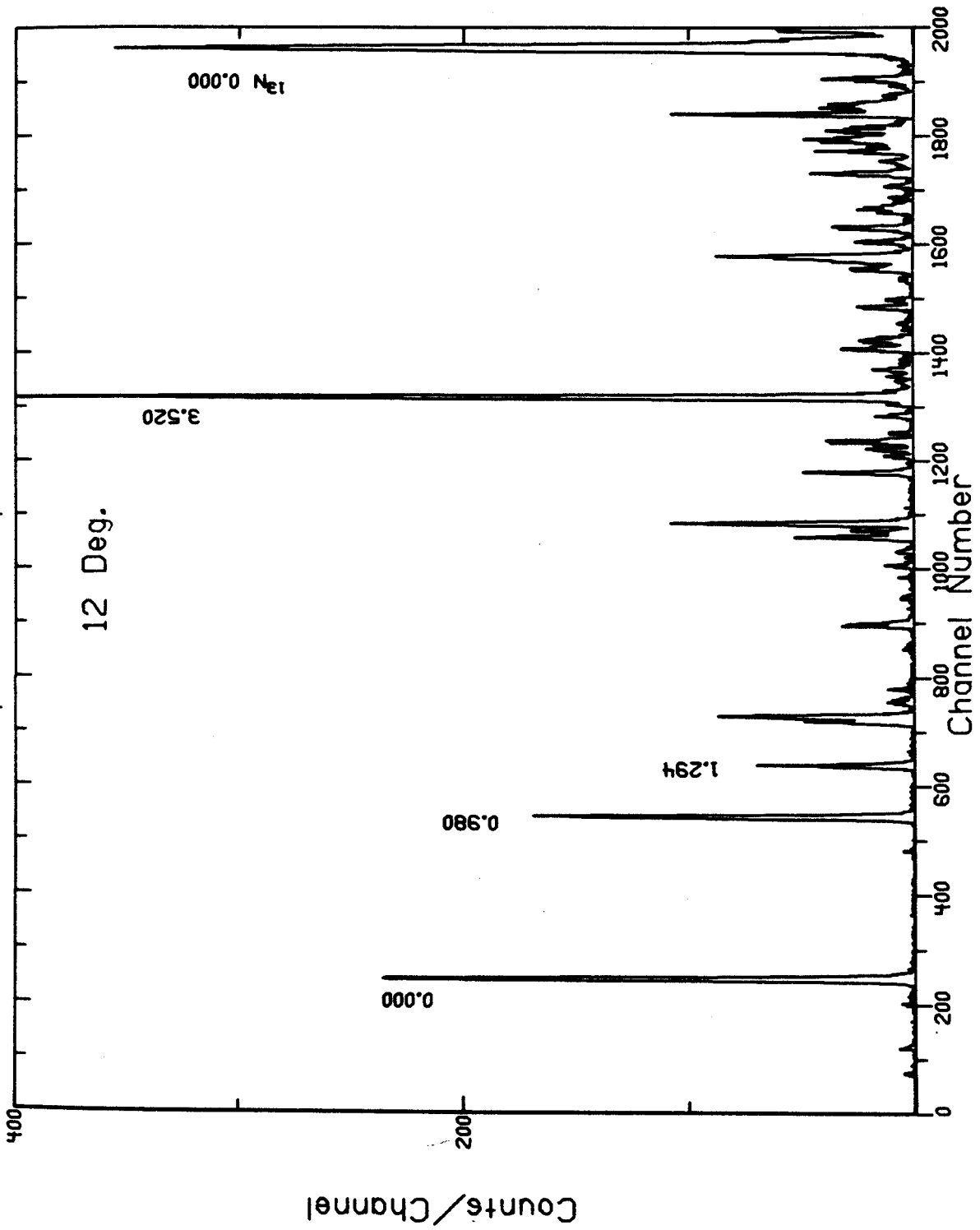
Figure V.1

Figure V.2

^{44}Ca(p,α)^{41}K angular distributions.
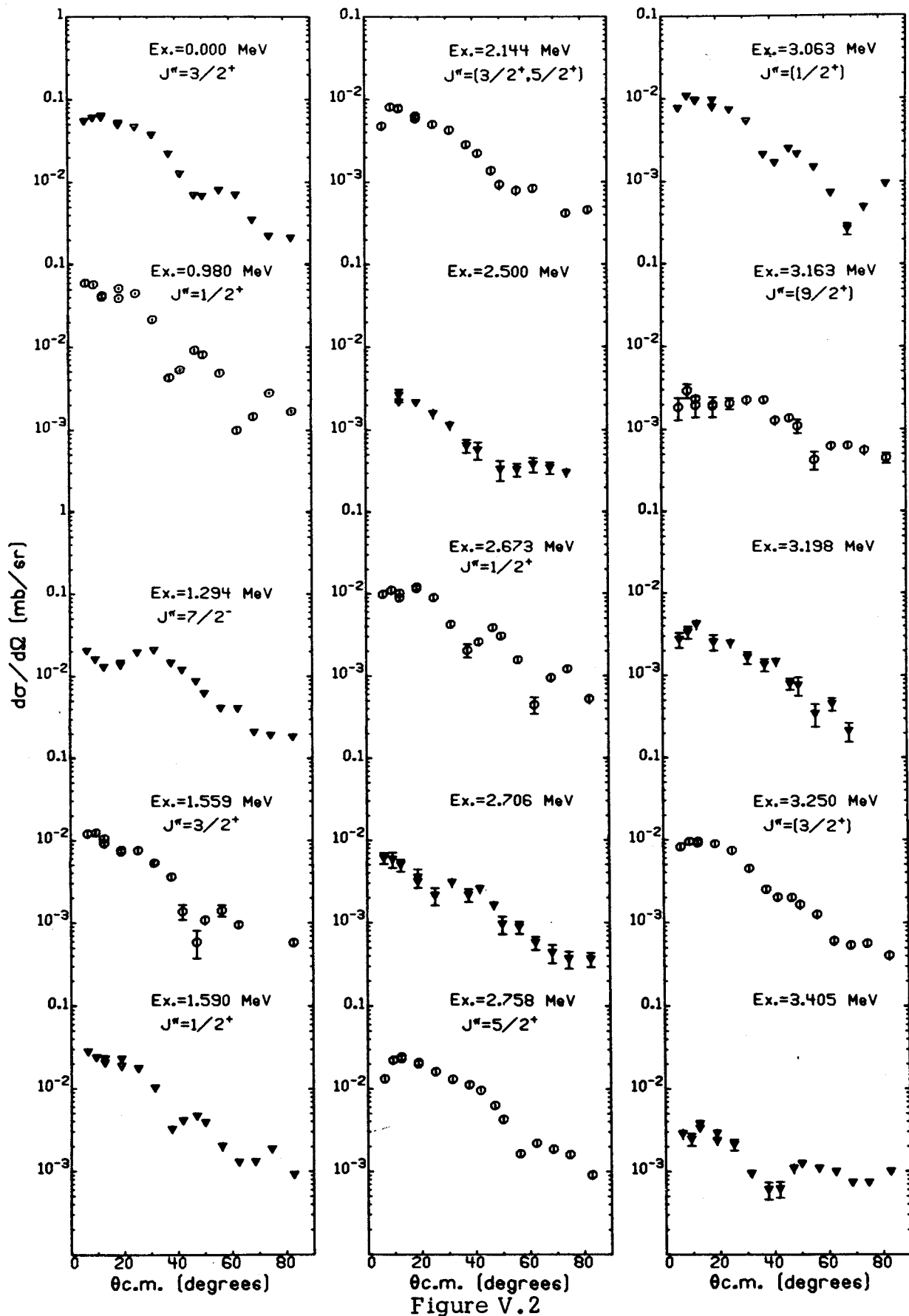
^{44}Ca(p,α)^{41}K Ep=35 MeV

Figure V.2

Figure V.3

^{44}Ca(p,α)^{41}K angular distributions.
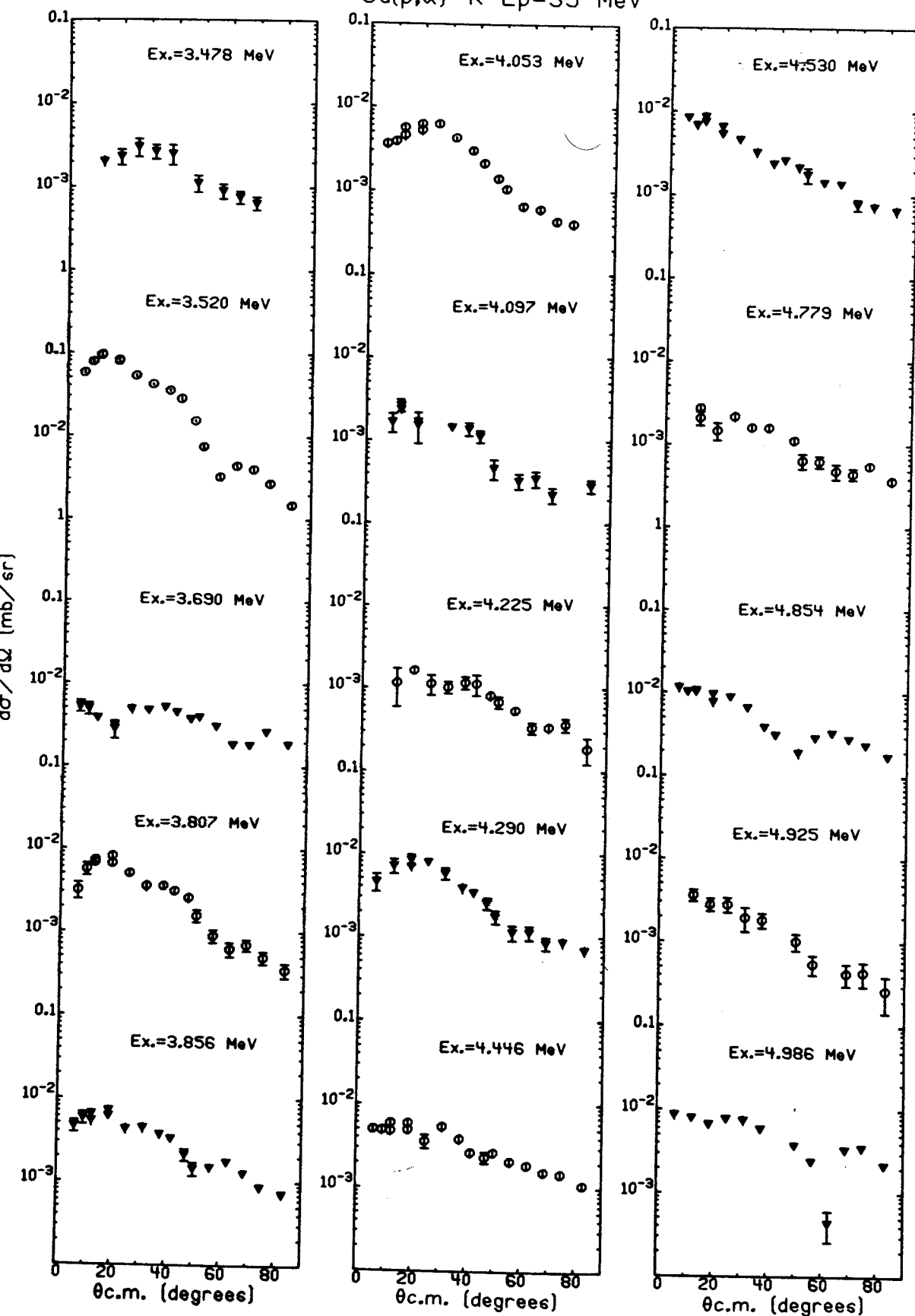
$^{44}Ca(p,\alpha)^{41}K$ Ep=35 MeV

Figure V.3

Figure V.4

^{44}Ca(p,α)^{41}K angular distributions.

$^{44}Ca(p,\alpha)^{41}K$ $E_p=35$ MeV

$d\sigma/d\Omega$ [mb/sr]

$\theta_{c.m.}$ [degrees]

T=5/2 $J^\pi=3/2^+$

T=5/2 $J^\pi=1/2^+$

T=5/2 $J^\pi=7/2^-$

Ex.=5.204 MeV

Ex.=5.417 MeV
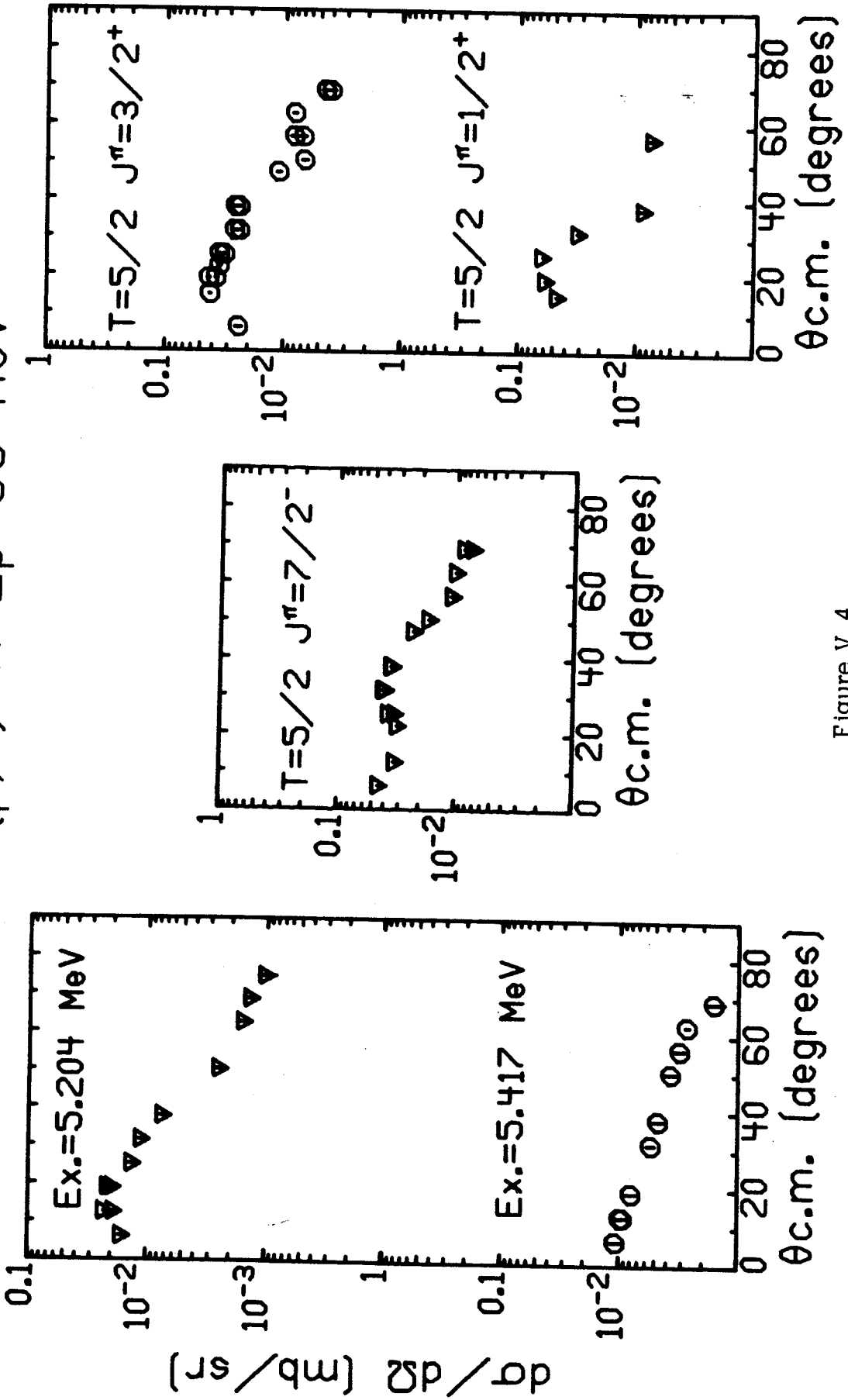
Figure V.4

Most of the 0d3/2 proton hole strength is in the ground state.

Other possible 3/2$^+$ assignments based on their angular distributions

are found at 1.559 MeV, 2.144 MeV, 2.500 MeV, 3.250 MeV,

4.053 MeV, and 4.446 MeV. Two of these levels have been reported

in other experiments. The 2.144 MeV state has been observed in

^{40}K(n,γ)^{41}K work (V.12). A 5/2$^+$ assignment is favored on the basis

of the γ-decays of this level. A level populated with an $\ell = 1$ transfer

is observed at 4.444 MeV in the ^{40}Ar(^{3}He,d)^{41}K reaction (V.13). If

the level at 4.446 MeV is the same state, then it must be a 3/2$^-$

level, since the angular distribution does not have the oscillatory

nature of a 1/2$^-$ transfer. Since 3/2$^-$ and 3/2$^+$ angular distributions

are expected to have similar angular distributions at this excitation, it

is not possible to distinguish between them. In addition, the

2.706 MeV level has been reported to have an $\ell = 2$ angular distribu-

tion in the ^{40}Ar(^{3}He,d)^{41}K experiment. Its angular distribution does

not look like either the 3/2$^+$ ground state or the 5/2$^+$, 3.520 MeV

state.

The 0d5/2 strength is largely contained in the 3.520 MeV state.

Other 5/2$^+$ shapes are seen at 2.758 MeV and 3.850 MeV.

The $\ell = 2$ j-dependence is well defined for this target. The j-

dependence, which is not as obvious as that of the $\ell = 1$ j-

dependence, is a small forward angle effect. This type of small-

angle j-dependence has been reported previously by Glenn et al.

(V.14). The $5/2^+$ angular distribution shows a distinct dip as the angle is decreased, a peak at about 14 degrees, and a flat shoulder, while the $3/2^+$ displays a smooth rounded fall-off as the angle increases. The j-dependence for $\ell = 2$ is illustrated in Figure V.5.

The maximum spin that can be made from $(0f7/2)^2 0d3/2$ is 15/2. A $15/2^+$ tentative assignment has been made from the results of a $(HI, xn, yp, z\alpha, \ldots, \gamma)$ experiment at 3.897 MeV (V.15). There is no evidence for a peak at this excitation in the (p, α) spectra. A tentative $19/2^-$ assignment has been made on the basis of results of the same experiment at 4.986 MeV. This level can be populated in the (p, α) reaction if there is a 2p-2h component of the ^{44}Ca ground state. A peak at this energy is observed. Its angular distribution is reasonably flat as would be expected for a high spin state. There is another angular distribution that is associated with a peak at 4.854 MeV that is nearly identical to the angular distribution of the 4.986 MeV level. The largest peak in the back angle spectra is a doublet located at 4.34 MeV. It is likely that at least one of these states has a spin greater than 11/2. Unfortunately, the data for the high spin states is not definitive because the because the density of states in this region is so high and empirical shapes for large angular momentum transfers are not known.

The only negative parity state that can be definitely identified in the low excitation spectra is the 1.294 MeV $7/2^-$ state. It is possible that the 4.446 MeV state is a $3/2^-$ state.

Figure V.5

^{44}Ca$(p,\alpha)^{41}$K L = 2 angular distributions.

L=2 Angular Distributions
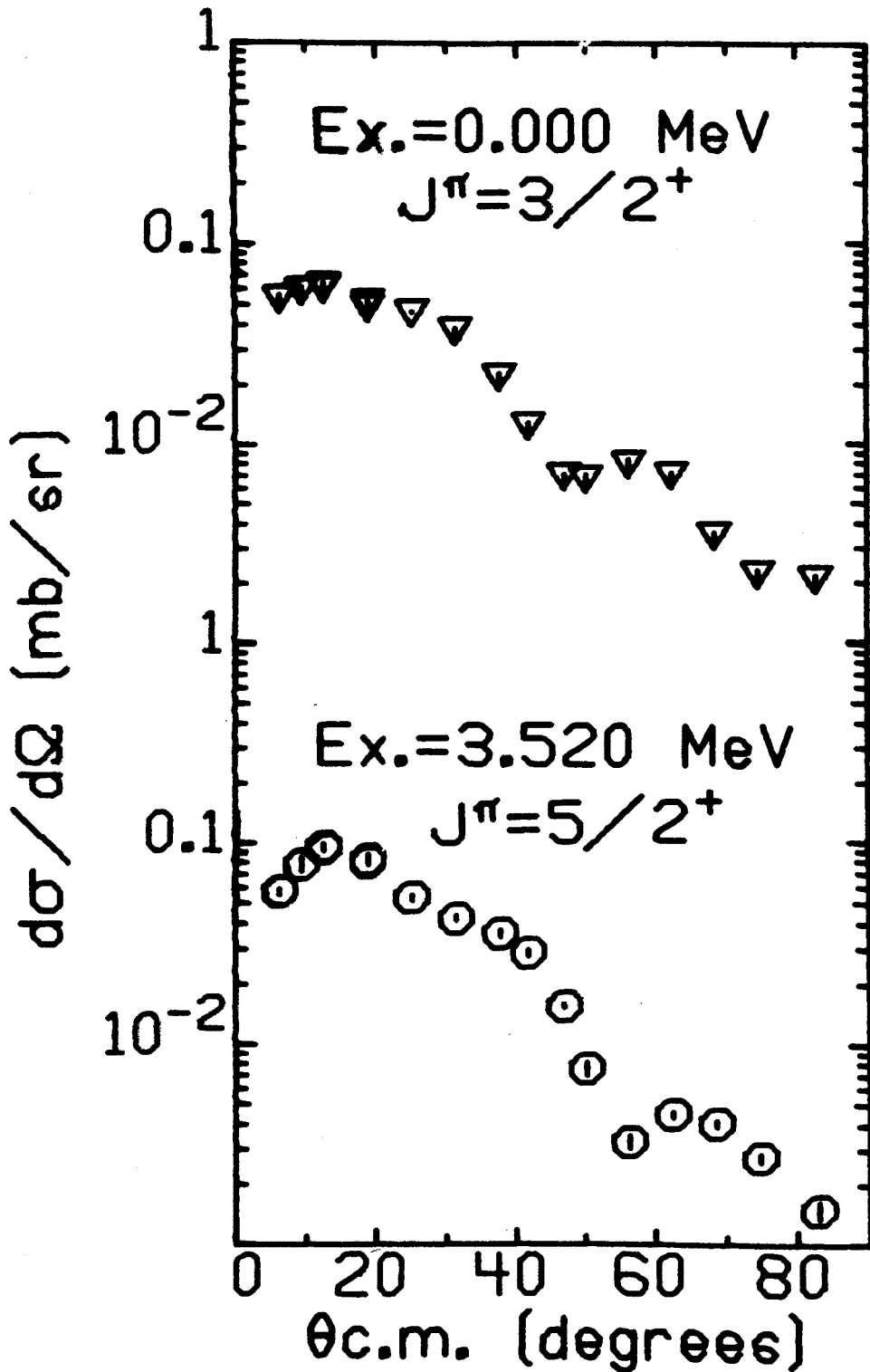
Figure V.5

In order to look for the $T = 5/2$ proton hole states, the spectrograph field was adjusted so that the excitation region from 6 MeV to 10 MeV fell on the counter. A spectrum of this region is shown in Figure V.6. The three strong peaks are the $7/2^-$ analog of the ^{41}Ar ground state and the $3/2^+$ and $1/2^+$, $T = 5/2$ proton hole states. This data suggests that the 1.03 MeV state in ^{41}Ar should be assigned $j^\pi = 3/2^+$. The angular distributions for these levels are found in Figure V.4.

A summary of the levels observed in this experiment and others is given in Table V.1. The j^π values which are given in ( ) in the (p, α) column are assignments made on the basis of the (p, α) data.

C. DWBA Calculations—Cluster Form Factors

Cluster model calculations have been used frequently because they are easily generated and because they can reproduce the shapes of many angular distributions. This type of calculation is especially useful for studying j-dependence and the effects of different optical potentials. Furthermore, continued study of cluster form factor parameters is desirable because of the wide range of choices that are found in the literature (see Chapter IV for a discussion of this point).

Because of the consistent success of the well-matching procedure for (p, α) reaction calculations, the ^{44}Ca α-elastic scattering data of Fernandez and Blair (V.16) were refit to obtain an optical potential with real well parameters: $V = 200$ MeV, $r_o = 1.22$ fm.,

Figure V.6

T = 5/2 proton hole states in ^{41}K.
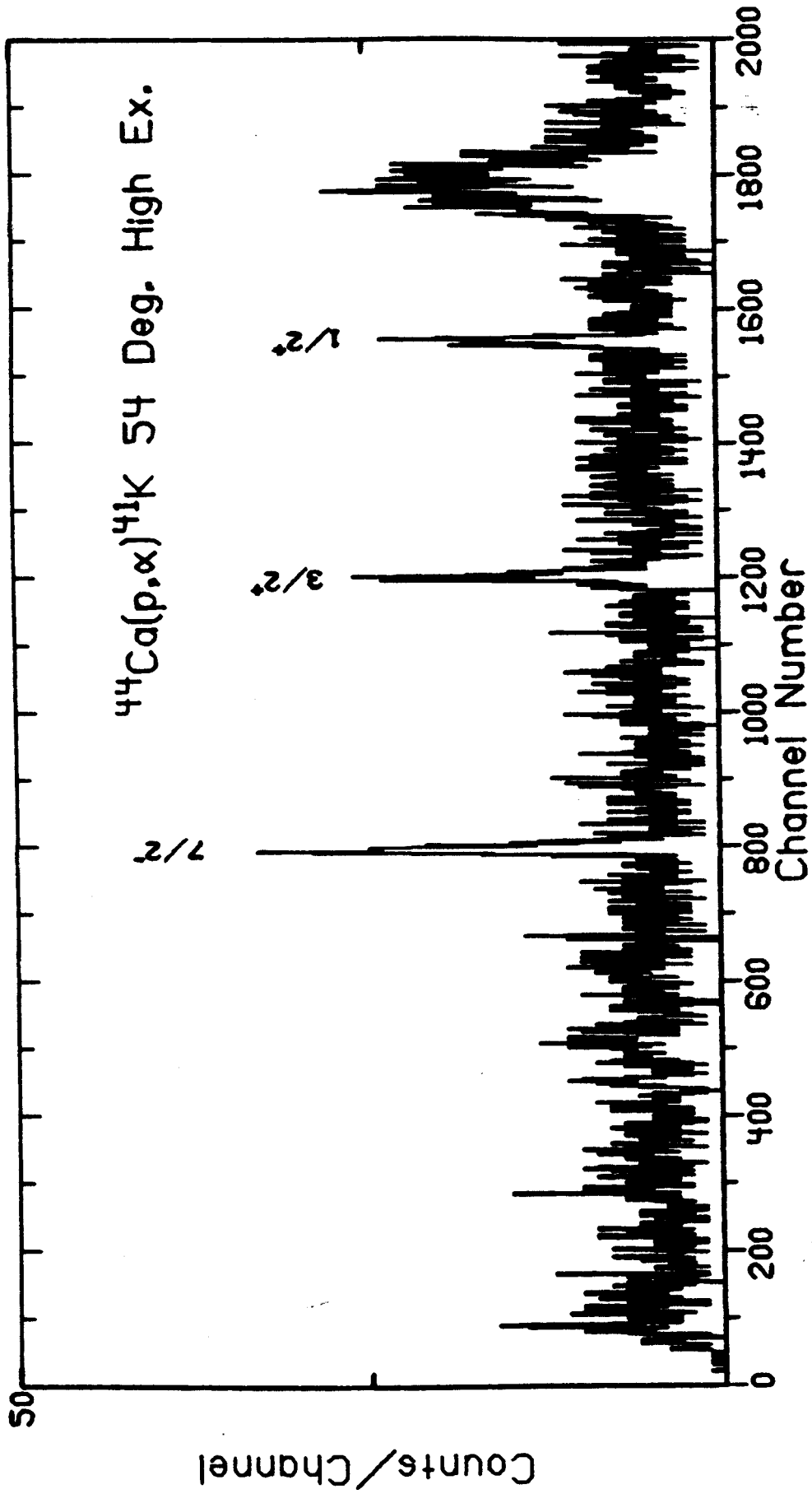
Figure V.6

TABLE V.1

ENERGY LEVELS OF ^{41}K

$(p,\alpha)^a$	$(d,{}^3\mathrm{He})^b$	$({}^3\mathrm{He},d)^c$	$(n,\gamma)^d$		$(\mathrm{HI},xn,yp,\dots\gamma)^f$	J^π
$0.000\ 3/2^+$	$0.000\ 3/2^+$	$0.000\ 3/2^+$		$0.000\ 3/2^+$		$3/2^+$
$0.980\ 1/2^+$	$0.98\ 1/2^+$	$0.980\ 1/2^+$	$0.9804\ 1/2^+$	$0.9804\ 1/2^+$		$1/2^+$
$1.294\ 7/2^-$	$1.29\ 7/2^-$	$1.293\ 7/2^-$	$1.2934\ 7/2^-$	$1.2936\ 7/2^-$	$1.294\ 7\ 2^-$	$7/2^-$
$1.559\ (3/2^+)$			$1.5599\ (1/2^+)$	$1.5599\ (\leq 5/2)$		$(3/2^+)$
	1.57	$1.582\ (1/2^-, 3/2)$	$1.5820\ (5/2^+)$	$1.582\ (\leq 5/2)$		
$1.590\ 1/2^+$				$1.594\ (\leq 5/2)$		$1/2^+$
1.680			$1.6775\ (5/2^+, 7/2^+)$	$1.6770\ (5/2^-, 7/2, 9/2^-)$	$1.6771\ (7/2^+)$	$(5/2^+, 7/2^+)$
1.696		1.693	$1.6981\ (5/2^+, 7/2^+)$	1.6981		$(5/2^\pm, 7/2^+)$
$2.144\ (3/2^+)$		$2.164\ (1/2^-, 3/2^-)$	$2.1441\ (5/2^+)$	$2.1441\ (\leq 5/2, 7/2^-)$		$(3/2^+, 5/2^+)$
		$2.313\ (5/2^-, 7/2^-)$	$2.1660\ (1/2, 3/2)$	$2.1660\ (\leq 5/2, 7/2^-)$		$(1/2^-, 3/2^-)$
2.307			$2.3165\ (5/2^+, 7/2^+)$			$(5/2, 7/2)$
2.427			$2.4479\ (1/2, 3/2)$			$(1/2, 3/2)$
$2.500\ (3/2^+)$			2.4947			
2.582			2.5079		$2.528\ (11/2^+)$	$(11/2^+)$
			2.5279			

TABLE V.1—Continued

(p,α)[a]	$(d,{}^{3}He)$[b]	$({}^{3}He,d)$[c]	(n,γ)[d]	$(HI,xn,yp,\dots,\gamma)$[f]	J^{π}
2.673 1/2$^+$	2.67 1/2$^+$	2.592 (1/2$^-$, 3/2$^-$)			(1/2$^-$, 3/2$^-$)
		2.672 1/2$^+$	2.6815		1/2$^+$
2.706		2.710 (3/2$^+$, 5/2$^+$)	2.7122		(3/2$^+$, 5/2$^+$)
2.758 (5/2$^+$)		2.755 (3/2$^+$,	2.7565		(5/2$^+$)
			2.7607	2.762 (11/2$^-$)	(11/2$^-$)
				2.774 (13/2$^+$)	(13/2$^+$)
3.063 (1/2$^+$)		3.046 (1/2$^-$, 3/2$^-$)	3.0421		(1/2$^-$, 3/2$^-$)
					(1/2$^+$)
3.163			3.142		
3.198	3.19 (3/2$^+$, 5/2$^+$)		3.1645		(3/2$^+$, 5/2$^+$)
3.250 (3/2$^+$)		3.216 (doublet)	3.2134		(3/2$^+$)
			3.2356		
3.303			3.2811		
3.405		3.446 (5/2$^-$, 7/2$^-$)			(5/2$^-$, 7/2$^-$)

TABLE V.1—Continued

(p,α) a)	$(d,{}^3\mathrm{He})$ b)	$({}^3\mathrm{He},d)$ c)	(n,γ) d)	$(\mathrm{HI},xn,yp,\ldots\gamma)$ f)	J^π
3.478	3.48 $(3/2^+, 5/2^+)$	3.480 $(5/2^-, 7/2^-)$			$(5/2^+)$
3.520 $(5/2^+)$		3.619 $(1/2^-, 3/2^-)$			$(1/2^-, 3/2^-)$
3.690		3.736 $(1/2^-, 3/2^-)$			$(1/2^-, 3/2^-)$
		3.773 $(5/2^-, 7/2^-)$			$(5/2^-, 7/2^-)$
					$(5/2^+)$
3.807 $(5/2^+)$		3.819 $(1/2^-, 3/2^-)$			$(1/2^-, 3/2^-)$
					$(5/2^+)$
3.850 $(5/2^+)$		3.858 $(5/2^-, 7/2^-)$			$(5/2^-, 7/2^-)$
				3.897 $(15/2^+)$	$(15/2^+)$
		3.916 $(1/2^-, 3/2^-)$			$(1/2^+)$
					$(3/2^-)$
		4.032 $(3/2^+, 5/2^+)$			$(3/2^+)$
					$(5/2^+)$
4.053 $(3/2^+)$					$(3/2^+)$

TABLE V.1—Continued

$(p,\alpha)^{a)}$	$(d, {}^3He)^{b)}$	$({}^3He, d)^{c)}$	$(n,\gamma)^{d)}$	$(HI, xn, yp, \ldots, \gamma)^{f)}$	J^π
4.097					
4.225		4.140		4.275 $(15/2^-)$	$(15/2^-)$
4.290		4.237 (doublet)			$(5/2^-, 7/2^-)$
	4.40 $(3/2^+, 5/2^+)$	4.339 $(5/2^-, 7/2^-)$			$(3/2^+, 5/2^+)$
4.446 $(3/2^\pm)$		4.478 $(1/2^-, 3/2^-)$			$(3/2^\pm)$
		4.478 $(1/2^-, 3/2^-)$			$(1/2^-, 3/2^-)$
4.530		4.587			
		4.661 (doublet)			
		4.728 $(1/2^-, 3/2^-)$			$(1/2^-, 3/2^-)$
4.779					
4.854	4.90 $(3/2^+, 5/2^+)$	4.848			$(3/2^+, 5/2^+)$
4.925		4.922 (doublet)		4.275 $(15/2^-)$	$(19/2^-)$
4.986					

TABLE V.1—Continued

$(p,\alpha)^a$	$(d,{}^3He)^b$	$({}^3He,d)^c$	$(n,\gamma)^d$	$(HI,xn,yp,\dots,\gamma)^f$	J^π
5.011		4.995 $(5/2^-,7/2^-)$			$(5/2^-,7/2^-)$
	5.06 $(3/2^+,5/2^+)$				$(3/2^+,5/2^+)$
		5.091 $(1/2^-,3/2^-)$ 5.160 $(5/2^-,7/2^-)$			$(1/2^-,3/2^-)$ $(5/2^-,7/2^-)$
5.204		5.235 $(1/2^-,3/2^-)$ 5.270 $(1/2^-,3/2^-)$ 5.335 $(1/2^-,3/2^-)$ 5.393 $(1/2^-,3/2^-)$			$(1/2^-,3/2^-)$ $(1/2^-,3/2^-)$ $(1/2^-,3/2^-)$ $(1/2^-,3/2^-)$
5.417 $(7/2^-,T=5/2)$ $(3/2^+,T=5/2)$ $(1/2^+,T=5/2)$					$(7/2^-,T=5/2)$ $(3/2^+,T=5/2)$ $(1/2^+,T=5/2)$

NOTE: Errors on (p,α) excitation energies are 5 keV below 3 MeV of excitation and 10 keV between 3 and 5.5 MeV.

[a]This experiment.

[b]Reference V.6.

[c]Reference V.13.

[d]Reference V.12.

[e]Reference V.21.

[f]Reference V.15.

$a = .72$ fm. The choice of proton parameters was determined by the success in fitting the α-elastic scattering data. Since the α-scattering was fit better by the choice $r_o = 1.22$ fm. than $r_o = 1.17$ fm., the $r_o = 1.22$ fm. Bechetti and Greenlees proton parameters were used (V.10). Given these choices, the bound state well should be chosen so that $r_o = 1.22$ fm., $a = .72$ fm., and $V \cong 150$ MeV. However, the well depth was allowed to vary to get the correct triton separation energy. For the most part, the depth was near 130 MeV. The fits to the data were not particularly good for the forward angles for this set of parameters. Since it was found that reducing the value of the diffuseness parameter slightly produced better fits to the $^{52}Cr(p,\alpha)^{49}V$ data (see Chapter IV), this was tried here. The best fit was found to occur for $a = .55$ fm., which is quite a bit smaller than was found to be necessary previously for the $^{52}Cr(p,\alpha)^{49}V$ reaction. The calculations are compared to the data in Figure V.7. The optical potentials are given in Table V.2.

TABLE V.2

OPTICAL POTENTIALS

	V	r_o	a	V_{so}*	r_{so}	a_{so}	W	r_I	a_I	W_D*
p	-43.2	1.22	.72	-25.0	1.06	.68	-5.0	1.32	.57	12.2
	-206.2	1.22	.72				-16.0	1.64	.57	

*Values for V_{so} and W_D include the factor of 4 required by DWUCK72 (V.17).

Figure V.7

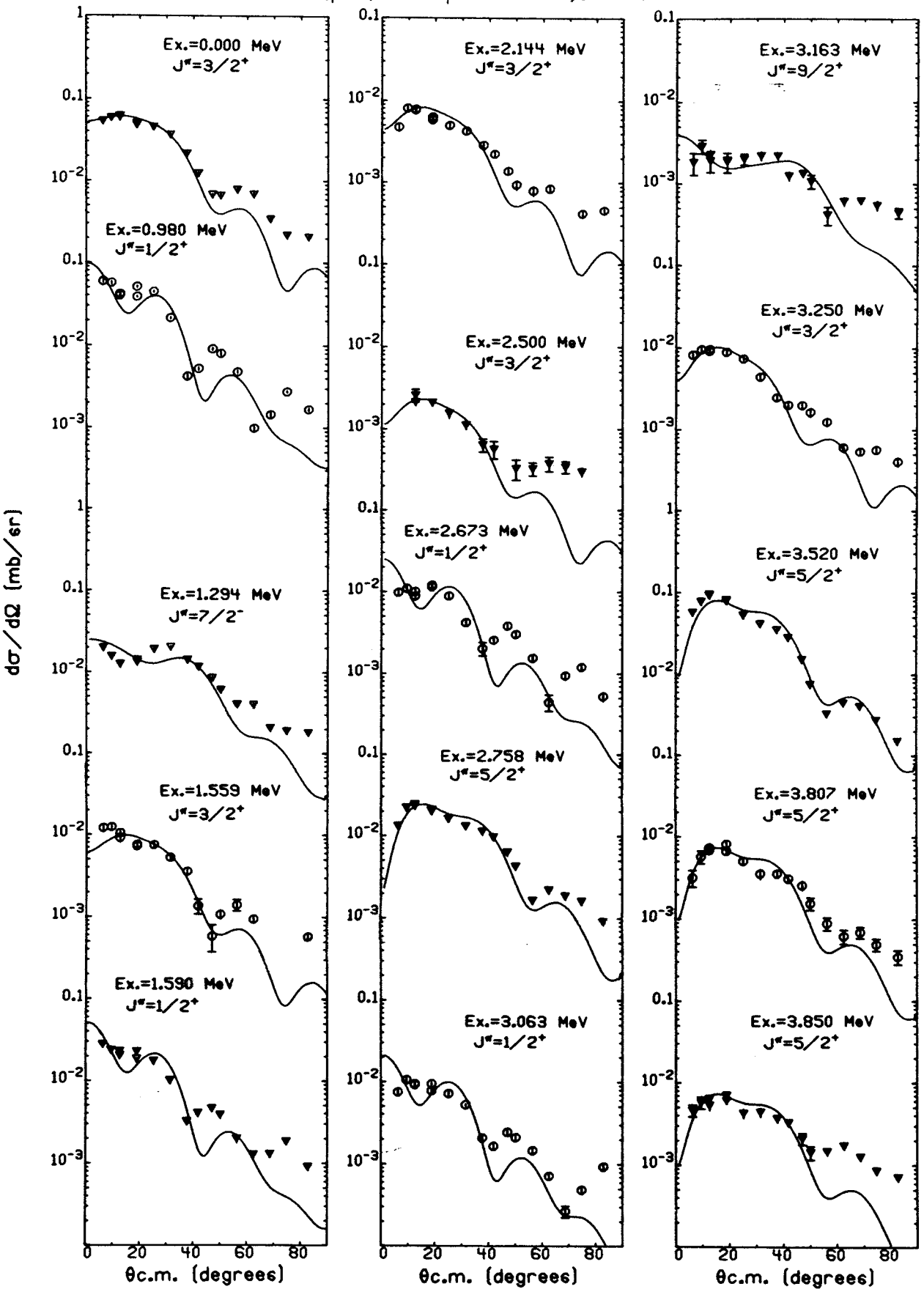DWBA calculations for the $^{44}Ca(p,\alpha)^{41}K$ reaction using cluster form factors.

$^{44}Ca(p,\alpha)^{41}K$ $Ep=35$ MeV;Cluster Model

Ex.=0.000 MeV
$J^\pi=3/2^+$

Ex.=0.980 MeV
$J^\pi=1/2^+$

Ex.=1.294 MeV
$J^\pi=7/2^-$

Ex.=1.559 MeV
$J^\pi=3/2^+$

Ex.=1.590 MeV
$J^\pi=1/2^+$

Ex.=2.144 MeV
$J^\pi=3/2^+$

Ex.=2.500 MeV
$J^\pi=3/2^+$

Ex.=2.673 MeV
$J^\pi=1/2^+$

Ex.=2.758 MeV
$J^\pi=5/2^+$

Ex.=3.063 MeV
$J^\pi=1/2^+$

Ex.=3.163 MeV
$J^\pi=9/2^+$

Ex.=3.250 MeV
$J^\pi=3/2^+$

Ex.=3.520 MeV
$J^\pi=5/2^+$

Ex.=3.807 MeV
$J^\pi=5/2^+$

Ex.=3.850 MeV
$J^\pi=5/2^+$

$d\sigma/d\Omega$ [mb/sr]

θc.m. (degrees)

θc.m. (degrees)

θc.m. (degrees)

Figure V.7

The $\ell = 2$ j-dependence is predicted properly by the calculations; however, the fits to the $1/2^+$ states are poor. It has not been possible to fit the $1/2^+$ and the $3/2^+$ and $5/2^+$ angular distributions simultaneously.
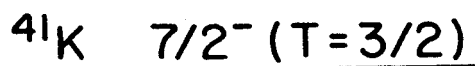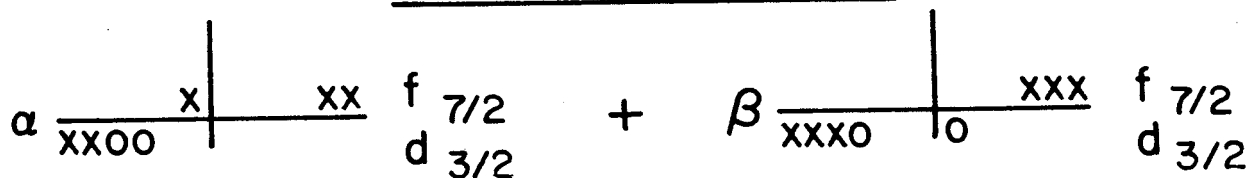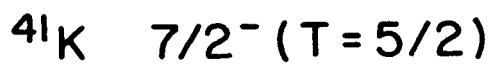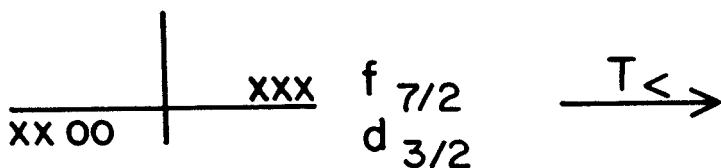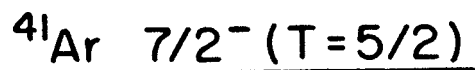
In general the normalization of the cluster model is not easily related to nuclear wavefunctions. If, however, two states have the same wavefunction in a p-n formalism, then the ratio of normalizations is independent of spectroscopic factors and reduces to $1/(2T+1)$. This has been discussed previously for the ground state of ^{49}V and the $T = 5/2$, $7/2^-$ state in ^{49}V that are observed in the $^{52}Cr(p,\alpha)^{49}V$ reaction (see Chapter IV). DWBA cluster model calculations where the well depth is allowed to vary to get the correct triton binding energy gave the analog state normalization to about 12.5 times too large for ^{49}V.

The two $7/2^-$ states observed in ^{41}K in the $^{44}Ca(p,\alpha)^{41}K$ are not related as those observed in ^{49}V. They are, however, related by being an analog-anti-analog pair for the ^{41}Ar ground state. This relation is illustrated in Figure V.8. If we assume that there is no mixed shell pick-up (see the section on microscopic calculations), the second term will not be involved and the ratio of spectroscopic factors using any form factor model should be

$$\frac{S_<}{S_>} = \frac{\alpha^2}{\beta^2} = \frac{3}{4}.$$

Figure V.8

Wavefunctions for analog states in the mass 41 system.

^{41}Ar   7/2$^-$ (T=5/2)

$\alpha \dfrac{\text{x}}{\text{XXOO}} \quad \overline{\qquad}^{\text{XX}} \quad \begin{matrix} \text{f }_{7/2} \\ \text{d }_{3/2} \end{matrix}$ $\xrightarrow{\;T<\;}$

^{41}K   7/2$^-$ (T=5/2)

$\alpha \dfrac{\text{x}}{\text{XXOO}} \quad \overline{\qquad}^{\text{XX}} \quad \begin{matrix} \text{f }_{7/2} \\ \text{d }_{3/2} \end{matrix}$ $+$ $\beta \dfrac{}{\text{XXXO}}\Big|_{\text{O}} \quad \overline{\qquad}^{\text{XXX}} \quad \begin{matrix} \text{f }_{7/2} \\ \text{d }_{3/2} \end{matrix}$

^{41}K   7/2$^-$ (T=3/2)

$\beta \dfrac{\text{x}}{\text{XXOO}} \quad \overline{\qquad}^{\text{XX}} \quad \begin{matrix} \text{f }_{7/2} \\ \text{d }_{3/2} \end{matrix}$ $-$ $\alpha \dfrac{}{\text{XXXO}}\Big|_{\text{O}} \quad \overline{\qquad}^{\text{XXX}} \quad \begin{matrix} \text{f }_{7/2} \\ \text{d }_{3/2} \end{matrix}$

$\alpha = \sqrt{3/7}$, $\beta = \sqrt{4/7}$

Figure V.8

The expected ratio of the normalizations, given these assumptions, will be

$$\frac{N_>}{N_<} = \frac{c_>^2 s_>}{c_<^2 s_<} = \frac{1}{2T+1} \frac{3}{4} = .15.$$

The ratio deduced from the fits shown in Figure V.9 is 1.92 which is 12.8 times the expected value. Once again the analog state is anomolously large with nearly the same enhancement that was observed in the $^{52}Cr(p,\alpha)^{49}V$ reaction.

D. DWBA Calculations—Microscopic Form Factors

The microscopic form factors were generated by the prescription given in Chapter II. $(0f7/2)^2 0d3/2$, $(0f7/2)^2 1s1/2$, $(0f7/2)^2 0d5/2$ pure configurations were assumed for the fragments of the sd-shell hole states. The fits that were obtained are shown in Figure V.10. In general they are not as satisfactory as the cluster model shapes. The calculations have been normalized to minimize χ^2.

Relative spectroscopic factors assuming a "spectator model" for the sd-shell hole states are given in Table V.3. The table has been normalized so that the total 0d3/2 spectroscopic factor is 1.0. For a zero order shell model assumption, the total 1s1/2 spectro-scopic factor should be .5 and the total 0d5/2 spectroscopic factor should be 1.5. The fractions are markedly different from the results obtained by the (d,^{3}He) reaction. The $3/2^+$ strength is found to be divided in the (p,α) data, though most of it is in the ground state.

Figure V.9

DWBA calculations for the two $7/2^-$ levels observed in the
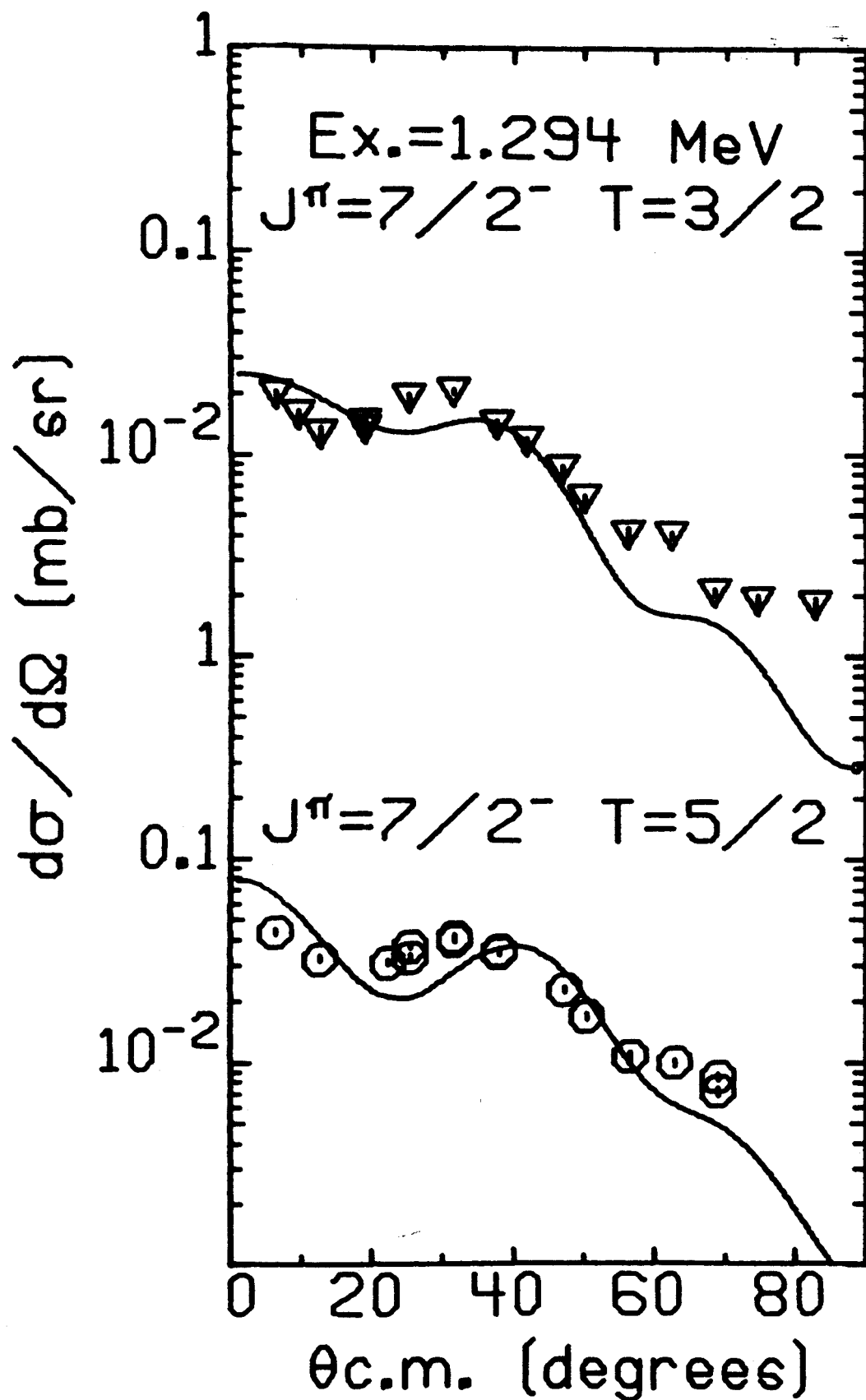$^{44}Ca(p,\alpha)^{41}K$ reaction using cluster form factors.

Cluster Model

Figure V.9

Figure V.10

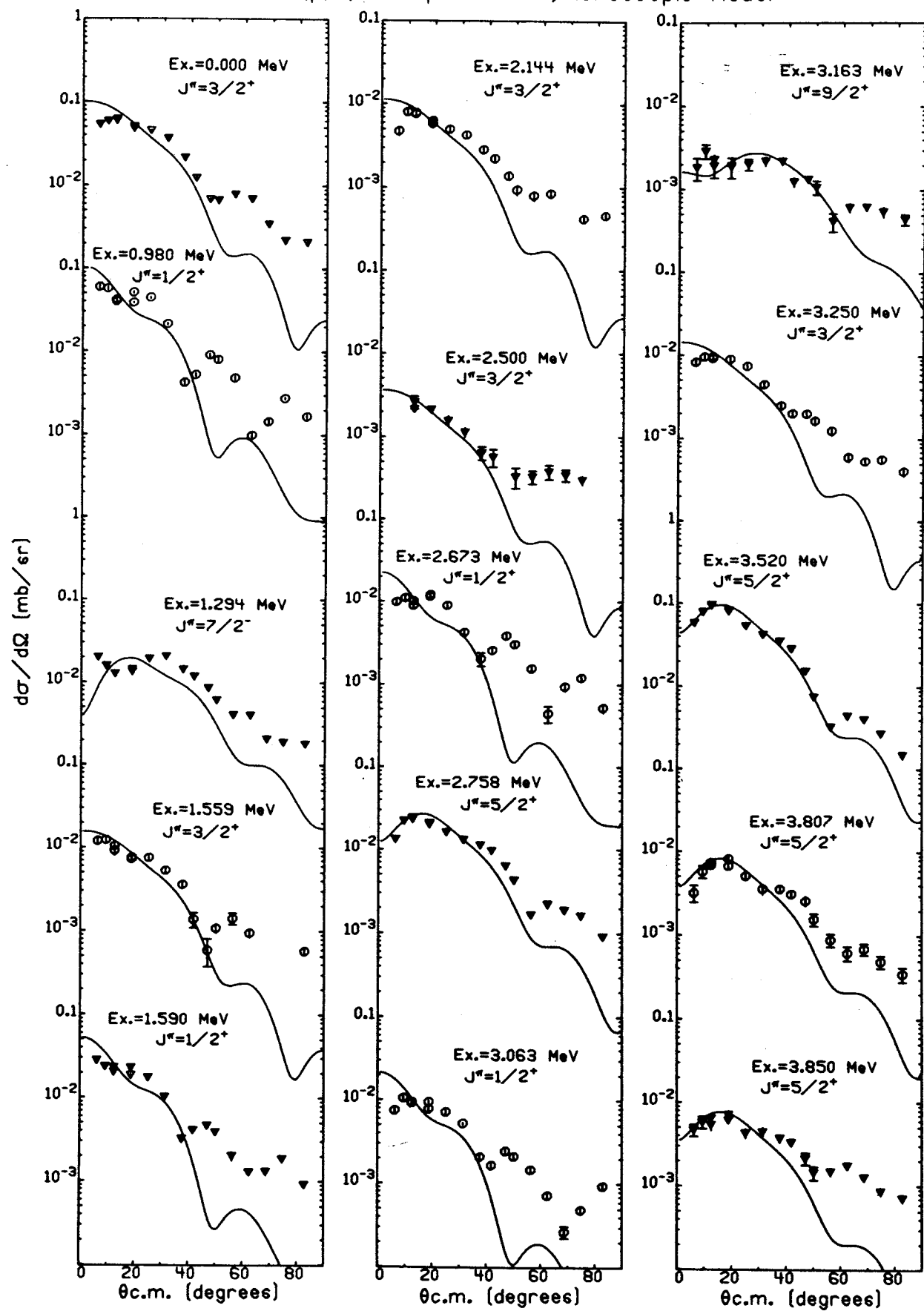DWBA calculations for ^{44}Ca$(p,\alpha)^{41}$K reaction using microscopic form factors.

$^{44}Ca(p,\alpha)^{41}K$ Ep=35 MeV;Microscopic Model

Figure V.10

TABLE V.3

RELATIVE PROTON HOLE SPECTROSCOPIC FACTORS

Excitation Energy	J^π	Relative C^2S[a]	$(d, {}^3He)$[b]
0.000	$3/2^+$	.69	1.0
0.980	$1/2^+$	.35	.22
1.559	$3/2^+$	.11	.05[c]
1.590	$1/2^+$	.12	.05[c]
2.144	$3/2^+$	.08	
2.500	$3/2^+$	.03	
2.673	$1/2^+$	.05	.19
2.758	$5/2^+$	.32	
3.063	$1/2^+$	.05	
3.250	$3/2^+$	.10	
3.520	$5/2^+$	1.13	.24
3.807	$5/2^+$	.10	
3.850	$5/2^+$	.06	

[a]Normalized so that $\sum(3/2^+) = 1.0$.

[b]From Reference V.6.

[c]Not resolved.

Some of the weaker $3/2^+$ levels may be seniority three couplings. The 1s1/2 strength is primarily located in the 0.980 MeV state in the (p,α) data, but is nearly equally divided with the 2.673 MeV state in the (d, ^{3}He) results. The grossest difference is in the $5/2^+$ levels where 70 percent of the 0d5/2 strength is found in the 3.520 MeV level in the (p,α) data. The (d, ^{3}He) data does not have a single strong $5/2^+$ transition. The authors choose to call all levels above 2 MeV $5/2^+$ levels with small spectroscopic factors in that study.

If all the levels of the same j^π in Table V.3 are totaled, the results shown in Table V.4 are obtained. The agreement with a zero order shell model is fortuitous given the quality of the fits.

TABLE V.4

TOTAL SPECTROSCOPIC FACTORS

Hole	Total	Zero Order Shell Model
0d3/2	1.0*	1.0
1s1/2	.57	.5
0d5/2	1.61	1.5

*Normalized to 1.0.

Calculations for the 1.294 MeV 7/2⁻ state were performed for the configurations: $(0f7/2\ 0d3/2)0d3/2$ and $(0f7/2)^3$. The proton occupation number for the 0f7/2 shell in ^{44}Ca has been deduced from the ^{44}Ca$(d,{}^3$He$)^{43}$K reaction to be .85. Therefore the occupation of the (1s1/2 + 0d3/2) orbits is 5.15 and the spectroscopic factor relative to the total (1s1/2 + 0d3/2) strength should be .165 for the $(0f7/2)^3$ configuration. A difference from this number would indicate a need for the mixed neutron configuration. The number which we get is .157 which is consistent with the $(d,{}^3$He$)$ result. There does not appear to be a need for a mixed neutron configuration for this transfer. This also implies that the relative spectroscopic factor of the 0d5/2

hole states should be larger than 1.5 since the 0d3/2 occupation is less than 4. The result shown in Table V.4 is in fact larger than 1.5.

E. Conclusions

The ^{44}Ca(p,α)^{41}K reaction has been found to strongly populate the sd-shell proton hole states that have been observed in previous ^{42}Ca(d,^{3}He)^{41}K work. Fragments of 1s1/2, 0d3/2, and 0d5/2 holes have been identified. A number of new states have been identified as parts of the 0d5/2 proton hole structure. The largest of these fragments is located at an excitation energy of 3.520 MeV.

In addition to the positive parity states, the 7/2$^-$ state at 1.294 MeV is populated with about the same relative strength as seen in the (d,^{3}He) spectrum.

A comparison of the 3/2$^+$ and 5/2$^+$ angular distributions shows that there is a definable j-dependence for this target. This j-dependence has made it possible to make 3/2$^+$ and 5/2$^+$ assignments to a number of levels below 4 MeV of excitation.

Three T = 5/2 states with probable spins of 7/2$^-$, 3/2$^+$, and 1/2$^+$ have been identified. These are the analogs of the neutron hole states in ^{41}Ar.

DWBA calculations have been performed using mass three cluster form factors. The best fit has been found with the bound state parameters r_o = 1.22 fm. and a = .55 fm. The ℓ = 2 j-dependence which is observed is predicted by these calculations.

DWBA calculations using microscopic form factors and pure configurations have also been performed. The fits to the data are not as good as the cluster model calculations. The normalization of the theory to the data indicates that relative spectroscopic factors for the 1/s1/2 and 0d5/2 fragments are quite different from those deduced from ^{42}Ca(d,^{3}He)^{41}K. This indicates a need to carefully include the coherence in the di-neutron coupling. The relative total spectroscopic factors are, however, consistent with the (d,^{3}He) result. The spectroscopic factor for the 7/2$^-$ state, deduced by assuming a (0f7/2)^3 pick-up, relative to the total (1s1/2+0d3/2) spectroscopic factor is consistent with the results of the ^{44}Ca(d,^{3}He)^{43}K reaction. There does not appear to be a need to include a (0d3/2 0f7/2)0d3/2 pick-up for this transition.

REFERENCES FOR CHAPTER V

V.1   R. G. Markham, M. A. M. Shahabuddin, R. K. Bhowmik,
       J. A. Nolen, Jr., P. A. Smith, Bull. Am. Phys. Soc.
       21 (1976), 634.

V.2   J. E. Finck, J. A. Nolen, Jr., R. Sherr, P. A. Smith,
       private communication.

V.3   S. H. Suck, W. R. Coker, Nucl. Phys. A176 (1971), 89.

V.4   J. W. Smits, F. Iachello, R. H. Siemssen, A. van der
       Woude, Phys. Lett. 53B (1974), 337.

V.5   J. W. Smits, R. H. Siemssen, Nucl. Phys. A261 (1976),
       385.

V.6   P. Doll, G. J. Wagner, K. T. Knopfele, G. Mairle,
       Nucl. Phys. A263 (1976), 210.

V.7   W. R. Falk, Phys. Rev. C8 (1973), 1957.

V.8   J. C. Hiebert, E. Newman, R. H. Bassel, Phys. Rev.
       137 (1965), B102.

V.9   W. R. Falk, A. Djaloeis, D. Ingham, Nucl. Phys. A252
       (1975),452.

V.10   R. G. Markham, R. G. H. Robertson, Nucl. Inst. and
       Meth. 129 (1975), 131.

V.11   F. D. Becchetti, Jr., G. W. Greenlees, Phys. Rev. 182
       (1968) 1190.

V.12   D. F. Berkstrand, E. B. Shera, Phys. Rev. C3 (1971),
       208.

V.13   L. R. Medsker, H. T. Fortune, S. C. Headly, J. N.
       Bishop, Phys. Rev. C11 (1975), 1937.

V.14   J. E. Glenn, C. D. Zafiratos, C. E. Zaidins, Phys.
       Rev. Lett. 26 (1971), 328.

7.15 P. Gorodetzky, J. J. Kolata, J. W. Olness, A. R. Poletti, E. K. Warburton, Phys. Rev. Lett. 31 (1973), 1067.

7.16 B. Fernandez, J. S. Blair, Phys. Rev. C1 (1970), 523.

7.17 P. D. Kunz, unpublished.

CHAPTER VI

SUMMARY

The features of the (p,α) reaction have been investigated from both a theoretical view and an experimental approach. Neither is complete and many aspects and implications need to be pursued in future work.

The theoretical side of the work has been directed toward developing a microscopic model for calculating angular distributions from detailed shell model wavefunctions. A microscopic form factor model which uses harmonic oscillator wavefunctions has been presented. This model, which is similar to one used previously by other researchers, has the advantages of being analytic and easily generalizable to multi-nucleon transfer with heavy ion beams. The oscillator has the disadvantage of not being realistic in the nuclear surface region. A microscopic form factor model which uses single particle wavefunctions generated in a Woods-Saxon well has been developed from a generalization of the popular Bayman and Kallio technique for calculating two nucleon form factors. This method has the advantage of being realistic in the nuclear surface region, but is restricted to

those reactions where the transferred particles are in a 0S state of internal motion.

A method for deriving spectroscopic amplitudes for the (p,α) reaction in terms of two nucleon reduced matrix elements and single nucleon reduced matrix elements has been presented. This method has the advantage of using the output of already existing shell model codes. It has the disadvantages of not being exact and not having simple sum rules.

The motion of the nuclear center of mass in a fixed center potential has been investigated for the harmonic oscillator model. It has been found that this motion can be approximated by a multiplicative factor introduced into the form factor. Even though the analysis cannot be carried out in a Woods-Saxon potential, it is reasonable to assume that the correction is similar to the harmonic oscillator result.

Part of the theoretical side of the investigation has concerned itself with the aspects of the DWBA for the (p,α) reaction. The angular momentum mismatch has been found to be severe. The effects of the mismatch are minimized by choosing "well matched" optical parameters. In the process of investigating the angular momentum dependence of the DWBA a brief excursion into the source of j-dependence in nuclear reactions has been taken. No conclusion can be drawn about j-dependence. Further investigation into this question is needed.

The experimental part of this thesis has been directed toward discovering the features of the (p,α) data. These features may be summarized as follows:

Proton hole states are strongly populated.

Many seniority three transfers are observed.

Many states that appear in the (p,α) spectra are not observed in (p,t) spectra or (t,α) spectra and vice versa indicating that coherence is important in the (p,α) reaction.

There may be j-dependence for $L = 2$ transfers, but this dependence is not consistent from target to target.

Candidates for high spin states are observed in back angle spectra.

Analog states are observed in the (p,α) spectra. These are the analogs of the neutron hole states in the neighboring nucleus.

DWBA calculations using cluster form factors have been found to be capable of reproducing the data if the well matched optical parameters are used and the diffuseness of the bound state well are reduced slightly.

DWBA calculations using microscopic form factors based on pure configuration wavefunctions are moderately successful in fitting the shapes of the angular distributions. The spectroscopic factors derived from these calculations have the correct behavior for the proton hole states observed in the $^{52}Cr(p,\alpha)^{49}V$ reaction. The

agreement for the proton hole states found in the ^{44}Ca$(p,\alpha)^{41}$ reaction is more limited.

APPENDICES

APPENDIX I

ELEMENTS OF NUCLEAR PHYSICS FOR

NON-TECHNICAL PEOPLE

The desk beneath my elbow is a hard object, yet it is mostly empty space. With a powerful enough microscope it is possible to see that this surface is really a large number of small fuzzy balls that bind together to form what we know as wood. These fuzzy balls are the basic building blocks of matter. They are the individual atoms of hydrogen, carbon, sulfur, iron, and numerous other elements that make up wood fiber.

Unfortunately, there are not any microscopes which allow us to look at the individual atoms in enough detail to see what they are made of. To answer this question, it is necessary to rely on evidence which is not nearly as direct as a picture of atoms.

An early picture of atomic structure comes from the famous experiment shown in Figure A.I.1. In this experiment α-particles, which are the result of the radioactive decay of radium, hit the thin gold foil. Most of them pass through and strike the forward scintillator. A scintillator is a material that glows when it is struck by α-particles. Small bursts of light indicate that α-particles are
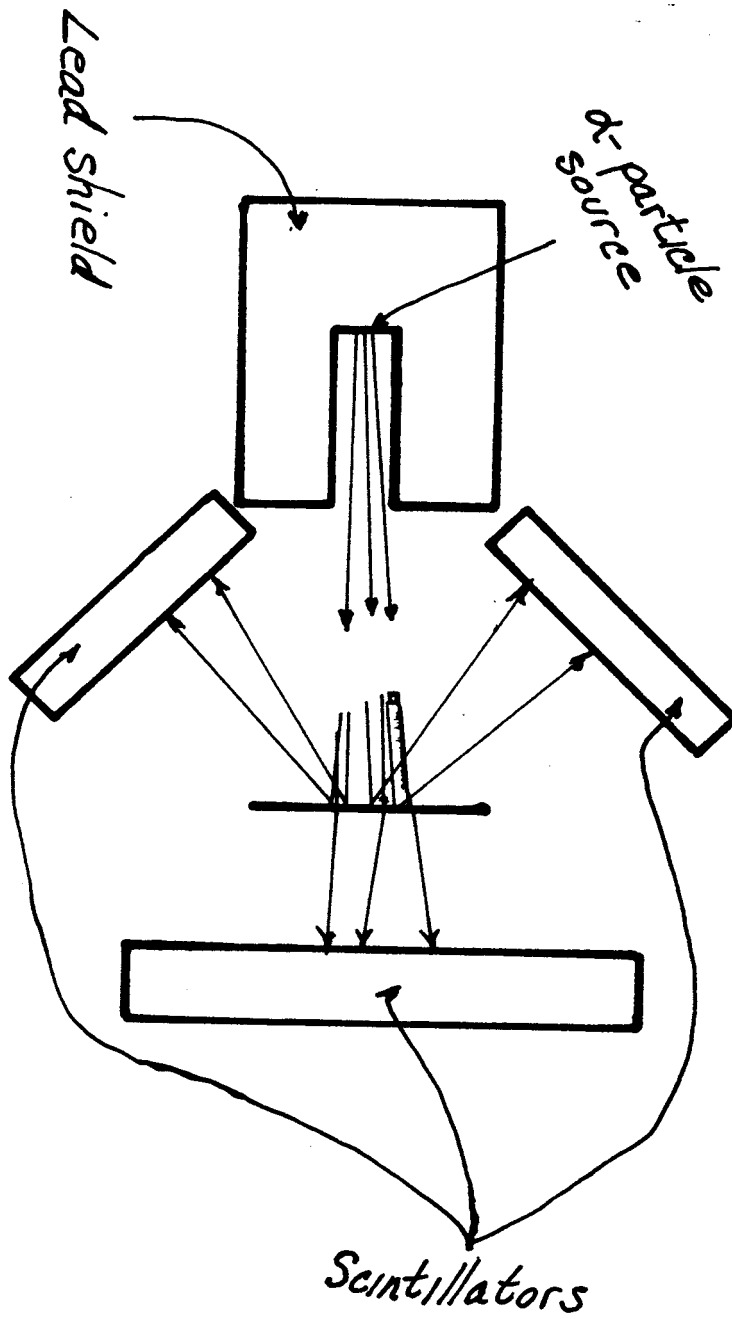
Figure A.I. 1

A sketch of the famous Rutherford experiment.

striking the scintillator. When the experiment was done, it was found that bursts of light were seen in the backward direction also. This could only occur if the projectile had struck something solid and massive.

From such evidence it was concluded that atoms have a small, hard core, which is called the nucleus. More refined experiments have shown that the nucleus is about one onehundredmillionth of the atomic size. It contains almost all the mass of the atom. The resulting picture is a small, positively charged hard core surrounded by a diffuse cloud of negative charge.

Atomic physics and chemistry are the branches of science that are concerned with the properties of atoms and the cloud of electrons that make up the ball of negative charge. It is the goal of nuclear physics to learn about the properties of the nucleus itself. This dissertation concerns itself with some details which should add to our understanding of nuclear phenomena.

Here are some of the questions that need to be answered in our quest toward understanding the nucleus:

1. What are nuclei made of?

2. Why do some of them decay, emitting radiation, when they do?

3. What holds nuclei together?

4. What happens when a projectile strikes a nucleus?

5. What shape is a nucleus?

6. How can we probe the nucleus to answer these questions?

The last question was the first to be answered. There are many known ways to probe the nucleus and there may be more which have not been invented yet. The experiment that has already been discussed contains an answer. To probe a nucleus you must hit it with a small fast projectile, such as an α-particle from a radioactive source. Unfortunately, radioactive sources do not emit fast enough particles to cause anything to happen other than scattering like billiard balls. To determine the constituent parts of the nucleus it is necessary to break it apart in a controlled way. So accelerators were invented to accelerate light particles such as hydrogen nuclei (protons) and helium nuclei (α-particles). In these accelerators the electrons are ripped from hydrogen or helium gas by an electric discharge. Then the free nuclei are accelerated toward a negatively charged piece of metal. There are a number of designs that do this. Later I shall describe how a cyclotron accomplishes the acceleration.

Early experiments showed that the nucleus was made of two types of matter. One type carries a positive charge. The other is neutral. Both particles have almost the same mass. We believe the answer to the first question is probably answered. Nuclei are made of protons and neutrons.

There are only partial answers to the other questions.

It is the fourth question that I have been working on during this project. It is this question to which the remainder of this part is addressed.

Today there are three basic pictures of nuclear reactions.

The first type of scattering is shape elastic scattering. This is the case where nothing happens. The projectile bounces off the target nucleus without causing any change in the state of the nucleus. This is the same thing that happens when two billiard balls collide.

The second picture is the compound nucleus view. In this instance, imagine that the projectile is absorbed by the target nucleus to form a new nucleus. A very short time later this nucleus comes apart at the seams and emits other particles which the experimenter detects. This model is illustrated in Figure A.I.2.

The third reaction model is called the direct reaction. In this picture the projectile makes a close pass, or grazing collision, with the target nucleus. As it passes by, a few protons or neutrons may be transferred, or the target nucleus may be made to vibrate or spin, without an intermediate nucleus being formed. Figure A.I.3 is a schematic of the direct reaction where x represents a cluster of nucleons which the projectile picks up as it passes by.

How do we know which type of reaction occurred?

The answer is that we do not. In fact, there is often a great deal of controversy over this point in nuclear physics literature. In general, one usually argues in the following way. If a compound
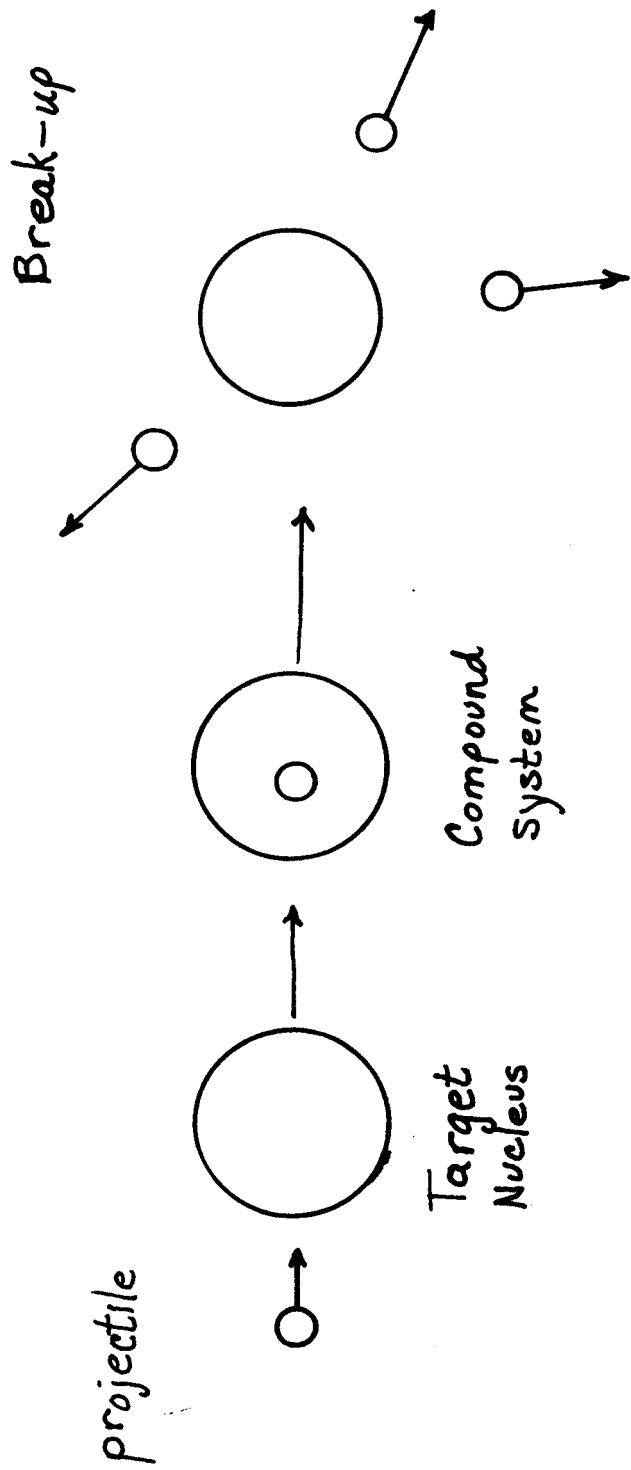
Figure A.I.2

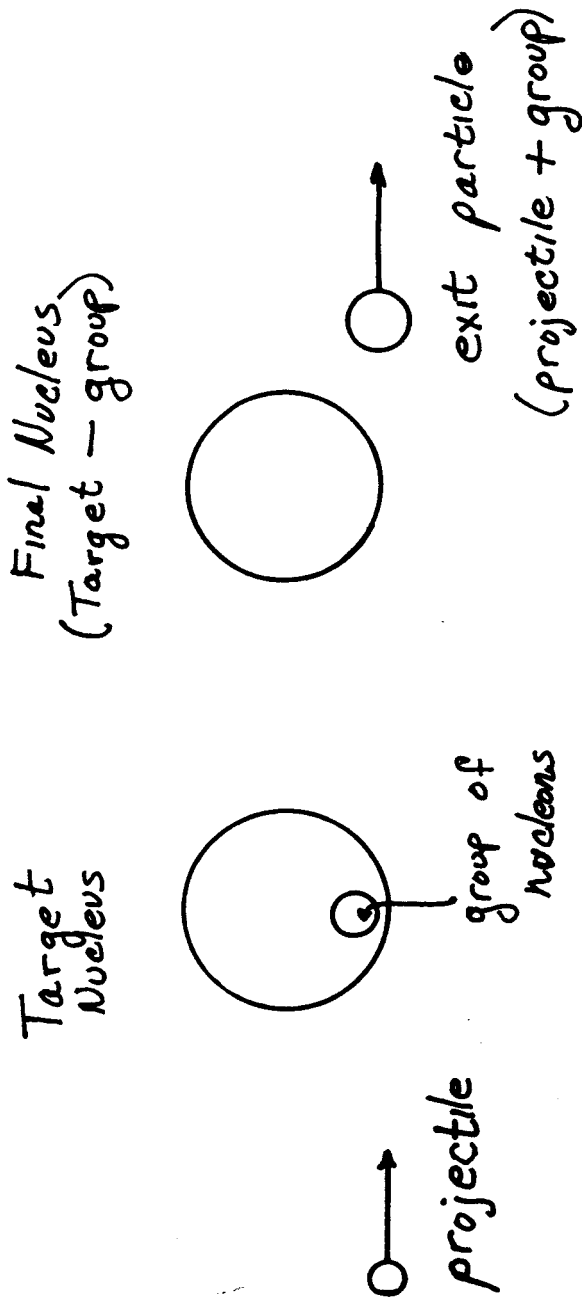The compound nuclear model of nuclear reactions.

Figure A.I.3

The direct nuclear reaction model.

nucleus is formed, it may fly apart in any direction. In this case, there will be lots of particles emitted in the backward directions. On the other hand, in the direct reaction the target nucleus is just barely grazed, so the reaction products should go primarily forward.

The research presented in this study is on a direct reaction. Various target nuclei have been bombarded with protons. These protons have picked up two neutrons and a proton from the target to make an α-particle as the out-going particle to be detected.

There are two questions which you should ask at this point. Why do this? What can be learned from nuclear reactions?

The answers lie in trying to find out whether question three can be answered using reactions as a tool.

The ideal way to answer the third question would be to bounce protons off of protons and neutrons individually to determine the forces between them. One could use these forces to predict the properties of nuclei. This has been tried with little success. Yet we are still interested in describing and predicting the properties of nuclei. So models have been invented that describe nuclei. One of these models is called a shell model. You can think of it in the following way.

Imagine that you are at the bottom of a well which has shelves on the walls above you. You have twelve balls with you which you may throw up. If you throw one up and it stays on a shelf, the system

of twelve balls has gained some potential energy. This is called an excited state of the system. It will subsequently lose this energy to heat radiation when the ball falls back to the bottom of the well. Experimentally, it has been observed that nuclei behave in this way. The twelve balls represent a carbon nucleus. The normal state of carbon is when all the balls are at the bottom of the well. However, it is observed that a reaction that results in the production of carbon produces excited states. This is analogous to having one or more of the balls on the shelves. Sometime later the nuclear excited state decays, emitting γ-radiation in the process.

It is the job of the shell model to predict how many excited states a nucleus has, the energies of these states, the probability that they will decay in a particular way, and a number of other properties including the chances of making any given excited state with a direct reaction. In other words, this model should predict the results of the work presented in this thesis.

The reason for studying direct reactions is to test the validity of the shell model.

A Simple Nuclear Experiment

The basic parts of a nuclear experiment are an accelerator, a transport system, a target, and a detector. The accelerator produces the beam of projectiles that are to be used to bombard the target. The transport system serves the purpose of carrying the beam from the

accelerator to the target and also determines the velocity of the beam. The detector analyzes the fragments that result from the reaction. In this section each of these components will be briefly described.

A Cyclotron—the Accelerator

A schematic top view of a cyclotron is shown in Figure A.I.4. Positive ions, usually hydrogen or helium nuclei, are produced in the ion source in the center of the cyclotron. Figure A.I.5 is a sketch of an ion source. A high current (about 400 amps) runs through the U-shaped tungsten filament. The filament becomes hot, just as the tungsten filaments in incandescent light bulbs do, and emits electrons. At the bottom of the cavity, which is filled with the gas that is to be ionized, is a block of tungsten which is at a high voltage compared to the filament. The high voltage causes the electrons to speed up. As they pass through the gas the accelerated electrons strike the gas atoms and knock off electrons. The result is that some atoms will not have any electrons. If the edge of the DEE which is just outside the ion source is negatively charged, the positive ions will be pulled out of the ion source through the hole in the side.

In the last paragraph we have already talked about the basic principle of all accelerators. Ions are accelerated when they are in a region of space where there is a high voltage. In other words, positive ions are accelerated toward a negative charge. The simplest possible accelerator is illustrated in Figure A.I.6.
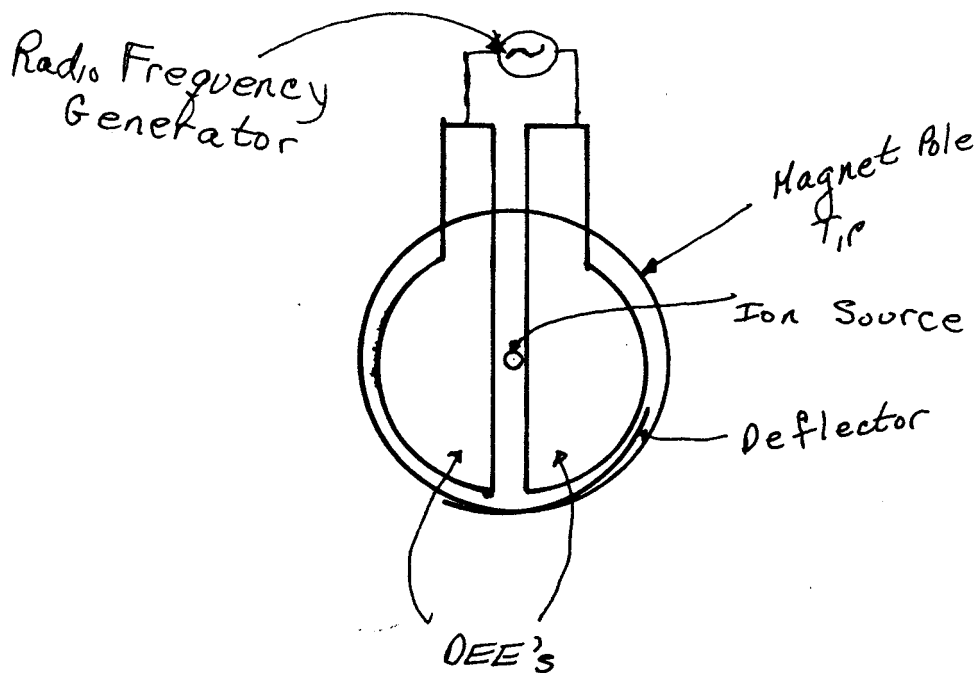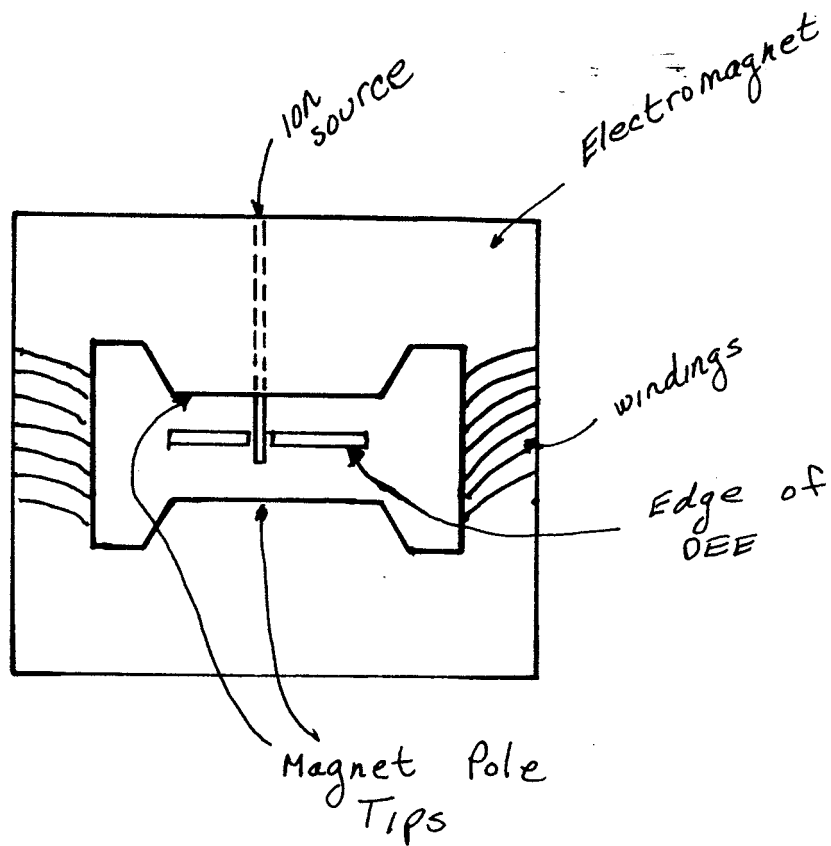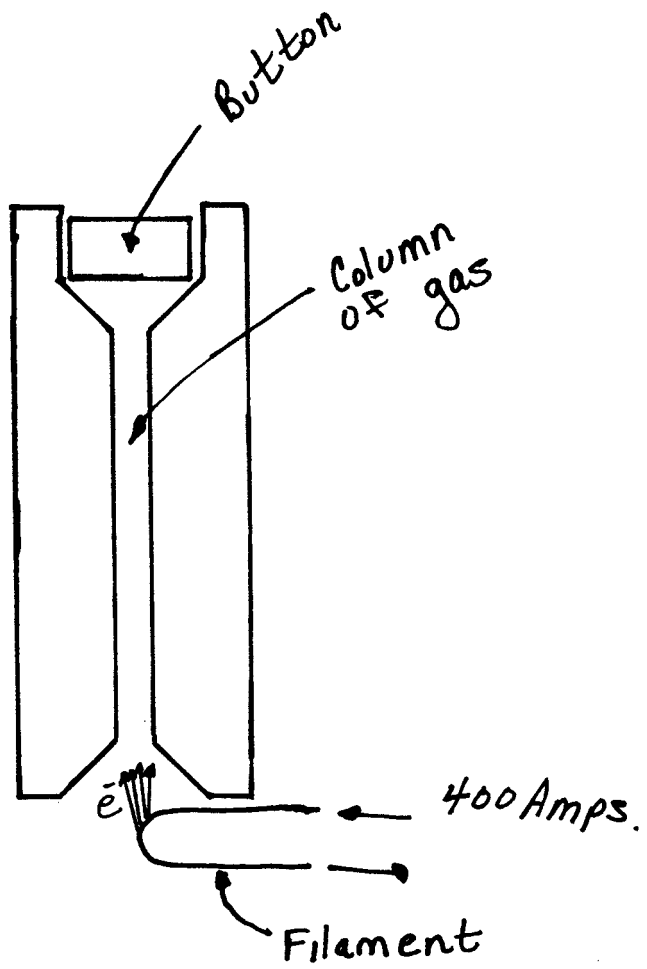
Figure A.I.4

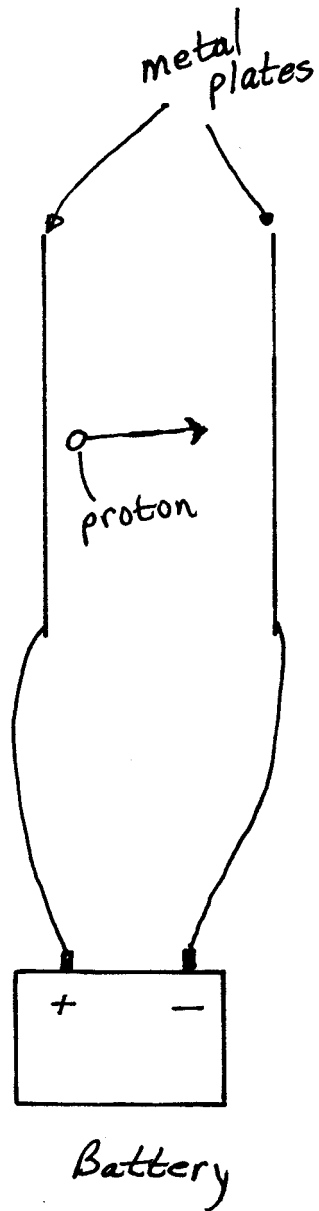A simple cyclotron

Figure A.I.5

A hot-filament ion source.

Figure A.I.6

A parallel plate accelerator.

It is hard to make a high enough voltage across a single gap to accelerate the ions to high enough energies. In the case of the research that is presented in this book, the voltage would have to be 35 million volts. In practice, it is practical to achieve 100,000 volts if there is good vacuum. The best way to attain high energies is to have many accelerations which add up. For example, the acceleration caused by 35 million volts can be attained by 350 100,000 volt accelerations.

This brings us to the second principle of cyclotrons. A charged particle that is moving between the pole tips of a magnet will follow a circular path. So now you can visualize how the machine works. First the ions are pulled through the hole in the side of the ion source by a negatively charged DEE. The DEE is hollow and between the pole tips of a magnet so the ions move in a circular path inside the DEE (see Figure A.I.4). After half a circle they return to the gap between the DEEs. When they get there the alternating voltage source which is attached to the DEEs has reversed and given the opposite DEE the negative charge. Thus the ions are accelerated across the gap again. Again they drift in a circle inside the DEE, and once again they are accelerated across the gap between the DEEs. In our cyclotron at MSU the ions make about 210 turns or 420 gap crossings and accelerations.

Each revolution the ions move a little faster in an orbit with a little larger radius. When they have spiraled to the outside edge of the machine, it is necessary to get them out of the machine. This means they must be deflected from their circular orbit. In many cyclotrons this is accomplished by placing a negatively charged plate near the outside orbit and pulling the particle out of the orbit. In the MSU cyclotron even fancier things are done to obtain a better beam outside the cyclotron.

The Transport System

A layout of the current status of the MSU cyclotron lab is shown in Figure A.I.7. There are a number of experimental setups available. This section deals with what must be done to get the beam from the cyclotron to one of these experimental areas.

This is really the simplest part of the system. We need only to apply the principle that charged particles follow curved orbits in a magnetic field. So every time the direction of the beam has to be changed, we pass it between the poles of a magnet. The magnets marked M3, M4, and M5 on Figure A.I.7 may be adjusted to send the beam whichever direction is desired.

While doing the accelerating and transporting of the beam, it is important to keep the beam in a high vacuum. Even a little air will result in a loss of beam because of collisions with the gas atoms.
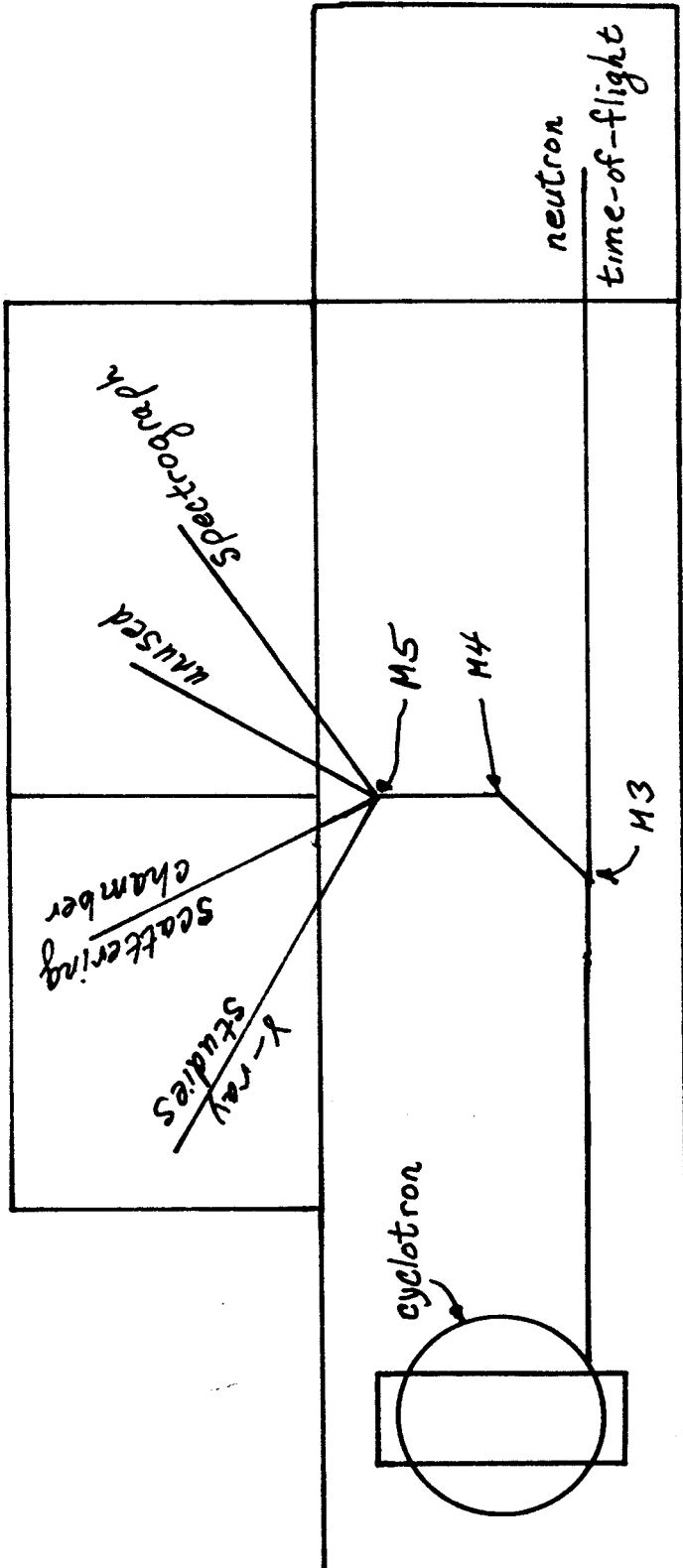
Figure A.I.7

The experimental facilities at M.S.U.

Besides transporting the beam to the experiment, the beam line may be used to define the beam energy. Consider the diagram in Figure A.I.8. The beam enters the magnet with some particles moving faster than others. The higher energy particles bend less than the low energy ones causing the beam to be spread out when it leaves the magnet. A set of metal jaws which only allow the central portion of the beam to pass through can then be used to define the spread in the energy.

The Target

There are two important qualities that a target must have. It must be pure and thin.

The purity requirement is different than just the idea of chemical purity. In this instance, isotopic purity is required. For example, the chromium found in nature is a mixture of four isotopes all of which have 24 protons but 26, 28, 29, or 30 neutrons. Although they are chemically the same, their nuclear properties are different.

The thinness is important since even these fast particles are greatly slowed down as they pass through any matter. They will go through only about 1/16 inch of brass. Good targets are only a couple hundred atomic layers thick. You can often see through them.

To make these thin targets the material must be made hot enough to melt and evaporate. A glass slide that has been coated with a water soluble salt may be placed above the hot metal so that
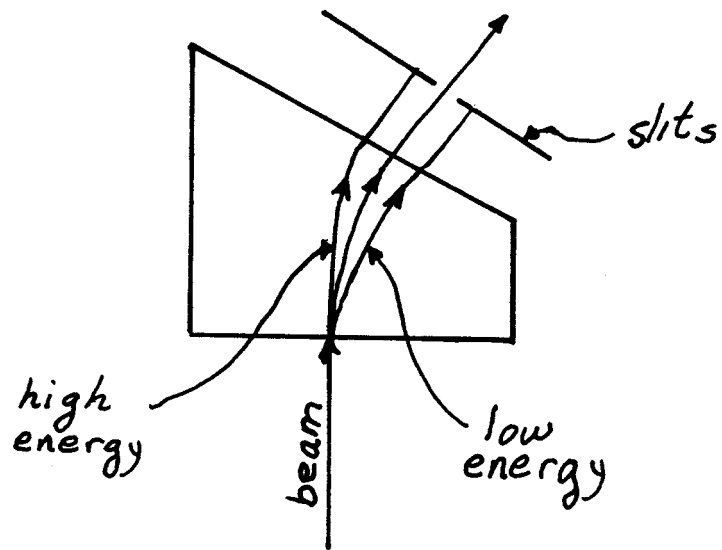
Figure A.I.8

Bending magnet and slits for beam energy definition.

the evaporating metal condenses on the slide. If the slide is slowly immersed in water at a later time, the soluble salt will dissolve leaving the target material floating on the surface. A metal slide with a hole in it may be used to pick up the floating foil in such a way that it is stretched across the hole.

The experimenter should put the beam through the hole in the target frame, thereby hitting the target foil only.

The Detector

The detector must be capable of giving three pieces of information. It must tell you what kind of particle has been seen, how much energy the particle had, and in what direction the particle was emitted from the target.

The detector used in this experiment is a rather complicated beast called a spectrograph. It works on the principle that fast particles bend less than slow ones in a magnetic field. A simple spectrograph sketch is given on Figure A.I.9.

Only particles that leave the target with the correct angle "θ" can enter the opening to the magnet. This requirement gives the directional information.

The energy information may be determined by finding the position that the particle hits the counter. High energy particles strike one end and low energy reaction products strike the other end.
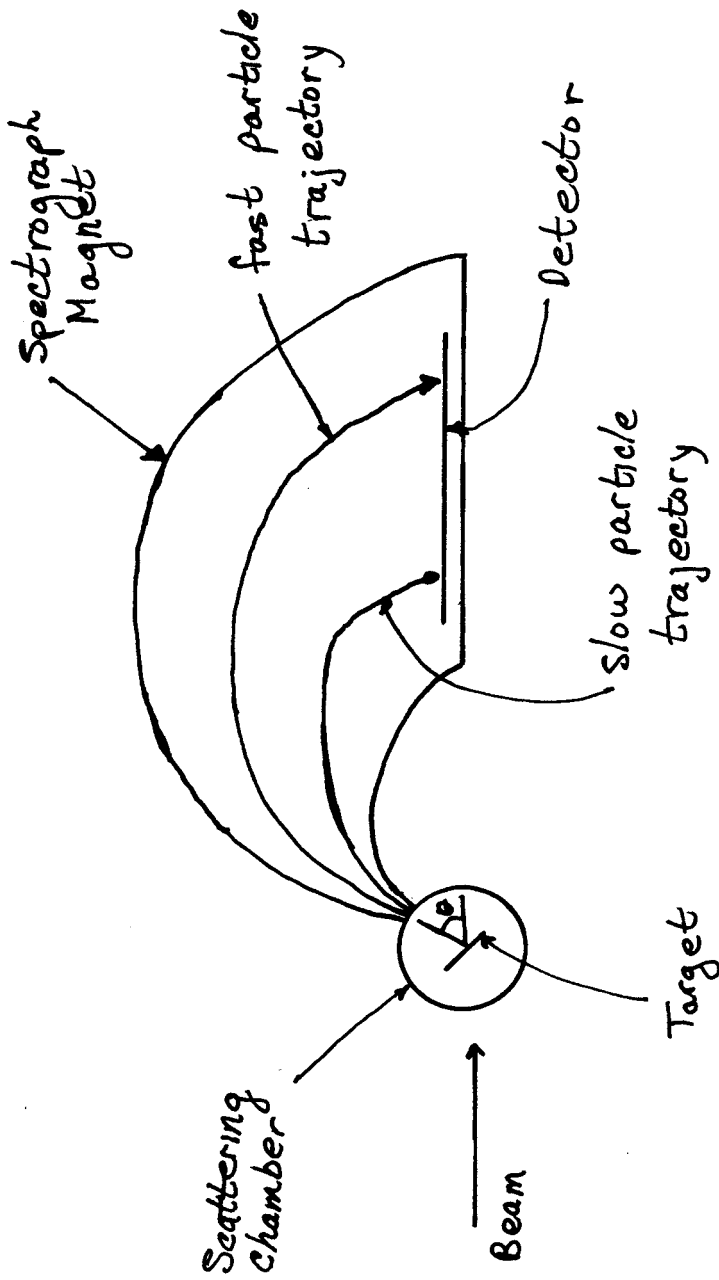
Figure A.I.9

A sketch of a magnetic spectrometer.

One type of counter is diagrammed in Figure A.I.10. When a fast charged particle passes through a gas, it leaves a track of ionized gas atoms along its path. The resulting charge is collected on the wire that runs the length of the gas region. More charge travels to the closer end of the wire than to the far end of the wire. Therefore, the position is given by the ratio:

$$\frac{end\ 1}{end\ 1 + end\ 2}.$$

The total signal will tell what kind of particle has been observed. You must keep in mind that all kinds of junk is being made in the target, but in this experiment we want to count α-particles only. The total signal (signal 1 + signal 2) is bigger for α-particles than protons, deuterons, tritons, and ^{3}He-particles. So by counting only the large total signals and rejecting the rest, it is possible to pick out the α-particles.

Doing the Experiment

The cyclotron is turned on and adjusted so that the beam goes down the beam pipe and strikes the target. This simple sounding operation may take half an hour or half a day depending on your luck.

The reaction products are allowed to strike the counter at the end of the spectrograph. At this point the work of finding out what is happening begins. The signals from the counter are very small so they must be amplified. After they are amplified they have to be added and then divided. Performing these operations requires the
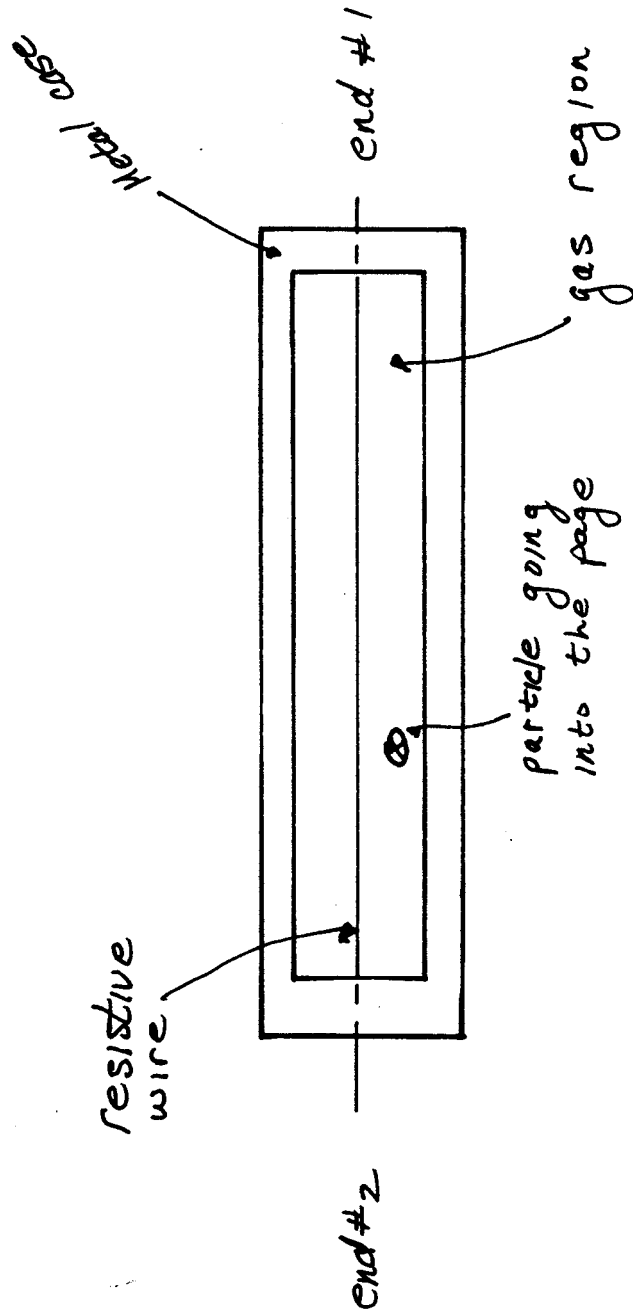
Figure A.I.10

A charge-division focal plane counter.

experimenter to process the signals with a number of electronic black boxes. One of these boxes adds the signals. The division is done by a computer. At the same time the computer will make a television display of the plot shown in Figure A.I.11. The bands in the display represent the different particles coming from the target. The bottom band may be protons and the top band might be α-particles. The computer program which we are using allows us to choose whichever band we want to study.

The desired result is a spectrum such as the one shown in Figure V.1. Each peak in the spectrum represents a different state of the nucleus that is left behind after the reaction has occurred. All the information about nuclei must come from spectra like this.

To complete the experiment it is necessary to move the spectrograph to many different angles and to record the spectrum at each of these angles. The relative sizes of the peaks at these different angles is important information. It is likely that about two days (48 hours) of beam time will be necessary to get all the necessary spectra for a given target.

Analysis of the Data

The data of an experiment similar to the one that was just described are a set of spectra (plots of number of α-particles vs. the energy of the α-particles). One of these spectra is shown in Figure V.1.
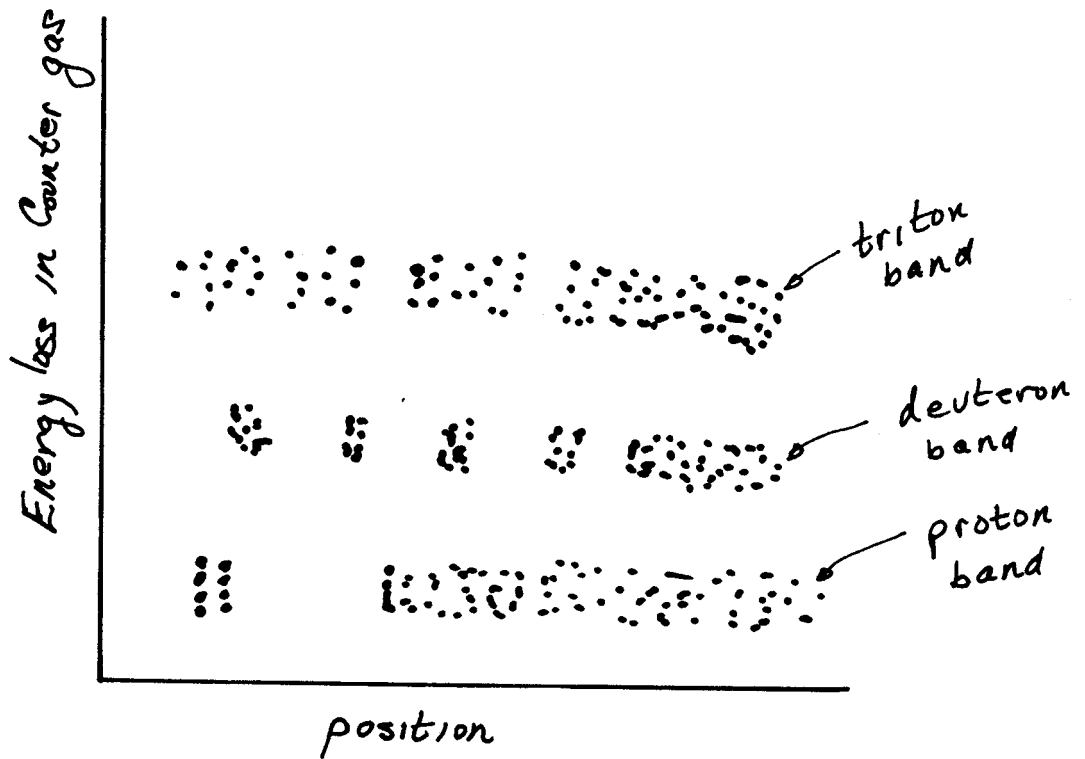
Figure A.I.11

Identification of the reaction products.

The analysis of this data begins by determining how much potential energy was left in the nucleus after the reaction for each peak that is observed. This list of energies can be compared with results from other experiments (see Table IV.2). It may also be compared with a list of energies predicted by the shell model.

There is also a lot of information contained in the sizes of the peaks. The relative sizes of the peaks changes as the detector angle changes. Some peaks become larger as the angle is increased, while others become smaller. This suggests that we should make graphs which show how big each peak is at each angle that a spectrum was taken. Such graphs are given in Figure V.2.

Many years of experimentation has shown that these shapes are characteristic of a property of the nucleus called spin. You can think of spin classically if you wish by considering the collision of two billiard balls. In general, both balls will be spinning after the collision. The spin is particularly evident if one of the balls is striped. Each time a nuclear reaction takes place, the resulting nucleus is caused to spin. The states of the final nucleus which we observe as peaks in the spectrum have various amounts of spin. The reasons the angular distributions (graphs of peak size vs. detector angle) are different is because the nucleus has different amounts of spin for each peak. With some reaction data, the spin of a particular nuclear excited state may be determined. When this is done, the list of

energies and spins may be compared to the predictions of the shell model. One of the principal reasons for the research presented in this thesis was to investigate the possibility of using the (p,α) reaction (incident proton, outgoing α-particle) to determine the spin of nuclear excited states.

There are two approaches we can take toward determining the utility of the (p,α) reaction for determining spins. First we may make a table of shapes for states whose spins have been determined previously. The table of known shapes can then be compared to data for new states and used to determine the spins of the new states. This method works only because it turns out that only certain amounts of spin may be realized, just as we saw that there were only certain energy shelves in the well.

The second method is theoretical. If the shell model works, it predicts both an energy and a spin value for all nuclear states. If a theory is developed to predict the angular distributions, given the shell model information, the resulting theoretical angular distributions can be compared to the data plotted on the peak size vs. angle graphs. Such a theory for the (p,α) reaction is developed in Chapter II and some comparisons can be found in Chapters IV and V.

Summary

The work which you find in this thesis may be summarized as follows. We have set out to use the (p,α) reaction to discover

nuclear energy levels and spins. We have done this by comparing the data with the results of other experiments and by developing a theory to predict the data that we have observed. In general, modest success has been realized.

APPENDIX II

AN INTRODUCTION TO SCATTERING THEORY

Part One: The First Year Quantum Mechanics Problem

Imagine a structureless projectile incident on a structureless

target. A classical analog of this situation would be a cue ball inci-

dent on a billiard ball.

The Schrödinger equation which describes the Quantum Mechani-

cal problem is

$$\nabla^2 \psi + \frac{2\mu}{\hbar^2} [E - V(r)] \psi = 0.$$ A.II.1

We will require the scattering potential to be short range, i.e.,

$$\lim_{r \to \infty} r V(r) \to 0.$$ A.II.2

(Notice that the Coulomb force does not satisfy this condition. A

screened Coulomb force does, however.) If this is the case, a detec-

tor which for all practical purposes is located at $r \to \infty$ will observe

the asymptotic form of ψ. Asymptotically, the solution must look like

a plane wave, which is the incident or non-scattered beam, and a

spherical scattered wave. In other words, the asymptotic form of ψ

should be

$$\psi^{(+)} \sim e^{ikz} + f(\theta) \frac{e^{ikr}}{r}.$$ A.II.3

k is the wavenumber

$$\left(\text{i.e.,} \quad p = \hbar k \quad \text{or} \quad E = \frac{p^2}{2\mu} = \frac{\hbar^2 k^2}{2\mu} \right)$$

and $f(\theta)$ is the scattering amplitude. $f(\theta)$, in other words, is the amplitude for scattering at a particular angle. $|f(\theta)|^2$ is, therefore, the probability for scattering at the angle θ. All the information about the interaction must be contained in $f(\theta)$. However, $f(\theta)$ is not the quantity which is derived experimentally. The experimentalist measures the differential cross section which is defined to be

$$\left(\frac{d\sigma}{d\Omega} \right) d\Omega = \frac{\text{number of particles scattered into } d\Omega \text{ at } \theta}{\text{number of particles incident per cm}^2} \qquad \text{. A.II.4}$$

The relation between $\left(\dfrac{d\sigma}{d\Omega} \right)$ and $f(\theta)$ can be found in the following way:

The incident probability current is

$$S_i = \frac{\hbar}{\mu} \, \text{Im} \, e^{-ikz} \frac{d}{dz} e^{ikz} = \frac{\hbar k}{\mu} \, . \qquad\qquad \text{A.II.5}$$

The outgoing current is

$$S_o = \frac{\hbar}{\mu} \, \text{Im} \, \frac{e^{-ikr}}{r} \frac{\partial}{\partial r} \left(f(\theta) \frac{e^{ikr}}{r} \right) = \frac{\hbar k}{\mu} \frac{|f(\theta)|^2}{r^2} \, . \qquad \text{A.II.6}$$

If N is the number of particles per cm^3 in the incident beam, then NS_i is the incident particle current (cm^2/sec). The number of particles striking the detector each second is $r^2 d\Omega \, NS_o$. So substitute these expressions into A.II.4 to find

$$\left(\frac{d\sigma}{d\Omega}\right) d\Omega = \frac{N r^2 d\Omega \, (\hbar k/\mu) \, (|f(\theta)|^2 / r^2)}{N \, (\hbar k/\mu)}$$

or

$$\left(\frac{d\sigma}{d\Omega}\right) = |f(\theta)|^2. \qquad\qquad \text{A.II.7}$$

In general there are two approaches to the problem. Either the experimentalist measures $|f(\theta)|^2$ at many angles and the theorist attempts to determine $V(r)$ from this, or the theorist guesses at $V(r)$ thereby determining $|f(\theta)|^2$ and the experimentalist measures it. In any event, it is necessary to find out how $f(\theta)$ is related to $V(r)$.

To do this, begin by rewriting Equation A.II.1

$$(\nabla^2 + k^2)\psi = \frac{2\mu}{\hbar^2} V(r)\psi. \qquad\qquad \text{A.II.8}$$

We are looking for a solution which has the asymptotic form given by Equation A.II.3. So it is reasonable to look for a solution that is good for all values of r which has the form

$$\psi = e^{i\underset{\sim}{k}\cdot\underset{\sim}{r}} + \psi_s \qquad\qquad \text{A.II.9}$$

where ψ_s is the scattered wave.

The plane wave satisfies

$$(\nabla^2 + k^2)e^{i\underset{\sim}{k}\cdot\underset{\sim}{r}} = 0. \qquad\qquad \text{A.II.10}$$

So if A.II.9 is used in A.II.8, the result is

$$(\nabla^2 + k^2)\psi_s = \frac{2\mu}{\hbar^2} V(r)\psi. \qquad\qquad \text{A.II.11}$$

Equation A.II.11 may be solved formally by using the Green's function method. We seek the Green's function which satisfies

$$(\nabla^2 + k^2) G(\underset{\sim}{r}, \underset{\sim}{r}') = -4\pi \, \delta(\underset{\sim}{r} - \underset{\sim}{r}').$$
A.II.12

Then the solution of A.II.11 will be given by

$$\psi_s = -\frac{1}{4\pi} \frac{2\mu}{\hbar^2} \int G(\underset{\sim}{r}, \underset{\sim}{r}') V(\underset{\sim}{r}') \psi(\underset{\sim}{r}') dr'.$$
A.II.13

Equation A.II.12 is the same relation that is found in the study of

electromagnetic radiation when solving the Helmholtz equation. The

Green's function for that problem is

$$G(r, r') = \frac{e^{ik(|\underset{\sim}{r} - \underset{\sim}{r}'|)}}{|\underset{\sim}{r} - \underset{\sim}{r}'|}.$$
A.II.14

It is the asymptotic form which is desired. This form is found by using

the relation

$$|\underset{\sim}{r} - \underset{\sim}{r}'| \cong |\underset{\sim}{r}| - \frac{\underset{\sim}{r}, \underset{\sim}{r}'}{|\underset{\sim}{r}|} \quad \text{when} \quad |\underset{\sim}{r}| \gg |\underset{\sim}{r}'|.$$
A.II.15

The asymptotic Green's function is then

$$G(\underset{\sim}{r}, \underset{\sim}{r}') \cong e^{-i\underset{\sim}{k}' \cdot \underset{\sim}{r}'} \frac{e^{ikr}}{r}.$$
A.II.16

where

$$\underset{\sim}{k}' = \frac{\underset{\sim}{r}}{|\underset{\sim}{r}|} |k|.$$

To get the asymptotic form of Equation A.II.9, we need to use

A.II.16 in Equation A.II.13.

$$\psi_{(r)}^{(+)} = e^{i\underset{\sim}{k} \cdot \underset{\sim}{r}} + \left(-\frac{1}{4\pi} \frac{2\mu}{\hbar^2} \int e^{-i\underset{\sim}{k}' \cdot \underset{\sim}{r}'} V(r') \psi(\underset{\sim}{r}') d\underset{\sim}{r}'\right) \frac{e^{ikr}}{r}.$$
A.II.17

Comparing A.II.17 to A.II.3, it is seen that

$$f(\theta) = -\frac{1}{4\pi} \frac{2\mu}{\hbar^2} \int e^{-i\underset{\sim}{k}' \cdot \underset{\sim}{r}'} V(r') \psi(\underset{\sim}{r}') d\underset{\sim}{r}'.$$
A.II.18

Although Equation A.II.18 looks like an answer, it is not because we

do not know $\psi(r')$—it is the solution of Equation A.II.1 which is what

we are trying to get. This is because Equation A.II.13 really only changes the problem from a differential equation to an integral equation. We can get an approximate solution if we make the assumption that the solution can be generated iteratively. We shall assume that

$$\psi^{(+)}(\underset{\sim}{r}') \cong \psi(\underset{\sim}{r}')$$

and proceed then by using $\psi^{(+)}(\underset{\sim}{r}')$ for $\psi(\underset{\sim}{r}')$ where

$$\psi^{(+)}(\underset{\sim}{r}') = e^{i\underset{\sim}{k}\cdot\underset{\sim}{r}'} - \frac{1}{4\pi}\frac{2\mu}{\hbar^2}\int e^{-i\underset{\sim}{k}''\cdot\underset{\sim}{r}''}V(r'')\psi(\underset{\sim}{r}'')d\underset{\sim}{r}''\,\frac{e^{ik'r'}}{r'} \qquad \text{A.II.19}$$

where

$$\underset{\sim}{k}'' = \frac{\underset{\sim}{r}'}{|\underset{\sim}{r}'|}\,|k'|\,.$$

Using A.II.19 in A.II.17 yields

$$\psi^{(+)}_{(r)} = e^{i\underset{\sim}{k}\cdot\underset{\sim}{r}} - \frac{1}{4\pi}\frac{2\mu}{\hbar^2}\int e^{-i\underset{\sim}{k}'\cdot\underset{\sim}{r}'}V(r')e^{i\underset{\sim}{k}\cdot\underset{\sim}{r}'}d\underset{\sim}{r}'$$

$$+\left(\frac{1}{4\pi}\frac{2\mu}{\hbar^2}\right)^2\iint e^{-i\underset{\sim}{k}'\cdot\underset{\sim}{r}'}V(r')e^{-i\underset{\sim}{k}''\cdot\underset{\sim}{r}''}V(r'')\psi(\underset{\sim}{r}'')d\underset{\sim}{r}''d\underset{\sim}{r}'\,. \qquad \text{A.II.20}$$

Presumably we can generate this series forever by replacing $\psi(r'') \to \psi^{(+)}(r'')$, etc. Instead we assume that the series converges rapidly and therefore keep only the first order term to yield the results

$$\psi^{(+)}(\underset{\sim}{r}) \cong e^{i\underset{\sim}{k}\cdot\underset{\sim}{r}} - \frac{1}{4\pi}\frac{2\mu}{\hbar^2}\left(\int e^{i\underset{\sim}{k}'\cdot\underset{\sim}{r}'}V(r')e^{i\underset{\sim}{k}\cdot\underset{\sim}{r}'}d\underset{\sim}{r}'\right)\frac{e^{ikr}}{r} \qquad \text{A.II.21}$$

and

$$f(\theta) = -\frac{1}{4\pi}\frac{2\mu}{\hbar^2}\int e^{-i\underset{\sim}{k}'\cdot\underset{\sim}{r}'}V(\underset{\sim}{r}')e^{i\underset{\sim}{k}\cdot\underset{\sim}{r}'}d\underset{\sim}{r}'\,. \qquad \text{A.II.22}$$

This is called the Born approximation. The convergence of the Born series is an open theoretical problem that remains unsolved. Nonetheless, it has been used with reasonable success for a long time now.

Part Two: Nuclear Scattering—The Distorted Wave Born Approximation

The first year quantum mechanics problem is not very useful for real problems since, in general, the projectile and the target have structure and, therefore, many different kinds of inelastic events may occur. Additionally, the target nucleus acts as a sink for particles that are incident on it in a way that is similar to the scattering of a beam of light by a cloudy crystal ball. It has been shown that this effect can be reproduced by using waves that are distorted by a short range optical potential which has real and imaginary parts instead of plane waves.

The simple problem shown in the first part of this appendix can be used as a guide for generalization. The approach here will be to proceed mostly by analogy to the first part.

Consider the reaction $A(a,b)B$. The Schrödinger equation which describes this system is

$$H\psi = E\psi \qquad\qquad A.II.23$$

where $H = H_\alpha + V_\alpha + T_\alpha$. Here α represents the aA system (the incident channel). H_α is the total internal Hamiltonian. In other words, $H_\alpha = H_a + H_A$ where H_a and H_A are the internal Hamiltonians for the projectile and the target. H_α, therefore, does not depend on the separation of aA. T_α is the kinetic energy of the relative aA motion, and V_α is the interaction between the projectile and the target.

Equivalently, we could write $H = H_\beta + V_\beta + T_\beta$ where β represents the bB system or exit channel.

Internal wavefunctions ψ_α and ψ_β may be defined by

$$H_\alpha \psi_\alpha = E_\alpha \psi_\alpha$$
$$H_\beta \psi_\beta = E_\beta \psi_\beta. \qquad \text{A.II.24}$$

Then

$$E = E_\alpha + \frac{\hbar^2 k_\alpha^2}{2\mu_\alpha} = E_\beta + \frac{\hbar^2 k_\beta^2}{2\mu_\beta}. \qquad \text{A.II.25}$$

The asymptotic form of ψ is what is desired. If three-body final states are neglected, Equation A.II.3 can be generalized to

$$\psi_\alpha^{(+)} = \psi_\alpha e^{i\underline{k}_\alpha \cdot \underline{r}_\alpha} + \sum_\gamma f_{\alpha\gamma}(\theta) \frac{e^{ik_\gamma r_\gamma}}{r_\gamma} \psi_\gamma. \qquad \text{A.II.26}$$

$f_{\alpha\gamma}(\theta)$ is the scattering amplitude for γ exit channel.

The generalization entails:

1. Including the projectile and target internal wavefunctions in the incident channel (ψ_α).

2. Allowing more than one exit channel, each with its own amplitude and internal wavefunction.

The functions ψ_γ form a complete set of orthogonal states of the (a + A) particles so we may expand

$$\psi_\alpha^{(+)} = \sum_\gamma \psi_\gamma \langle \psi_\gamma | \psi_\alpha^{(+)} \rangle. \qquad \text{A.II.27}$$

The overlap on the right hand side of Equation A.II.27 is an integral over the internal coordinates only, hence we may write

$$\langle \psi_\gamma | \psi_\alpha{}^{(+)} \rangle = \varphi_\gamma(\underline{r}_\gamma). \qquad \text{A.II.28}$$

The relative motion in the β channel is then given by

$$\langle \psi_\beta | \psi_\alpha{}^{(+)} \rangle = \varphi_\beta(\underline{r}_\beta). \qquad \text{A.II.28a}$$

An equation for the relative motion may be found by rewriting Equation A.II.23 as

$$(E - H)\psi_\alpha{}^{(+)} = 0$$

so

$$(E - H_\beta - T_\beta - V_\beta)\psi_\alpha{}^{(+)} = 0. \qquad \text{A.II.29}$$

We can now multiply Equation A.II.29 on the left by ψ_β and integrate over the internal coordinates to get

$$\langle \psi_\beta | (E - H_\beta - T_\beta - V_\beta) | \psi_\alpha{}^{(+)} \rangle = 0$$

$$(E - E_\beta - T_\beta)\langle \psi_\beta | \psi_\alpha{}^{(+)} \rangle = \langle \psi_\beta | V_\beta | \psi_\alpha{}^{(+)} \rangle. \qquad \text{A.II.30}$$

To perform the last step we have used $[\psi_\beta, T_\beta] = 0$ which is true because ψ_β is a function of internal coordinates while T_β is a function of the relative motion only.

Now

$$E - E_\beta = \mathcal{E}_\beta = \frac{\hbar^2 k_\beta^2}{2\mu_\beta}$$

from Equation A.II.24, so we finally get an equation for the relative motion which is

$$\left(\frac{\hbar^2 k^2}{2\mu_\beta} - T_\beta\right)\varphi_\beta(r_\beta) = \langle \psi_\beta | V_\beta | \psi_\alpha{}^{(+)} \rangle$$

so

$$(\nabla^2 + k^2)\varphi_\beta(r_\beta) = \frac{2\mu_\beta}{\hbar^2}\langle \psi_\beta | V_\beta | \psi_\alpha{}^{(+)} \rangle. \qquad \text{A.II.31}$$

This is exactly the same form as Equation A.II.11 to which we applied

the Green's function method previously. We can solve it again by the

same method and the resulting expression for $f_{\alpha\beta}(\theta)$ will be

$$f_{\alpha\beta}(\theta) = -\frac{1}{4\pi}\frac{2\mu_\beta}{\hbar^2}\iint d\xi_\beta dr_\beta \psi_\beta^*(\xi_\beta) e^{-i\underset{\sim}{k}_\beta \cdot \underset{\sim}{r}_\beta} V(r_\beta, \xi_\beta)\psi_\alpha^{(+)} \qquad \text{A.II.32}$$

where the ξ_β are the internal coordinates of b and B. The Plane

Wave Born Approximation demonstrated in Equation A.II.22 is to

replace

$$\psi(r') \rightarrow e^{i\underset{\sim}{k}\cdot\underset{\sim}{r}'}.$$

The appropriate generalization to make is to replace

$$\psi_\alpha^{(+)} \rightarrow \psi_\alpha(\xi_\alpha) e^{i\underset{\sim}{k}_\alpha \cdot \underset{\sim}{r}_\alpha}$$

and integrate over the internal coordinates ξ_α and r_α so that final

expression for the scattering amplitude in the first order Plane Wave

Born Approximation (PWBA) is

$$f_{\alpha\beta}^{PWBA}(\theta) = -\frac{1}{4\pi}\frac{2\mu_\beta}{\hbar^2}\iiint d\xi_\alpha d\xi_\beta d\underset{\sim}{r}_\beta d\underset{\sim}{r}_\alpha \psi_\beta^*(\xi_\beta) e^{-i\underset{\sim}{k}_\beta \cdot \underset{\sim}{r}_\beta}$$

$$V_\beta(r_\beta, \xi_\beta)\psi_\alpha(\xi_\alpha) e^{i\underset{\sim}{k}_\alpha \cdot \underset{\sim}{r}_\alpha}. \qquad \text{A.II.33}$$

As a convenient notation, we define a transition matrix element by

$$T_{\alpha\beta}^{PWBA} = \int d\underset{\sim}{r}_\alpha d\underset{\sim}{r}_\beta e^{-i\underset{\sim}{k}_\beta \cdot \underset{\sim}{r}_\beta}\langle\psi_\beta|V_\beta|\psi_\alpha\rangle e^{i\underset{\sim}{k}_\alpha \cdot \underset{\sim}{r}_\alpha}. \qquad \text{A.II.34}$$

The potential V_β is the interaction between all the nucleons in

the projectile and all the nucleons in the target. In practice, we only

want to consider one or two interactions. For example, we are only

interested in the p-n interaction in the (p,d) reaction. The rest of the interactions cannot be neglected, however. We hope that these interactions can be treated as an average overall potential, which may be complex. To incorporate this potential, we subtract a potential U_β from both sides of Equation A.II.31 to get

$$(\mathcal{E}_\beta - T_\beta - U_\beta)\varphi_\beta(r_\beta) = \langle \psi_\beta | (V_\beta - U_\beta) | \psi_\alpha^{(+)} \rangle. \qquad \text{A.II.35}$$

We will choose U_β in such a way that $V_\beta - U_\beta$ contains only interactions between the nucleons involved in the scattering and so that U_β does not cause any transitions; i.e., U_β is diagonal in the β system. This equation can also be solved by a Green's function method which involves making a multipole expansion of the Green's function. The procedure is complicated and amounts to proving the Gell-Mann-Goldberg relation for scattering from two potentials. Instead of carrying out this procedure, we will simply use the relation to get the transition matrix element

$$T_{\alpha\beta} = \langle \psi_\beta \chi_\beta^{(-)} | U_\beta | \psi_\alpha e^{i\underset{\sim}{k}_\alpha \cdot \underset{\sim}{r}_\alpha} \rangle + \langle \psi_\beta \chi_\beta^{(-)} | (V_\beta - U_\beta) | \psi_\alpha^{(+)} \rangle, \qquad \text{A.II.36}$$

where $\chi_\beta^{(-)}$ is the incoming solution of the homogeneous equation

$$(\mathcal{E}_\beta - T_\beta - U_\beta)\chi_\beta(r_\beta) = 0.$$

By choice, U_β does not cause any transitions or, in other words, is diagonal in the β system. So the first term reduces to $t_o \delta_{\alpha\beta}$ and

$$T_{\alpha\beta} = t_o \delta_{\alpha\beta} + \langle \psi_\beta \chi_\beta^{(-)} | (V_\beta - U_\beta) | \psi_\alpha^{(+)} \rangle. \qquad \text{A.II.37}$$

This form is called the _post-interaction_ form. There is another form

called the _prior-interaction_ form which is related by time-reversal symmetry and is

$$T_{\alpha\beta} = t_o \delta_{\alpha\beta} + \langle \psi_\beta^{(-)} | (V_\alpha - U_\alpha) | \psi_\alpha \chi_\alpha^{(+)} \rangle .$$ A.II.37a

Once again, A.II.37 is not a solution because it contains $\psi_\alpha^{(+)}$ or $\psi_\beta^{(-)}$. We still need to make some approximations. Using Equation A.II.37a, expand $\psi_\beta^{(-)}$ as

$$\psi_\beta^{(-)} = \sum_\gamma a_\gamma \varphi_\gamma^{(-)}(\underset{\sim}{r}_\gamma) \psi_\gamma(\xi_\gamma)$$ A.II.38

or, in other words,

$$\psi_{d+^{15}0}^{(-)} = a_1 \varphi_{d+^{15}0}^{(-)} \psi_{d+^{15}0} + a_2 \varphi_{d+^{15}0*}^{(-)} \psi_{d+^{15}0*} + a_3 \varphi_{t+^{14}0} \psi_{t+^{14}0} + \cdots$$

Now we assume that $a_1 \cong 1$ and $a_i \cong 0$; $i = 2 \ldots$; hence,

$$\psi_{d+^{15}0}^{(-)} \cong \varphi_{d+^{15}0}^{(-)} \psi_{d+^{15}0} \quad ; \quad \psi_\beta^{(-)} \cong \varphi_\beta^{(-)}(r_\beta) \psi_\beta(\xi_\beta) .$$

This amounts to neglecting multiple excitations such as inelastic scattering (second term) and two-step processes such as $(d,t)(t,d)$ (third term).

The eigenfunctions of U_β accurately reproduce $\varphi_\beta^{(-)}$ in the asymptotic region. We now will assume that $\varphi_\beta^{(-)}$ can be approximated by the eigenfunctions of the optical potential, $\chi_\beta^{(-)}$ even during the interaction. Then

$$T_{\alpha\beta}^{DWBA} = T_o \delta_{\alpha\beta} + \langle \chi_\beta^{(-)} \psi_\beta | (V_\alpha - U_\alpha) | \psi_\alpha \chi_\alpha^{(+)} \rangle .$$ A.II.39

This is called the distorted Wave Born Approximation. All the nuclear structure information is contained in the internal matrix element

$\langle \psi_\beta | (V_\alpha - U_\alpha) | \psi_\alpha \rangle$. The method of evaluating this matrix element depends on the reaction being considered. In Chapter II of this book the internal matrix elements for the (p,α) and (α,p) reactions are evaluated.

The purpose of this appendix was to present a non-rigorous guide to the DWBA. More detailed and complete derivations may be found in:

A.II.1. The Theory of Direct Nuclear Reactions by W. Toborman, Oxford University Press (1961), London, England.